

DRAFT: Shielding benchmark calculations with MCNP-4C3 using ENDF/B-VII beta2 nuclear data

S.C. van der Marck

Petten, June 13, 2006

21616/05.70023/P

rev. no	date	description
B	2006/06/13	Calculations based on beta2 version of ENDF/B-VII
A	2005/11/02	Calculations based on beta1 version of ENDF/B-VII

author : S.C. van der Marck

reviewed : A.J. Koning

69 page(s)
shield.tex

approved : R.P.C. Schram

Abstract

Shielding benchmark calculations were performed with MCNP-4C3 using the new ENDF/B-VII beta2 nuclear data library. The benchmarks used were Oktavian (for Al, Co, Cr, Cu, LiF, Mn, Mo, Si, Ti, W, Zr), FNS (for Be, C, Fe, and Pb), LLNL Pulsed Spheres (for concrete), and NIST Water Spheres (for water and Cd). The results of these calculations are reported as graphs of the neutron spectra, and in some cases also the photon spectrum, as well as in graphs and tables of calculated over experimental values of the neutron spectra.

Keywords

MCNP-4C3
ENDF/B-VII beta2
nuclear data
shielding benchmarks

Contents

1	Introduction	5
2	Brief description of the shielding benchmarks	6
2.1	Oktavian	6
2.2	FNS	7
2.3	LLNL Pulsed Spheres	8
2.4	NIST Water Spheres	10
3	Results	11
3.1	Oktavian	11
3.1.1	Oktavian, Al	11
3.1.2	Oktavian, Co	12
3.1.3	Oktavian, Cr	13
3.1.4	Oktavian, Cu	14
3.1.5	Oktavian, LiF	15
3.1.6	Oktavian, Mn	16
3.1.7	Oktavian, Mo	17
3.1.8	Oktavian, Si	18
3.1.9	Oktavian, Ti	19
3.1.10	Oktavian, W	20
3.1.11	Oktavian, Zr	21
3.2	FNS	22
3.2.1	Calculational methods	22
3.2.2	FNS, Be, 5 cm	22
3.2.3	FNS, Be, 15 cm	24
3.2.4	FNS, C, 5 cm	26
3.2.5	FNS, C, 20 cm	28
3.2.6	FNS, C, 40 cm	30
3.2.7	FNS, N, 20 cm	32
3.2.8	FNS, O, 20 cm	34
3.2.9	FNS, Fe, 5 cm	36
3.2.10	FNS, Fe, 20 cm	38
3.2.11	FNS, Fe, 40 cm	40
3.2.12	FNS, Fe, 60 cm	42
3.2.13	FNS, Pb, 5 cm	44
3.2.14	FNS, Pb, 20 cm	46
3.2.15	FNS, Pb, 40 cm	48
3.3	LLNL Pulsed Spheres	50
3.3.1	LLNL Pulsed Spheres, ⁶ Li	50
3.3.2	LLNL Pulsed Spheres, ⁷ Li	51
3.3.3	LLNL Pulsed Spheres, Be	52
3.3.4	LLNL Pulsed Spheres, C	53
3.3.5	LLNL Pulsed Spheres, N	54

3.3.6	LLNL Pulsed Spheres, O	55
3.3.7	LLNL Pulsed Spheres, Mg	56
3.3.8	LLNL Pulsed Spheres, Al	57
3.3.9	LLNL Pulsed Spheres, Ti	58
3.3.10	LLNL Pulsed Spheres, Fe	59
3.3.11	LLNL Pulsed Spheres, Pb	60
3.3.12	LLNL Pulsed Spheres, D ₂ O	61
3.3.13	LLNL Pulsed Spheres, H ₂ O	62
3.3.14	LLNL Pulsed Spheres, Concrete	63
3.3.15	LLNL Pulsed Spheres, Polyethylene	64
3.3.16	LLNL Pulsed Spheres, Teflon	65
3.4	NIST Water Spheres	67
4	Summary	68
References		69

1. Introduction

On April 25, 2006 a new beta version of the ENDF/B-VII general purpose nuclear data library was released: ENDF/B-VII beta2. Over the last several years there has been a concerted effort by many people to bring the quality of this nuclear data library to a new, higher level.

In this report, the results of many shielding benchmark runs are presented.

All results reported in this report were obtained by use of the Monte Carlo neutronics code MCNP, version 4C3 [1].

2. Brief description of the shielding benchmarks

2.1 Oktavian

The Oktavian benchmark specifications are given on the IAEA web site [3]. The measured quantity

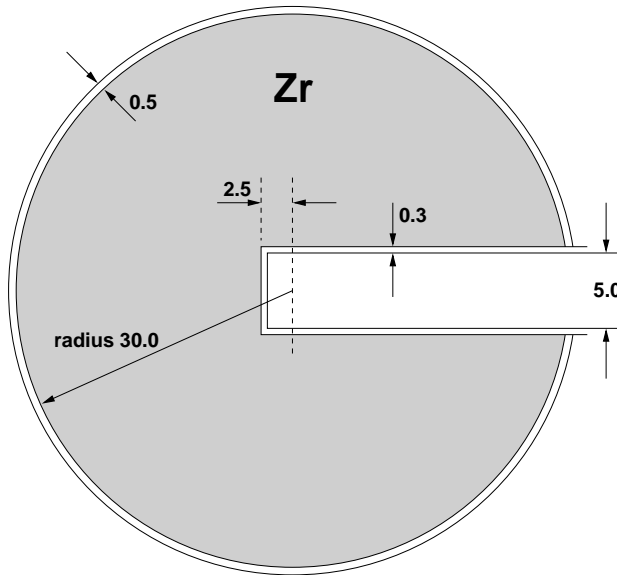


Figure 2.1 Schematic drawing of the Oktavian geometry for the Zr benchmark (not to scale). All dimensions are in cm.

was the leakage current spectrum from the outer surface of a spherical pile of a material. At the center of a pile a 14 MeV D-T neutron source was located. The leakage spectrum is given in units of neutrons per MeV per source neutron.

The materials for which benchmark calculations have been performed are listed in Table 2.1. A schematic drawing of one of the models is given in Fig. 2.1 (see Ref. [4]).

material		outer diameter
aluminum	Al	40 cm
cobalt	Co	40 cm
chromium	Cr	40 cm
copper	Cu	61 cm
lithium fluoride	LiF	61 cm
molybdenum	Mo	61 cm
manganese	Mn	61 cm
silicon	Si	60 cm
titanium	Ti	40 cm
tungsten	W	40 cm
zirconium	Zr	61 cm

Table 2.1 The materials used in the Oktavian shielding benchmarks

2.2 FNS

The FNS Time-of-Flight benchmark specifications are given on the IAEA web site [5]. The neu-

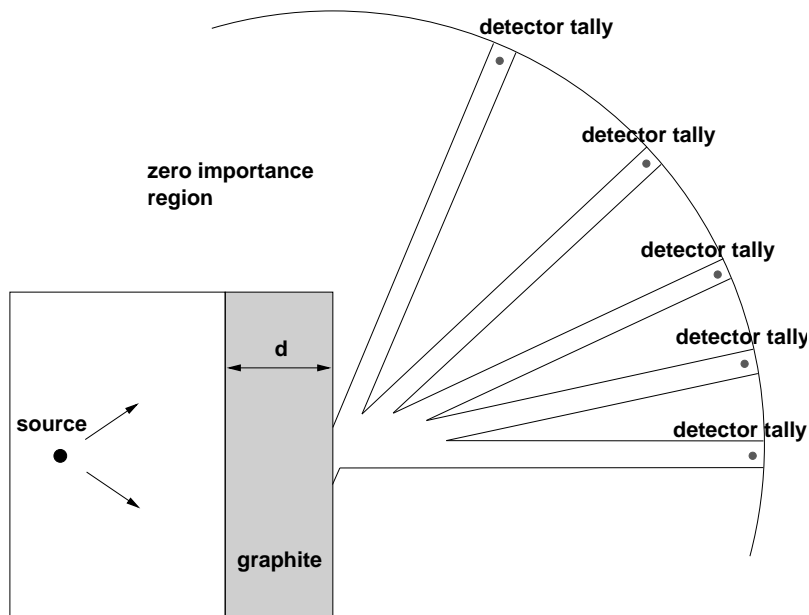


Figure 2.2 Schematic drawing of the MCNP model for the FNS benchmark for graphite (not to scale).

tron spectrum emerging from slabs of material of varying thickness, was measured at five different angles. The slabs were placed at 20 cm distance from a 14 MeV D-T neutron source. The materials for which benchmark calculations have been performed are listed in Table 2.2. A schematic drawing of the MCNP model for this benchmark is given in Fig. 2.2 [6].

material		slab thickness	angles
beryllium	Be	5 cm	0°, 24.9°, 42.8°, 66.8°
		15 cm	0°, 12.2°, 24.9°, 42.8°, 66.8°
graphite	C	5 cm	0°, 24.9°, 42.8°, 66.8°
		20 cm	0°, 12.2°, 24.9°, 42.8°, 66.8°
		40 cm	0°, 12.2°, 24.9°, 42.8°, 66.8°
nitrogen	N	20 cm	0°, 12.2°, 24.9°, 42.8°, 66.8°
oxygen	O	20 cm	0°, 12.2°, 24.9°, 42.8°, 66.8°
iron	Fe	5 cm	0°, 24.9°, 42.8°, 66.8°
		20 cm	0°, 12.2°, 24.9°, 42.8°, 66.8°
		40 cm	0°, 12.2°, 24.9°, 42.8°, 66.8°
		60 cm	0°, 12.2°, 24.9°, 42.8°
lead	Pb	5 cm	0°, 24.9°, 42.8°, 66.8°
		20 cm	0°, 12.2°, 24.9°, 42.8°, 66.8°
		40 cm	0°, 12.2°, 24.9°, 42.8°, 66.8°

Table 2.2 The materials used in the FNS shielding benchmarks

2.3 LLNL Pulsed Spheres

The description of the experiments performed in the Livermore Pulsed Sphere Program is given in Ref. [7]. Time-of-flight measurements were performed for neutrons passing through spherical shells of varying thickness, containing different materials. The source was a 14 MeV D-T neutron source.

material	thickness [mfp]
⁶ Li	0.5, 1.1, 1.6
⁷ Li	0.5, 1.1, 1.6
Be	0.8
C	0.5, 1.3, 2.9
N	1.1, 3.1
O	0.7
Mg	0.7, 1.2, 1.9
Al	0.9, 1.6, 2.6
Ti	1.2, 2.2, 3.5
Fe	0.9, 2.9, 4.8
Pb	1.4
D ₂ O	1.2, 2.1
H ₂ O	1.1, 1.9
Concrete	2.0, 3.8
Polyethylene	0.8, 1.8, 3.5
Teflon	1.8, 2.9

Table 2.3 The materials used in the LLNL pulsed sphere benchmarks. The thickness of the material is given in units of the mean free path.

Calculations were performed for many cases, see Table 2.3. The geometry of the sample materials for these cases varies; one for concrete is depicted schematically in Fig. 2.3. The composition of the concrete is given in Table 2.4; the density of the concrete was 2.35 g/cm³. The MCNP model used in the present work was taken over from Ref. [8].

Material	at%
O	55.7
H	15.1
Si	14.9
Ca	3.6
Al	3.2
C	3.1
Mg	1.8
Na	1.3
other	< 1.0 each

Table 2.4 The composition of the concrete used in the LLNL Pulsed Sphere experiments.

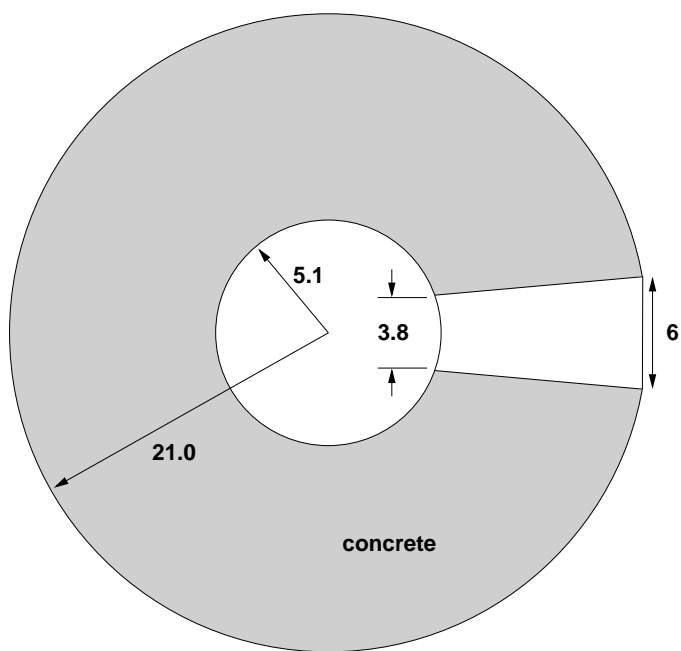


Figure 2.3 Schematic drawing of the MCNP model for the LLNL benchmark for concrete (not to scale). All dimensions are in cm.

2.4 NIST Water Spheres

A description of the experiments performed at NIST with water and cadmium shielding is given in Ref. [10]. A Cf source was placed at the center of the experiment, and fission foils were placed at two, diametrically opposed positions. Between the source and the fission foils were several combinations of shielding materials, see Table 2.5. The fission foils used were ^{235}U , ^{239}Pu , ^{238}U , ^{237}Np .

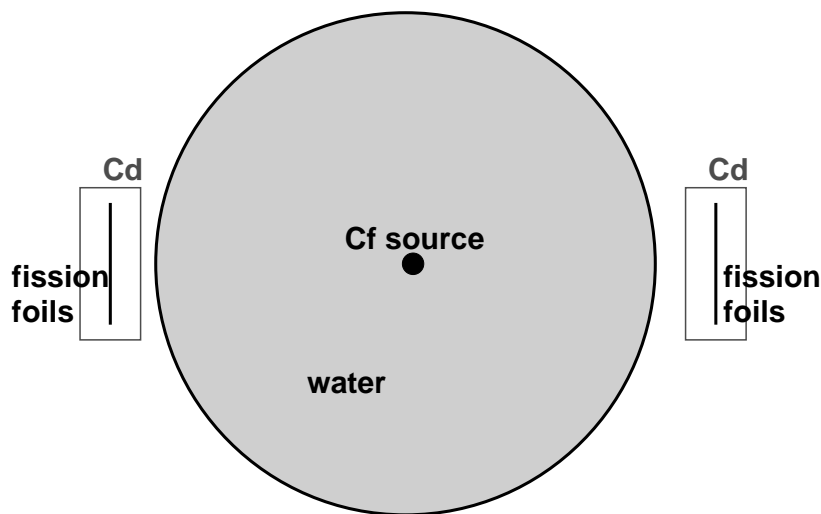


Figure 2.4 Schematic drawing of the MCNP model for the NIST benchmark (not to scale).

radius (inch)	material
1.5	—
2.0	—
1.5	Cd
2.0	Cd
1.5	H_2O
2.0	H_2O
2.5	H_2O
1.5	$\text{H}_2\text{O}+\text{Cd}$
2.0	$\text{H}_2\text{O}+\text{Cd}$
2.5	$\text{H}_2\text{O}+\text{Cd}$

Table 2.5 The radius and material combinations for which experiments have been performed.

3. Results

In this section we report on the results of our calculations. These results are reported as graphs of the neutron spectra, and in some cases also the photon spectrum, as well as in graphs and tables of calculated over experimental values of the neutron spectra.

3.1 Oktavian

3.1.1 Oktavian, Al

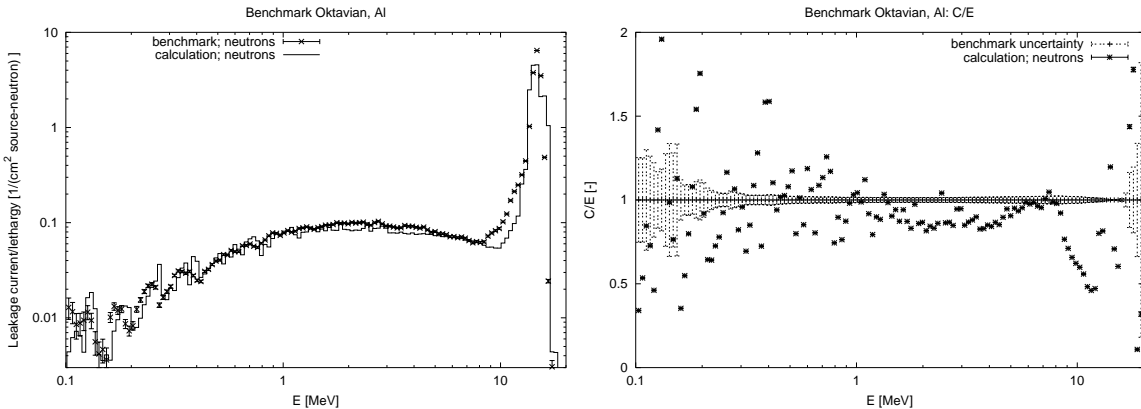


Figure 3.1 The result for the neutron leakage spectrum for the Oktavian Al benchmark.

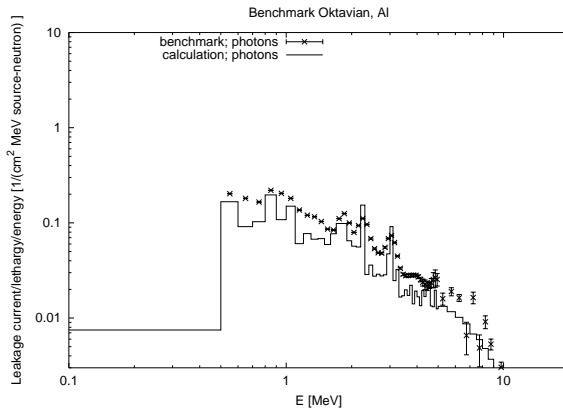


Figure 3.2 The result for the photon leakage spectrum for the Oktavian Al benchmark.

	energy range	C/E
Al	0.1– 1.0	1.00 ± 0.01
Al	1.0– 5.0	0.90 ± 0.01
Al	5.0– 10.0	0.92 ± 0.01
Al	10.0– 20.0	1.06 ± 0.01

Table 3.1 C/E values for the neutron spectrum of the Oktavian Al benchmark.

3.1.2 Oktavian, Co

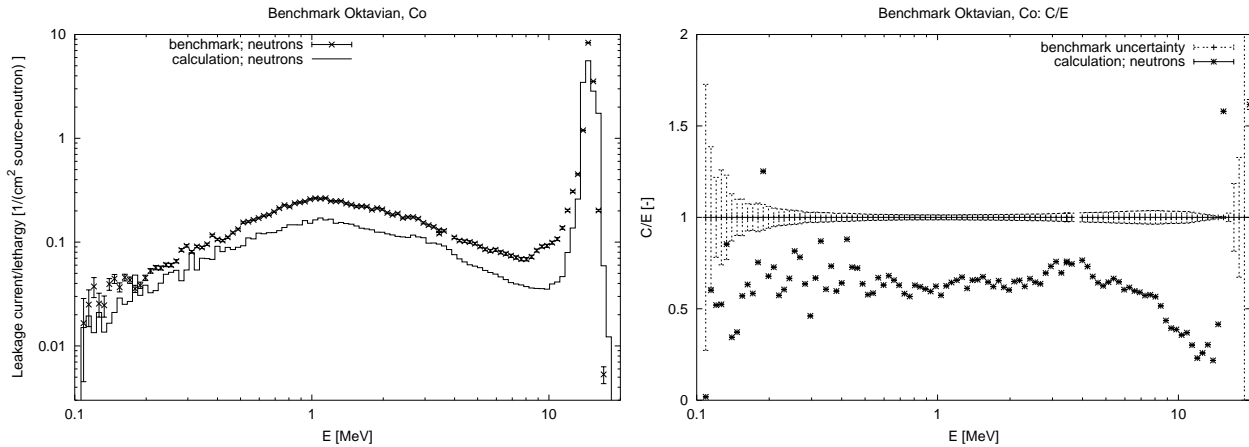


Figure 3.3 The result for the neutron leakage spectrum for the Oktavian Co benchmark.

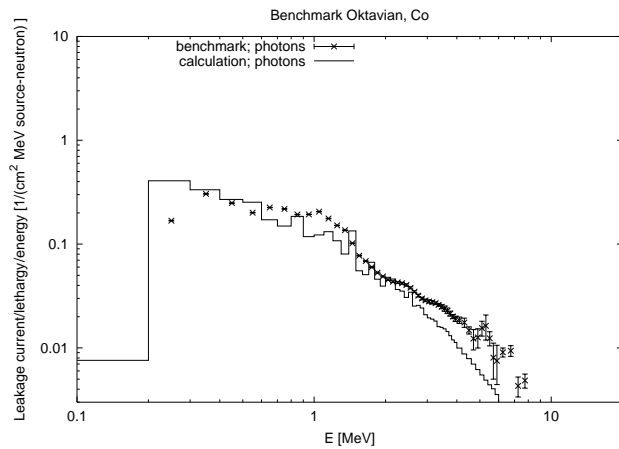


Figure 3.4 The result for the photon leakage spectrum for the Oktavian Co benchmark.

	energy range		C/E
Co	0.1–	1.0	0.64 ± 0.01
Co	1.0–	5.0	0.66 ± 0.01
Co	5.0–	10.0	0.55 ± 0.01
Co	10.0–	20.0	0.98 ± 0.01

Table 3.2 C/E values for the neutron spectrum of the Oktavian Co benchmark.

3.1.3 Oktavian, Cr

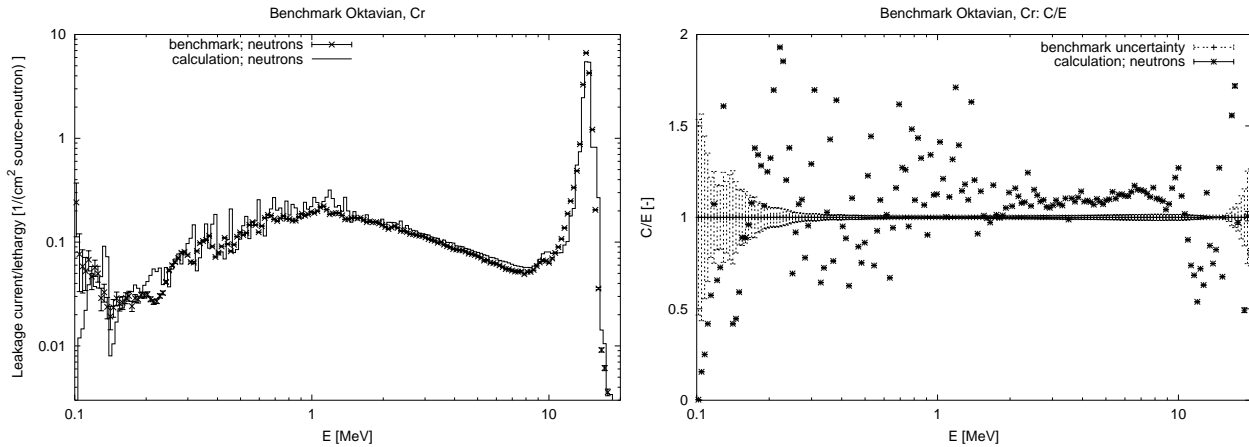


Figure 3.5 The result for the neutron leakage spectrum for the Oktavian Cr benchmark.

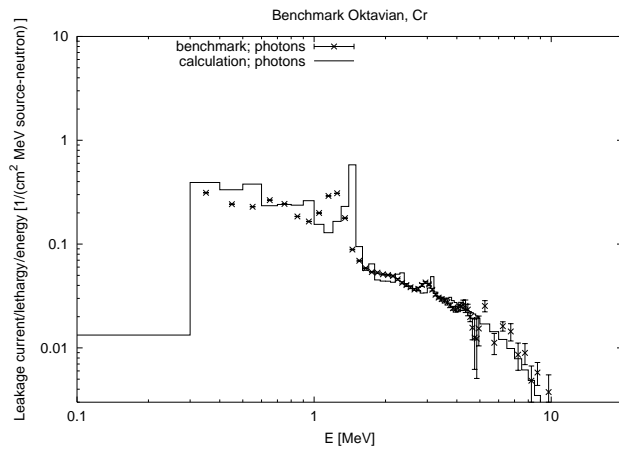


Figure 3.6 The result for the photon leakage spectrum for the Oktavian Cr benchmark.

	energy range	C/E
Cr	0.1– 1.0	1.10 ± 0.02
Cr	1.0– 5.0	1.14 ± 0.01
Cr	5.0– 10.0	1.12 ± 0.01
Cr	10.0– 20.0	0.96 ± 0.01

Table 3.3 C/E values for the neutron spectrum of the Oktavian Cr benchmark.

3.1.4 Oktavian, Cu

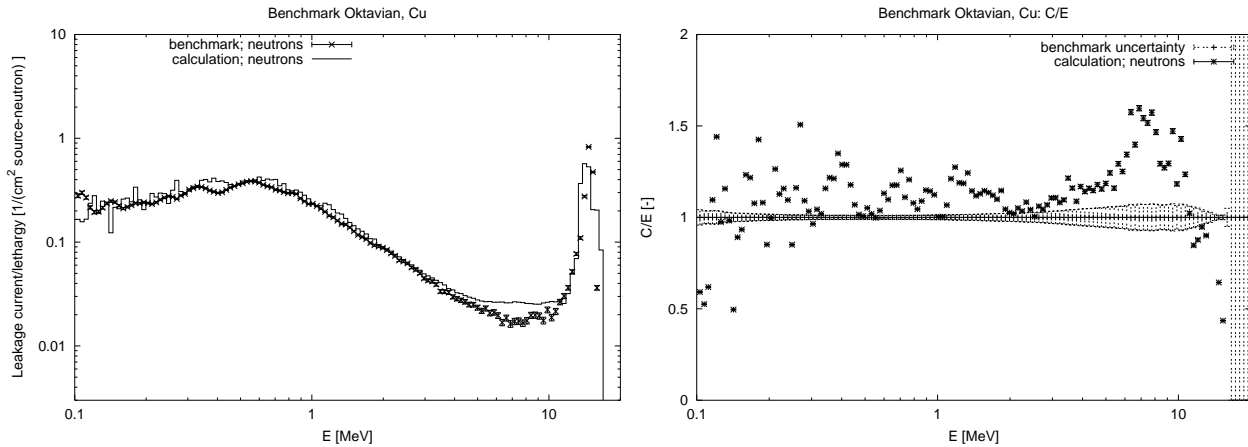


Figure 3.7 The result for the neutron leakage spectrum for the Oktavian Cu benchmark.

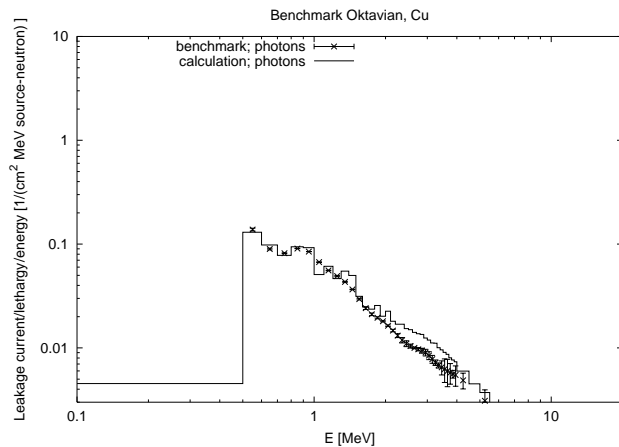


Figure 3.8 The result for the photon leakage spectrum for the Oktavian Cu benchmark.

	energy range	C/E
Cu	0.1– 1.0	1.07 ± 0.01
Cu	1.0– 5.0	1.11 ± 0.01
Cu	5.0– 10.0	1.37 ± 0.02
Cu	10.0– 20.0	1.12 ± 0.01

Table 3.4 C/E values for the neutron spectrum of the Oktavian Cu benchmark.

3.1.5 Oktavian, LiF

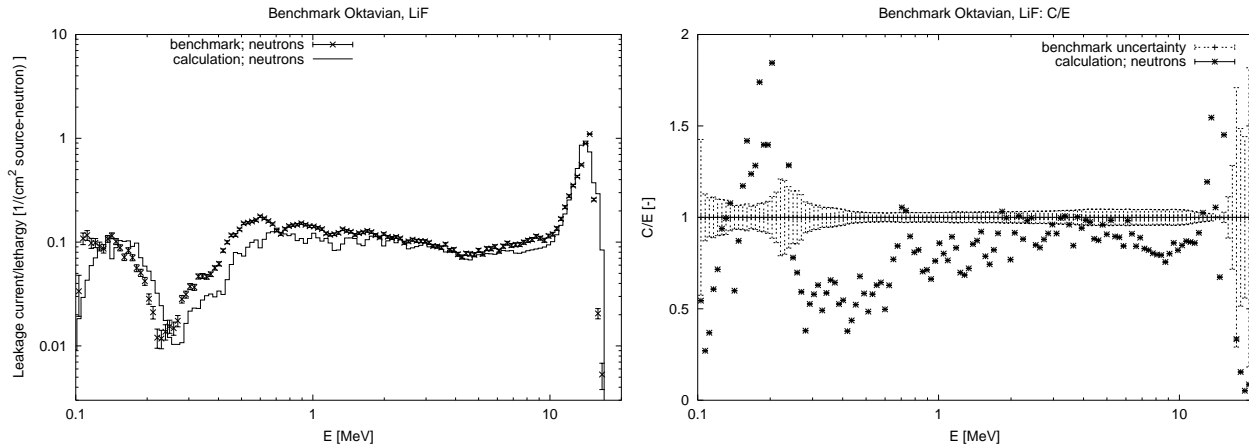


Figure 3.9 The result for the neutron leakage spectrum for the Oktavian LiF benchmark.

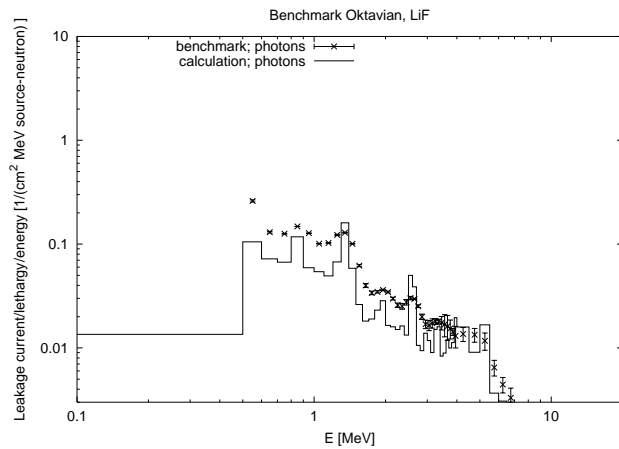


Figure 3.10 The result for the photon leakage spectrum for the Oktavian LiF benchmark.

	energy range	C/E
LiF	0.1 – 1.0	0.76 ± 0.01
LiF	1.0 – 5.0	0.88 ± 0.01
LiF	5.0 – 10.0	0.85 ± 0.01
LiF	10.0 – 20.0	1.09 ± 0.01

Table 3.5 C/E values for the neutron spectrum of the Oktavian LiF benchmark.

3.1.6 Oktavian, Mn

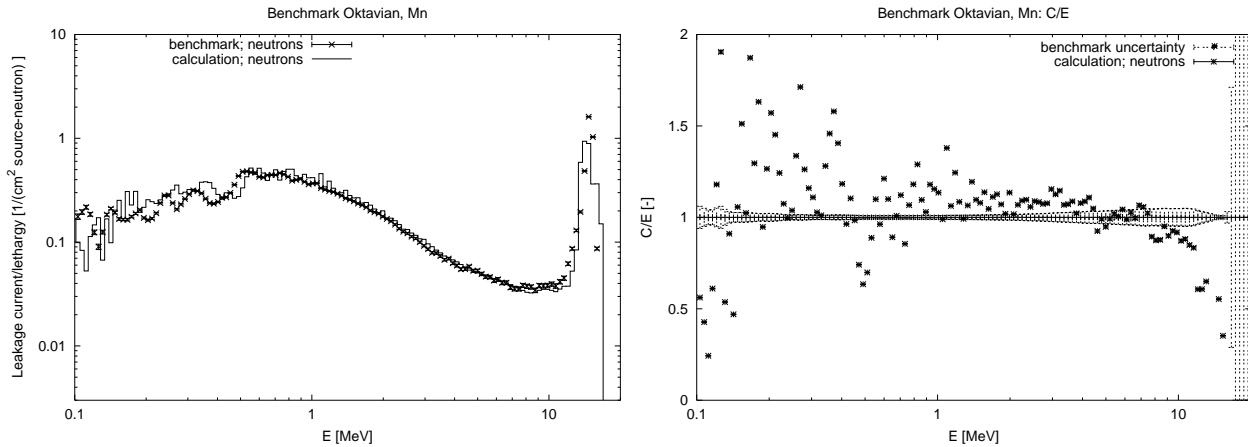


Figure 3.11 The result for the neutron leakage spectrum for the Oktavian Mn benchmark.

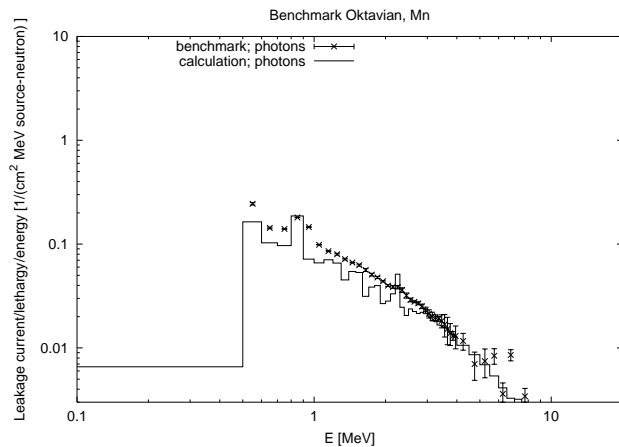


Figure 3.12 The result for the photon leakage spectrum for the Oktavian Mn benchmark.

	energy range	C/E
Mn	0.1– 1.0	1.06 ± 0.01
Mn	1.0– 5.0	1.10 ± 0.01
Mn	5.0– 10.0	0.98 ± 0.01
Mn	10.0– 20.0	0.94 ± 0.01

Table 3.6 C/E values for the neutron spectrum of the Oktavian Mn benchmark.

3.1.7 Oktavian, Mo

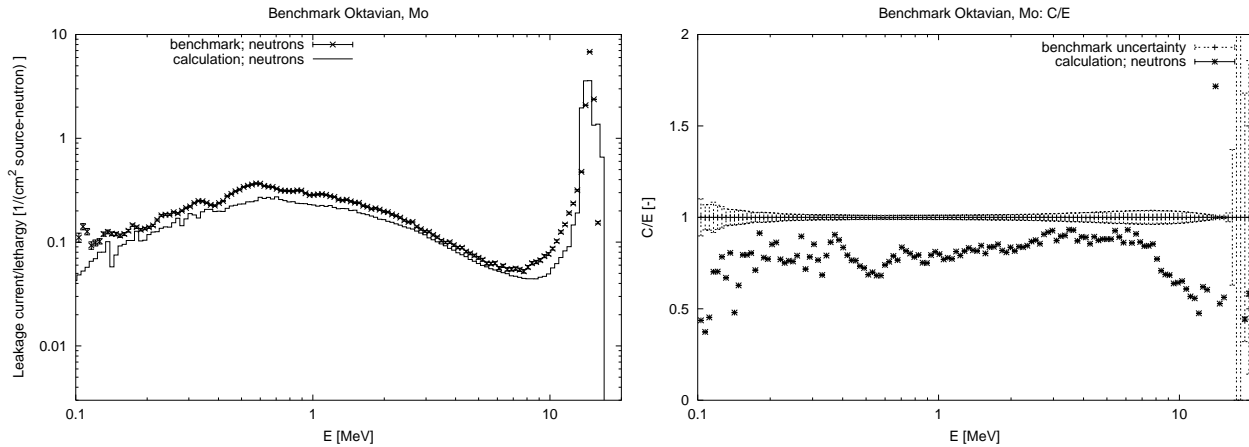


Figure 3.13 The result for the neutron leakage spectrum for the Oktavian Mo benchmark.

	energy range		C/E
Mo	0.1–	1.0	0.76 ± 0.01
Mo	1.0–	5.0	0.84 ± 0.01
Mo	5.0–	10.0	0.82 ± 0.01
Mo	10.0–	20.0	1.01 ± 0.01

Table 3.7 C/E values for the neutron spectrum of the Oktavian Mo benchmark.

3.1.8 Oktavian, Si

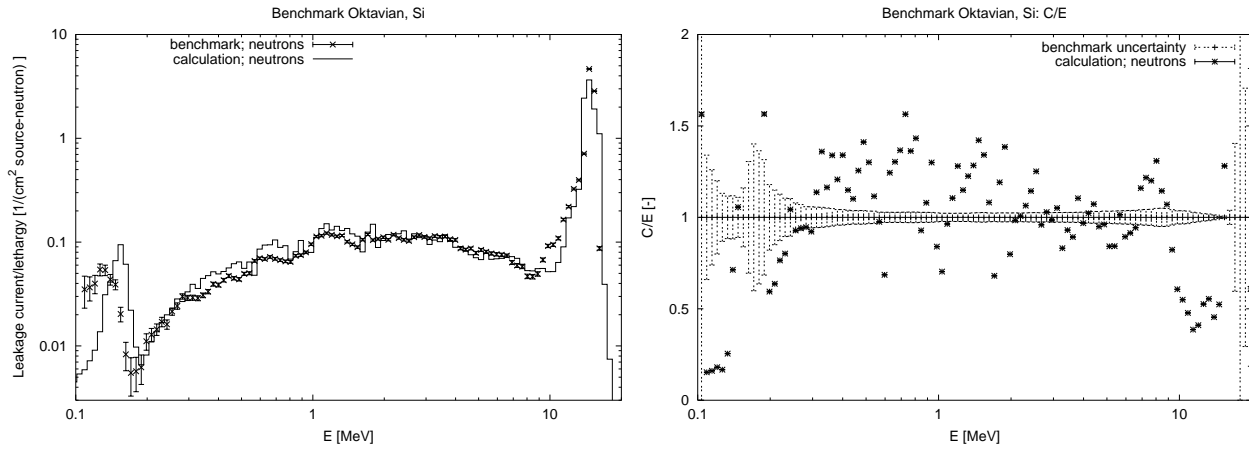


Figure 3.14 The result for the neutron leakage spectrum for the Oktavian Si benchmark.

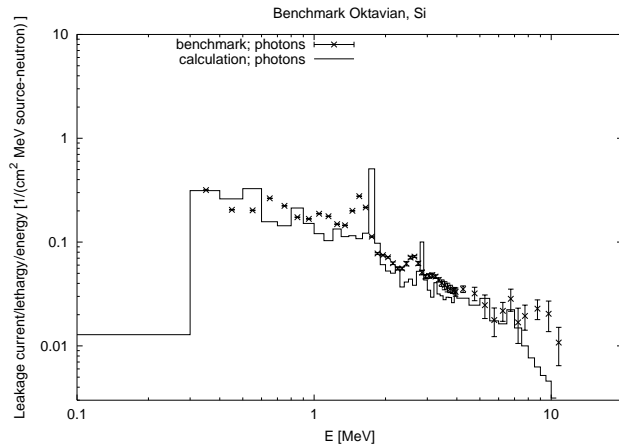


Figure 3.15 The result for the photon leakage spectrum for the Oktavian Si benchmark.

	energy range	C/E
Si	0.1– 1.0	1.13 ± 0.02
Si	1.0– 5.0	1.05 ± 0.01
Si	5.0– 10.0	0.98 ± 0.01
Si	10.0– 20.0	1.05 ± 0.01

Table 3.8 C/E values for the neutron spectrum of the Oktavian Si benchmark.

3.1.9 Oktavian, Ti

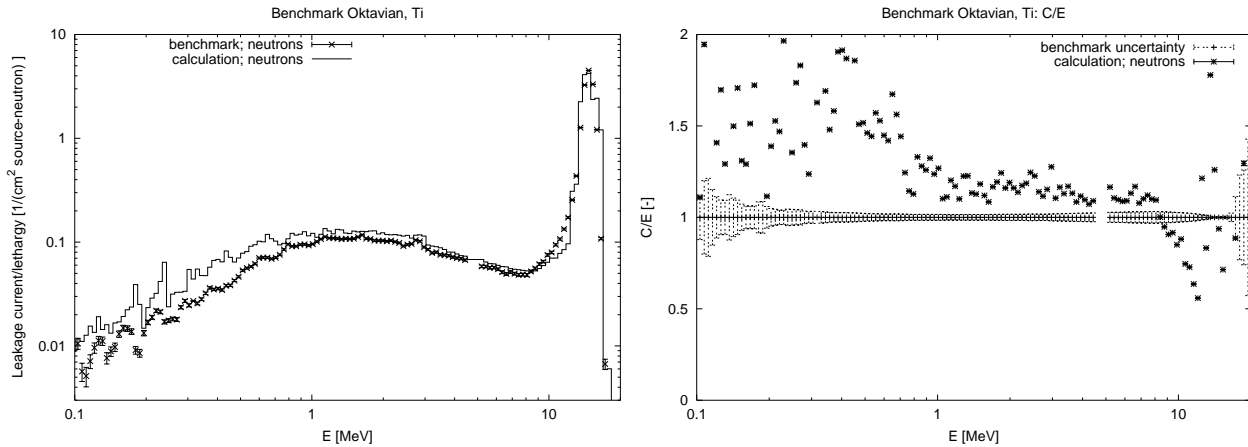


Figure 3.16 The result for the neutron leakage spectrum for the Oktavian Ti benchmark.

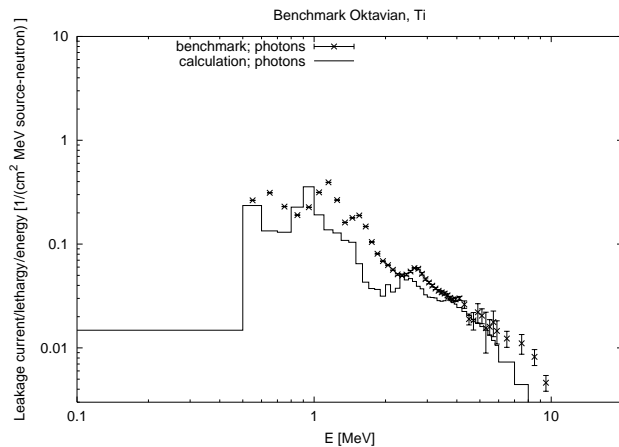


Figure 3.17 The result for the photon leakage spectrum for the Oktavian Ti benchmark.

	energy range	C/E
Ti	0.0– 0.1	1.16 ± 0.11
Ti	0.1– 1.0	1.51 ± 0.01
Ti	1.0– 5.0	1.16 ± 0.01
Ti	5.0– 10.0	1.07 ± 0.01
Ti	10.0– 20.0	1.18 ± 0.01

Table 3.9 C/E values for the neutron spectrum of the Oktavian Ti benchmark.

3.1.10 Oktavian, W

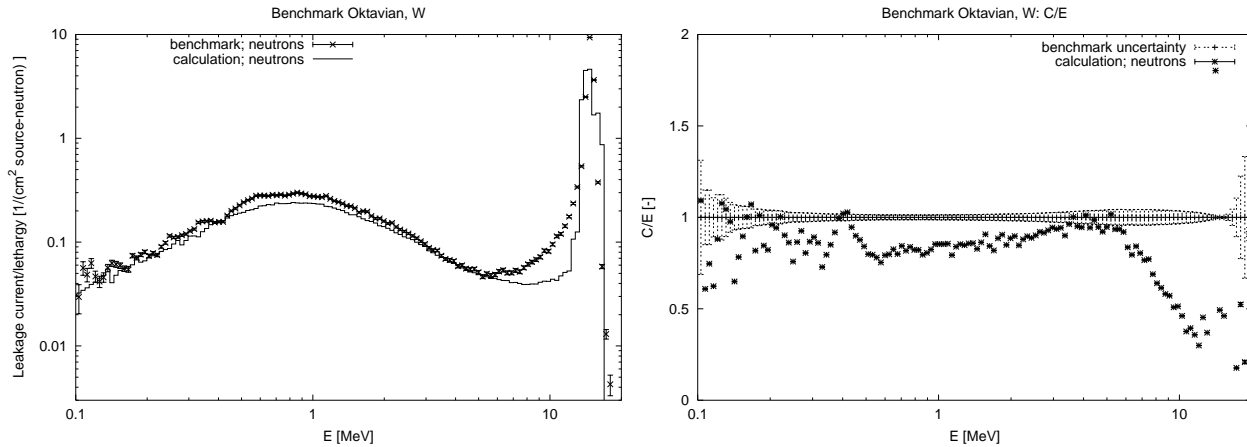


Figure 3.18 The result for the neutron leakage spectrum for the Oktavian W benchmark.

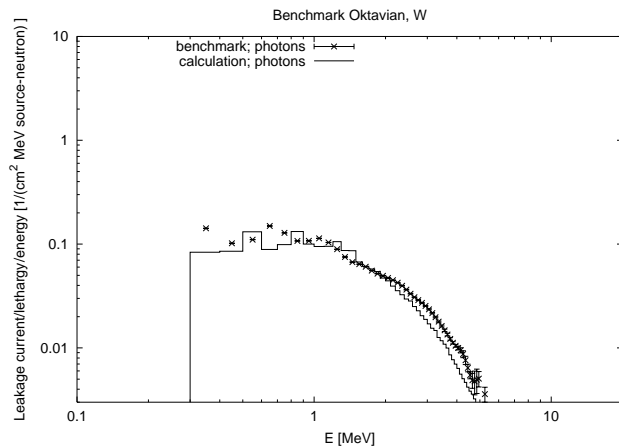


Figure 3.19 The result for the photon leakage spectrum for the Oktavian W benchmark.

	energy range	C/E
W	0.1— 1.0	0.85 ± 0.01
W	1.0— 5.0	0.88 ± 0.01
W	5.0— 10.0	0.75 ± 0.01
W	10.0— 20.0	0.91 ± 0.01

Table 3.10 C/E values for the neutron spectrum of the Oktavian W benchmark.

3.1.11 Oktavian, Zr

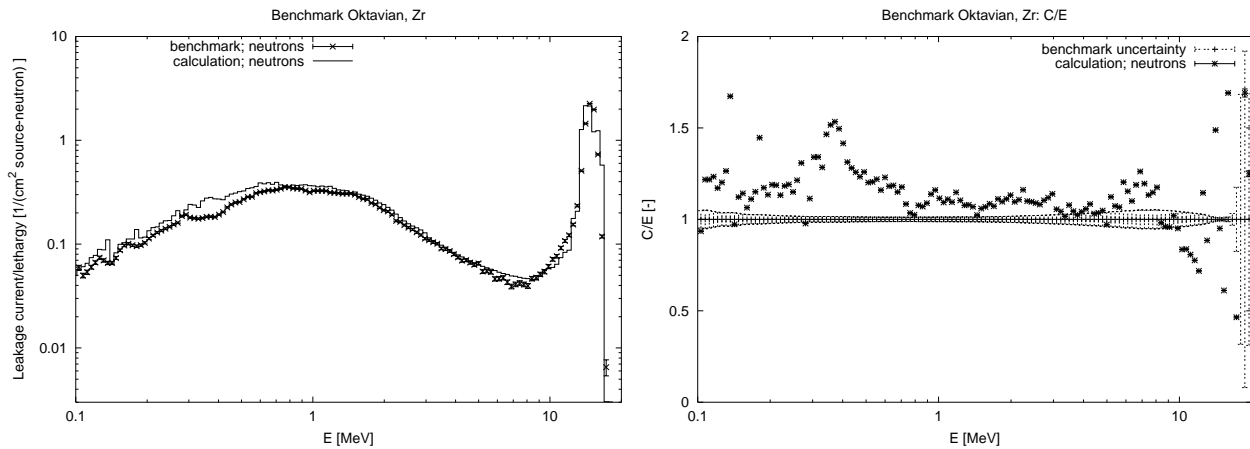


Figure 3.20 The result for the neutron leakage spectrum for the Oktavian Zr benchmark.

	energy range		C/E
Zr	0.0–	0.1	0.88 ± 0.04
Zr	0.1–	1.0	1.20 ± 0.01
Zr	1.0–	5.0	1.09 ± 0.01
Zr	5.0–	10.0	1.09 ± 0.01
Zr	10.0–	20.0	1.18 ± 0.01

Table 3.11 C/E values for the neutron spectrum of the Oktavian Zr benchmark.

3.2 FNS

3.2.1 Calculational methods

For each of the experiments mentioned in Section 2 the neutron source spectrum was taken from the underlying reference. Hence, in Oktavian and FNS analyses an isotropic neutron distribution was assumed. However, it is known that the neutron source has a peak energy of 14.8 MeV in the forward direction, and a peak at 13.3 MeV in the backward direction (see Ref. [9]).

The assumption of isotropy will slightly influence the calculated angular spectra for the FNS benchmarks. This influence is expected to be of the order of several percent only.

3.2.2 FNS, Be, 5 cm

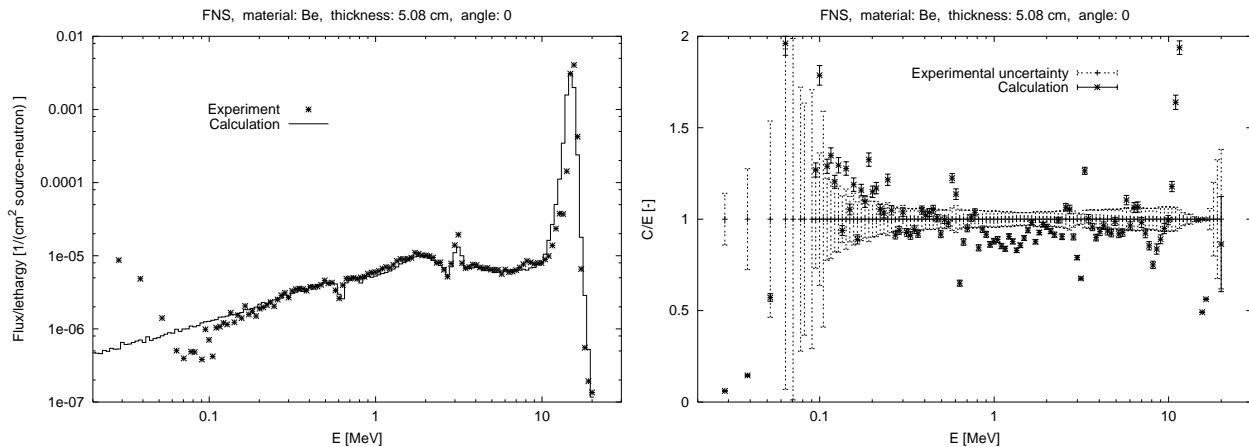


Figure 3.21 Neutron spectrum for the FNS, Be, $d=5\text{cm}$ benchmark at 0° angle.

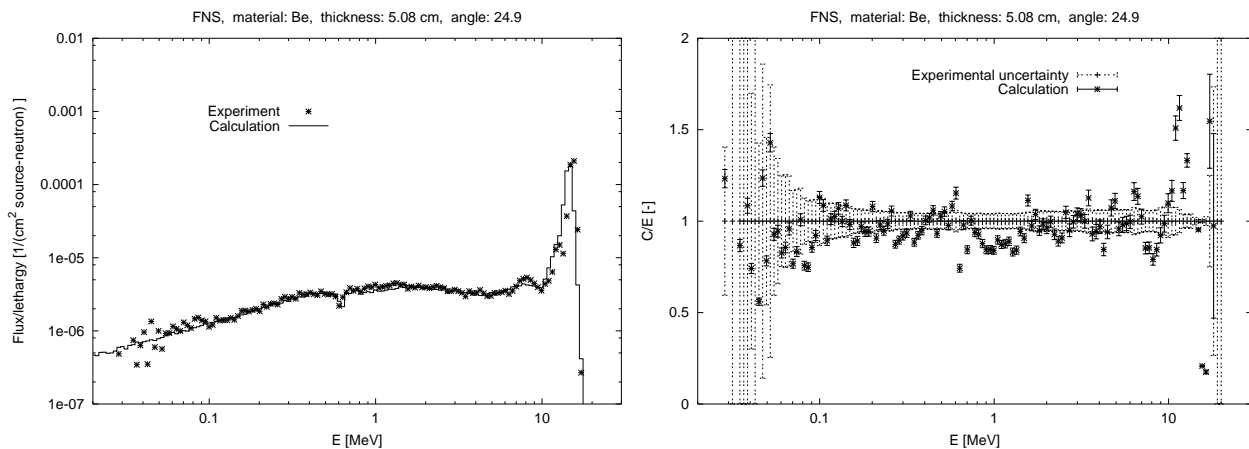


Figure 3.22 Neutron spectrum for the FNS, Be, $d=5\text{cm}$ benchmark at 24.9° angle.

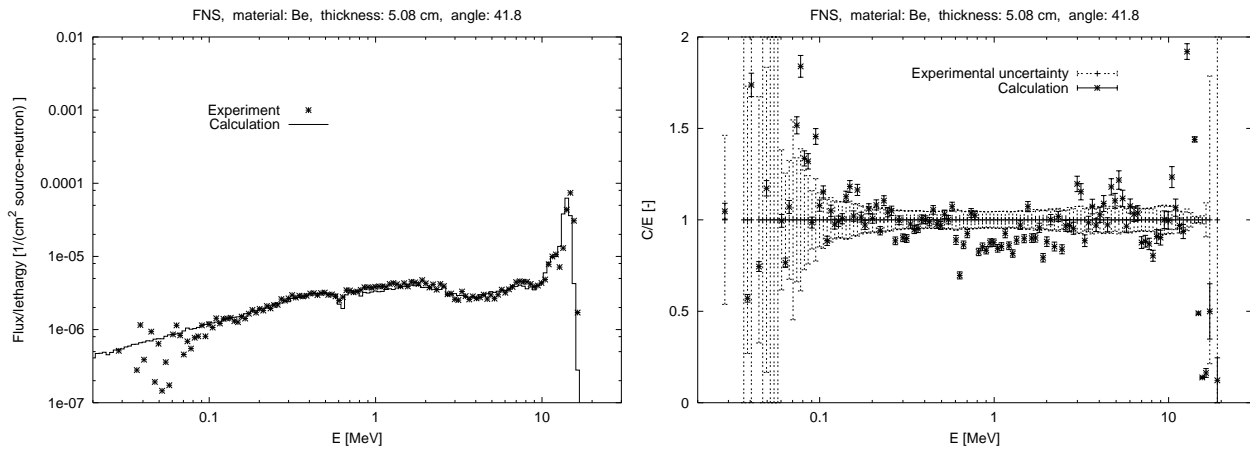


Figure 3.23 Neutron spectrum for the FNS, Be, $d=5\text{cm}$ benchmark at 42.8° angle.

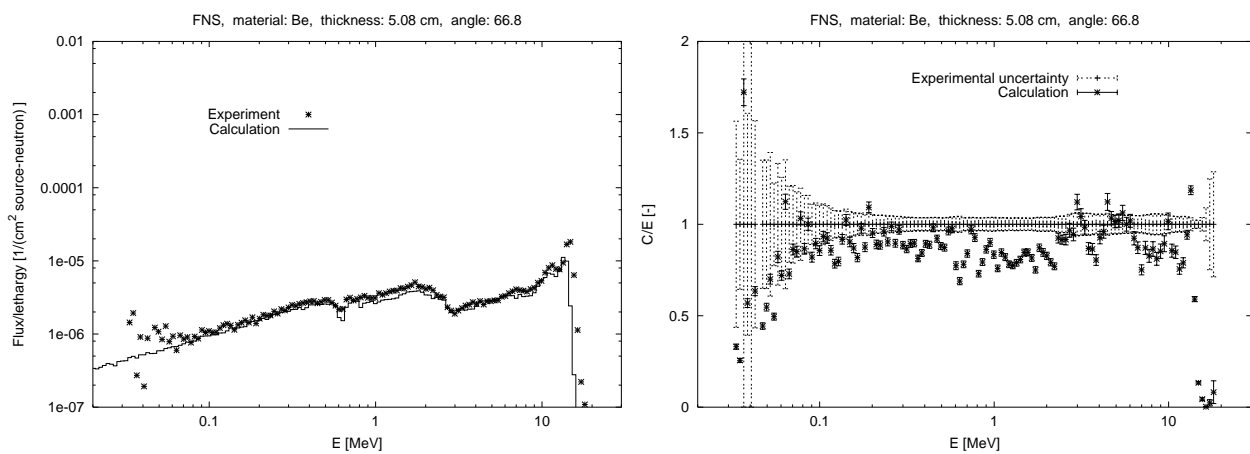


Figure 3.24 Neutron spectrum for the FNS, Be, $d=5\text{cm}$ benchmark at 66.8° angle.

energy range		0°	12.2°	24.9°	42.8°	66.8°
0.1—	1.0	0.97 ± 0.01		0.93 ± 0.01	0.95 ± 0.01	0.87 ± 0.01
1.0—	5.0	0.91 ± 0.01		0.96 ± 0.01	0.95 ± 0.01	0.86 ± 0.01
5.0—	10.0	0.92 ± 0.01		0.94 ± 0.01	0.94 ± 0.01	0.86 ± 0.01
10.0—	20.0	0.95 ± 0.01		0.96 ± 0.01	0.95 ± 0.01	0.68 ± 0.01

Table 3.12 C/E values for the neutron spectrum of the FNS Be 5cm benchmark.

3.2.3 FNS, Be, 15 cm

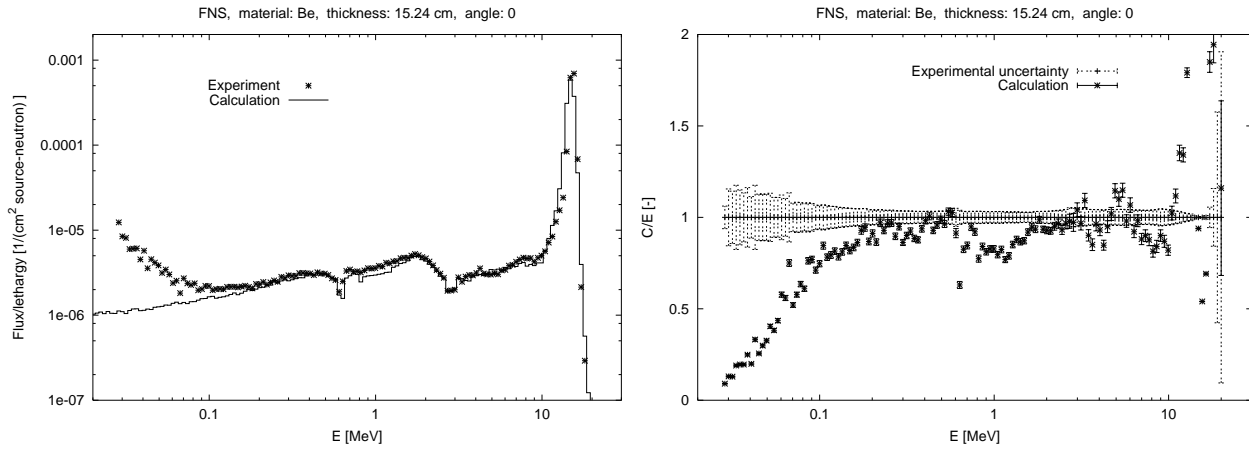


Figure 3.25 Neutron spectrum for the FNS, Be, $d=15\text{cm}$ benchmark at 0° angle.

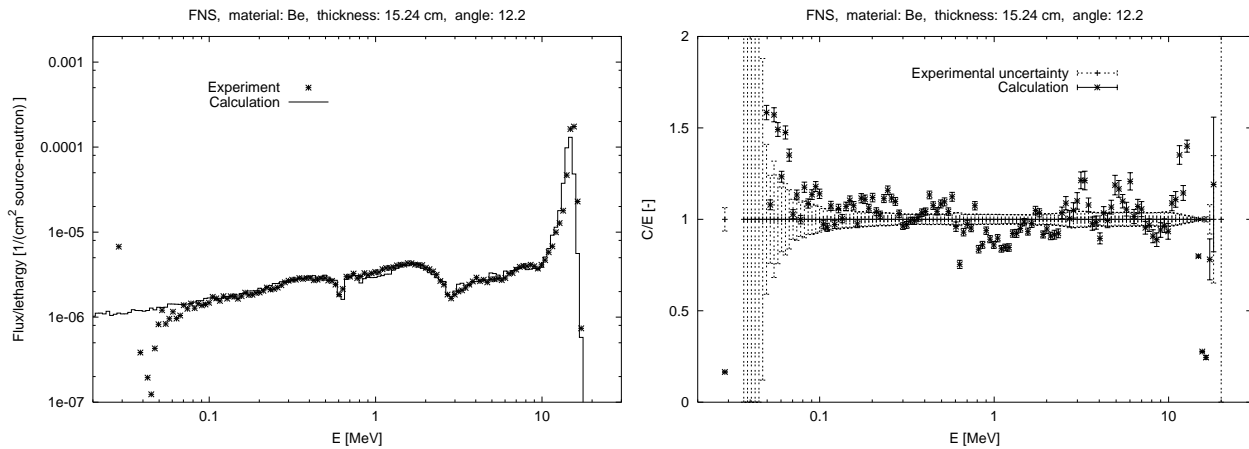


Figure 3.26 Neutron spectrum for the FNS, Be, $d=15\text{cm}$ benchmark at 12.2° angle.

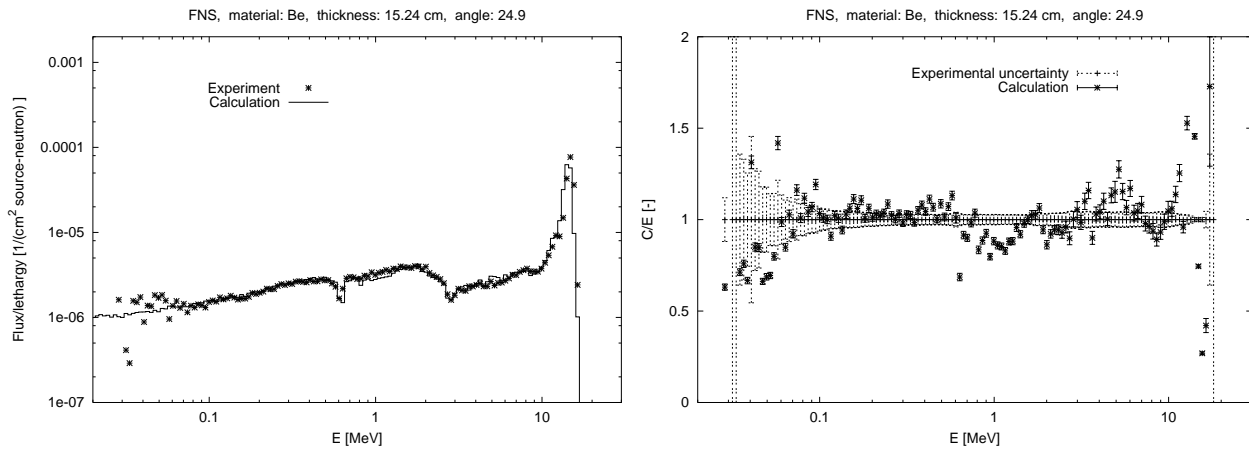


Figure 3.27 Neutron spectrum for the FNS, Be, $d=15\text{cm}$ benchmark at 24.9° angle.

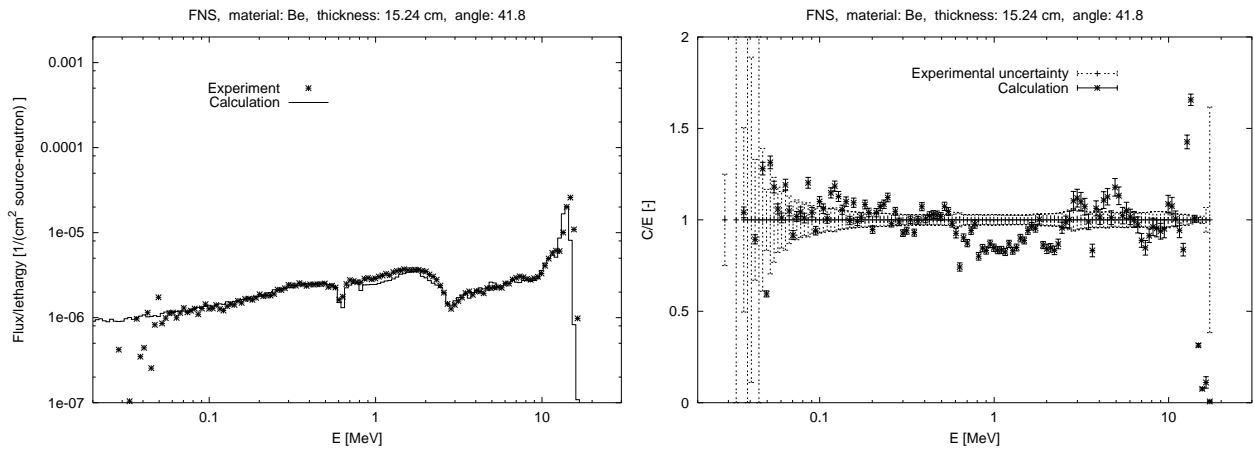


Figure 3.28 Neutron spectrum for the FNS, Be, $d=15\text{cm}$ benchmark at 42.8° angle.

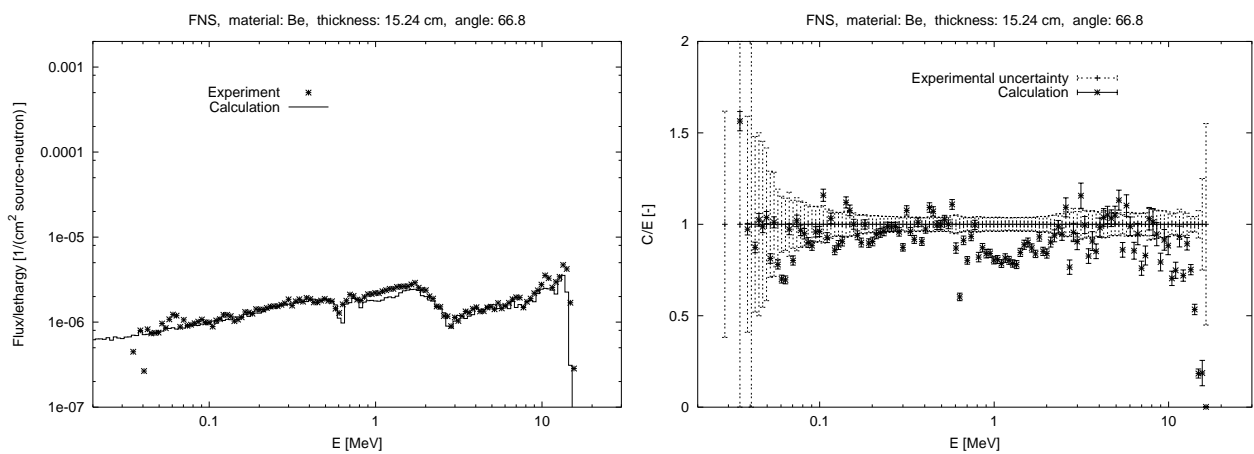


Figure 3.29 Neutron spectrum for the FNS, Be, $d=15\text{cm}$ benchmark at 66.8° angle.

energy range	0°	12.2°	24.9°	42.8°	66.8°	
0.1–	1.0	0.88 ± 0.01	1.00 ± 0.01	0.98 ± 0.01	0.97 ± 0.01	0.93 ± 0.01
1.0–	5.0	0.92 ± 0.01	0.97 ± 0.01	0.97 ± 0.01	0.93 ± 0.01	0.89 ± 0.01
5.0–	10.0	0.91 ± 0.01	0.99 ± 0.01	1.01 ± 0.01	0.95 ± 0.01	0.89 ± 0.02
10.0–	20.0	0.96 ± 0.01	0.80 ± 0.01	1.00 ± 0.01	0.82 ± 0.01	0.79 ± 0.02

Table 3.13 C/E values for the neutron spectrum of the FNS Be 15cm benchmark.

3.2.4 FNS, C, 5 cm

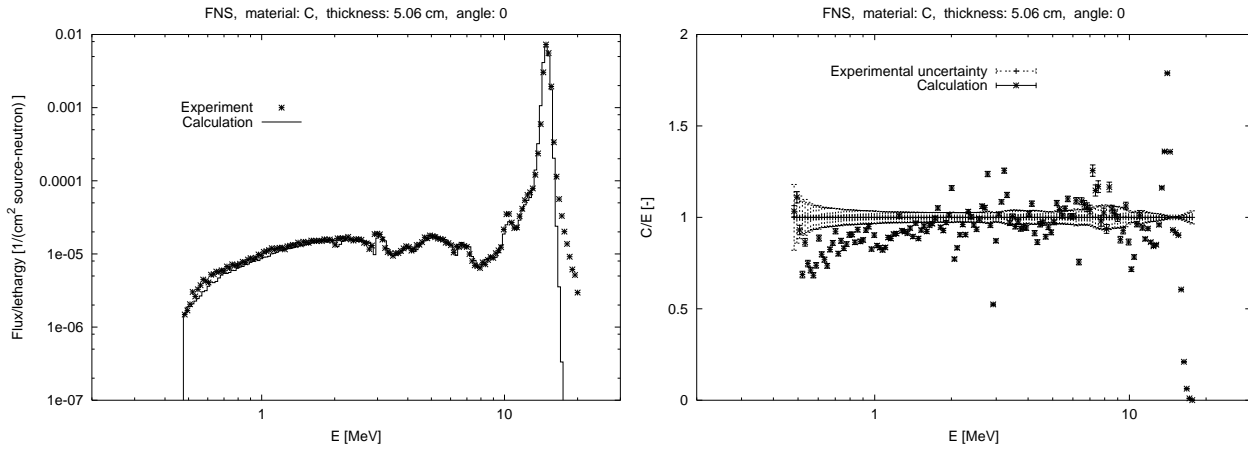


Figure 3.30 Neutron spectrum for the FNS, C, $d=5\text{cm}$ benchmark at 0° angle.

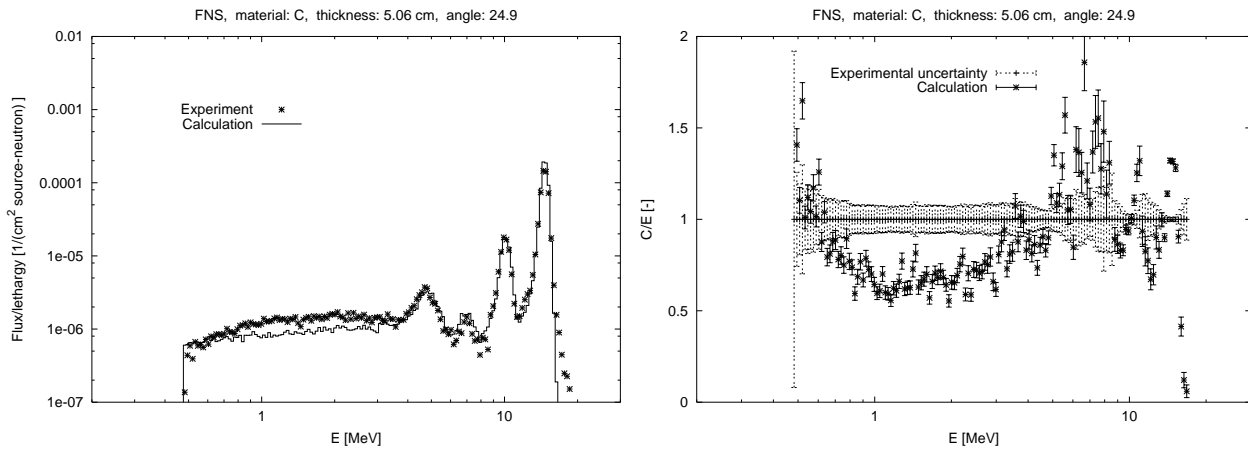


Figure 3.31 Neutron spectrum for the FNS, C, $d=5\text{cm}$ benchmark at 24.9° angle.

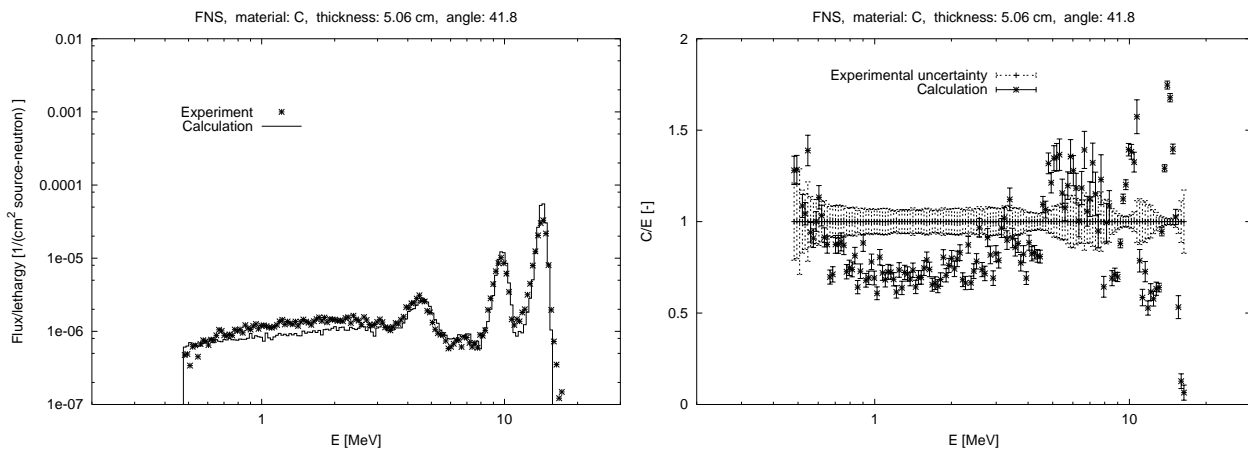


Figure 3.32 Neutron spectrum for the FNS, C, $d=5\text{cm}$ benchmark at 42.8° angle.

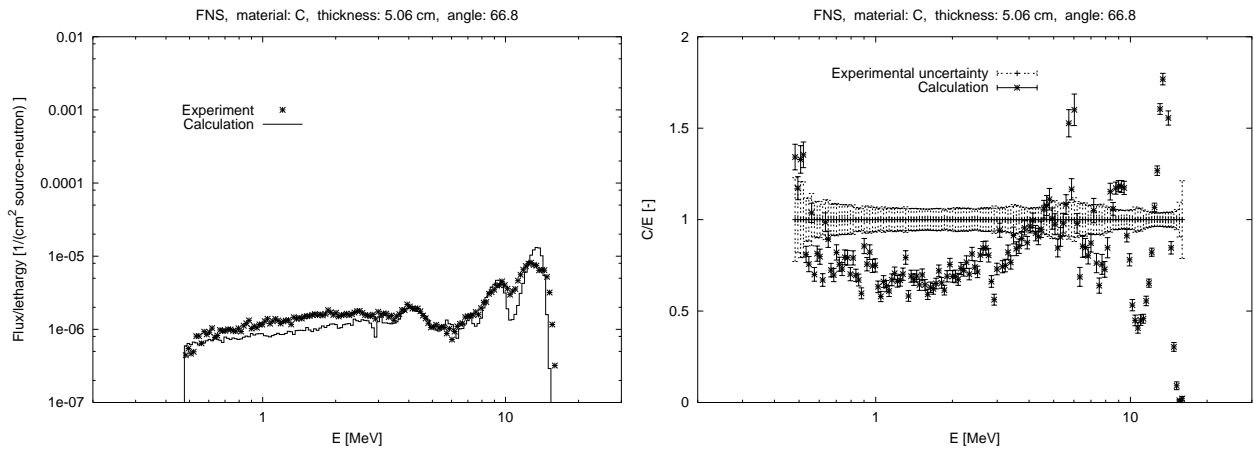


Figure 3.33 Neutron spectrum for the FNS, C, d=5cm benchmark at 66.8° angle.

energy range	0°	12.2°	24.9°	42.8°	66.8°
0.1— 1.0	0.81 ± 0.01		0.84 ± 0.01	0.83 ± 0.01	0.77 ± 0.01
1.0— 5.0	0.94 ± 0.01		0.73 ± 0.01	0.79 ± 0.01	0.76 ± 0.01
5.0— 10.0	1.01 ± 0.01		0.83 ± 0.01	0.93 ± 0.01	0.95 ± 0.01
10.0— 20.0	1.01 ± 0.01		1.23 ± 0.01	1.39 ± 0.01	1.01 ± 0.01

Table 3.14 C/E values for the neutron spectrum of the FNS C 5cm benchmark.

3.2.5 FNS, C, 20 cm

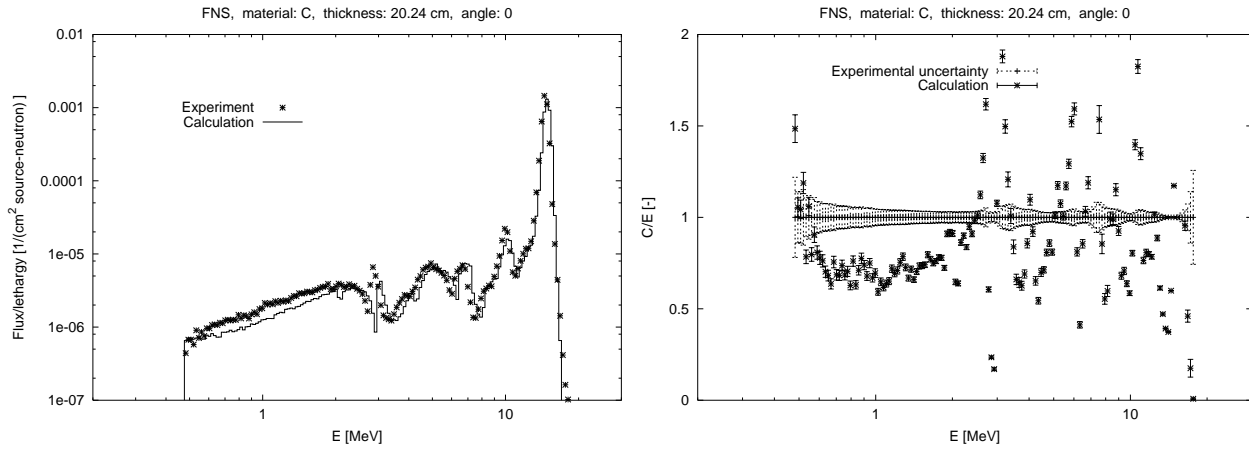


Figure 3.34 Neutron spectrum for the FNS, C, $d=20\text{cm}$ benchmark at 0° angle.

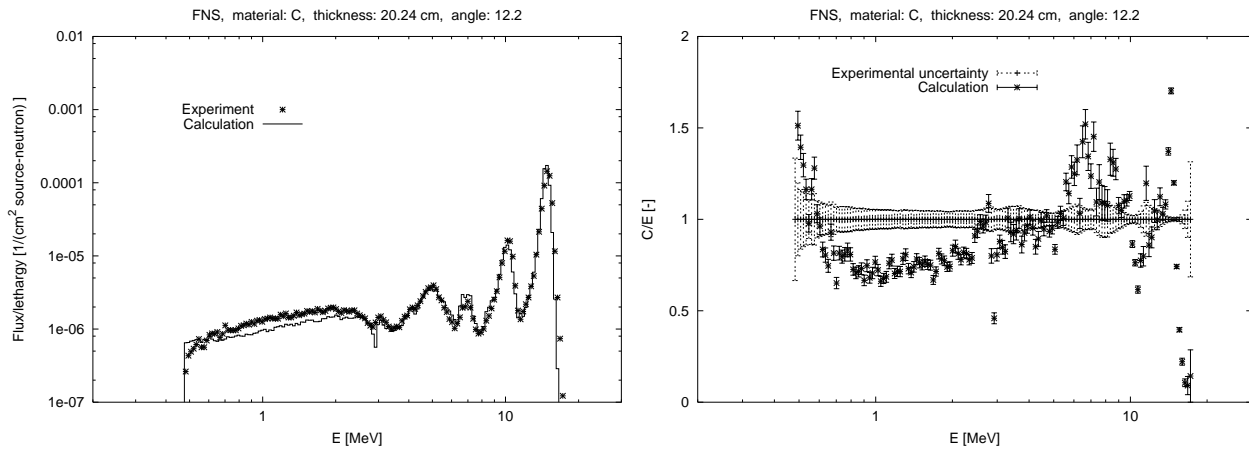


Figure 3.35 Neutron spectrum for the FNS, C, $d=20\text{cm}$ benchmark at 12.2° angle.

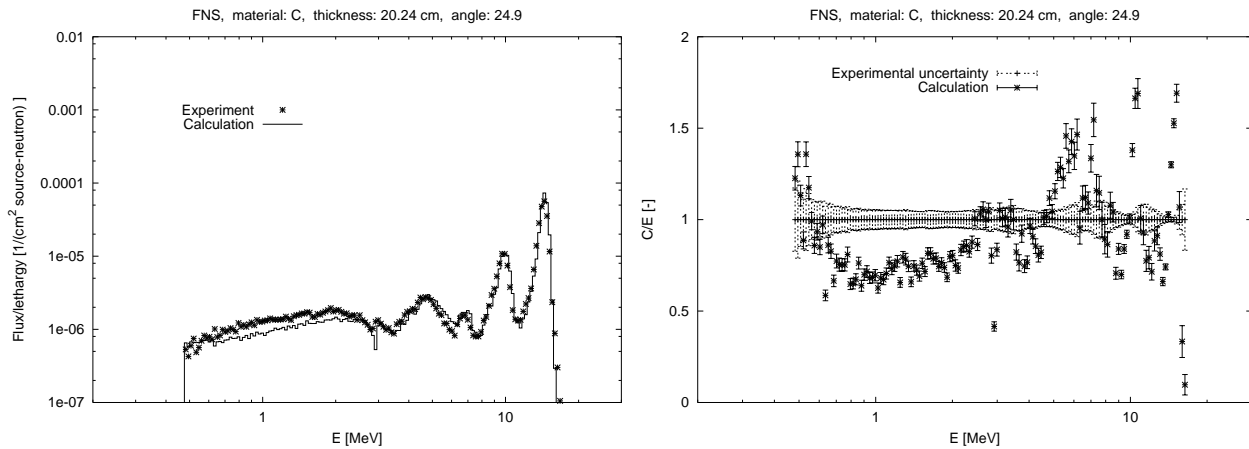


Figure 3.36 Neutron spectrum for the FNS, C, $d=20\text{cm}$ benchmark at 24.9° angle.

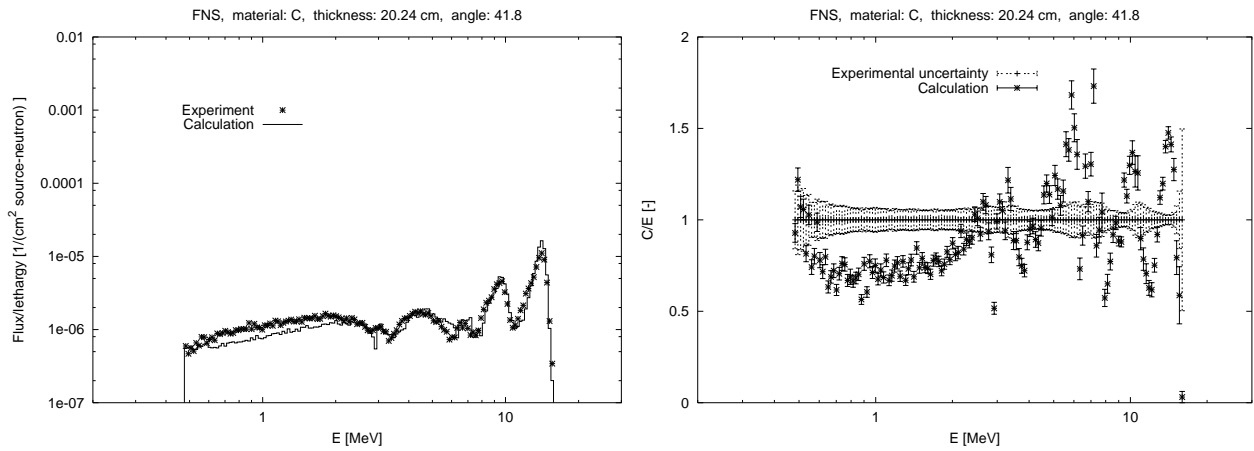


Figure 3.37 Neutron spectrum for the FNS, C, $d=20\text{cm}$ benchmark at 42.8° angle.

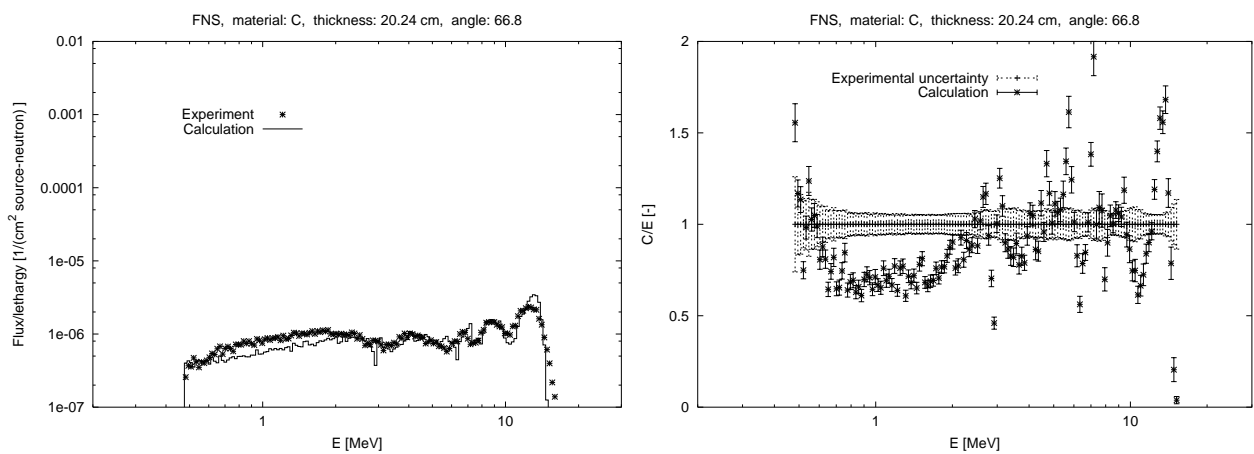


Figure 3.38 Neutron spectrum for the FNS, C, $d=20\text{cm}$ benchmark at 66.8° angle.

energy range	0°	12.2°	24.9°	42.8°	66.8°	
0.1–	1.0	0.72 ± 0.01	0.82 ± 0.01	0.76 ± 0.01	0.72 ± 0.01	0.75 ± 0.01
1.0–	5.0	0.77 ± 0.01	0.81 ± 0.01	0.81 ± 0.01	0.84 ± 0.01	0.83 ± 0.01
5.0–	10.0	0.90 ± 0.01	1.01 ± 0.01	0.89 ± 0.01	1.01 ± 0.01	1.04 ± 0.01
10.0–	20.0	0.98 ± 0.01	1.07 ± 0.01	1.20 ± 0.01	1.24 ± 0.01	1.07 ± 0.01

Table 3.15 C/E values for the neutron spectrum of the FNS C 20cm benchmark.

3.2.6 FNS, C, 40 cm

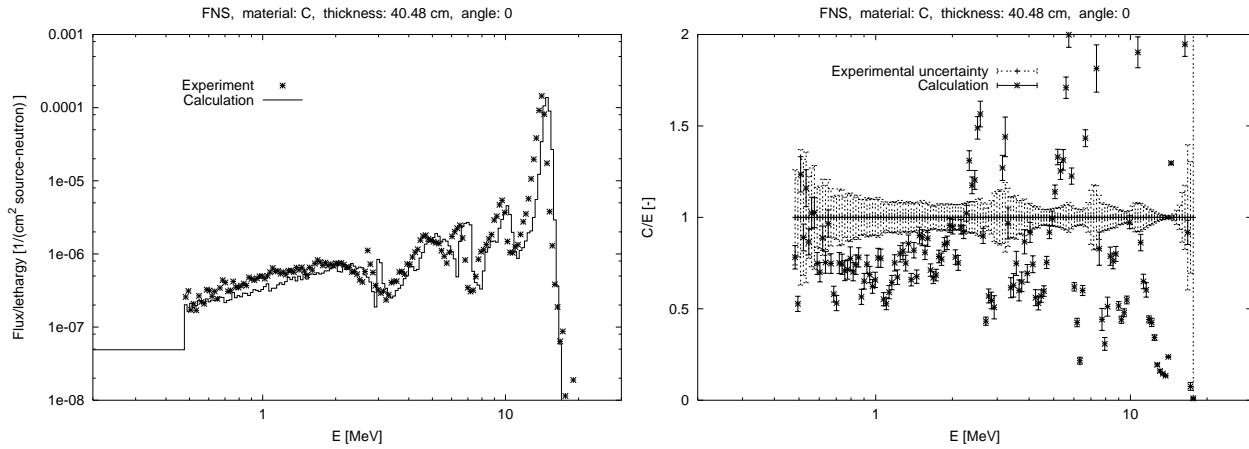


Figure 3.39 Neutron spectrum for the FNS, C, $d=40\text{cm}$ benchmark at 0° angle.

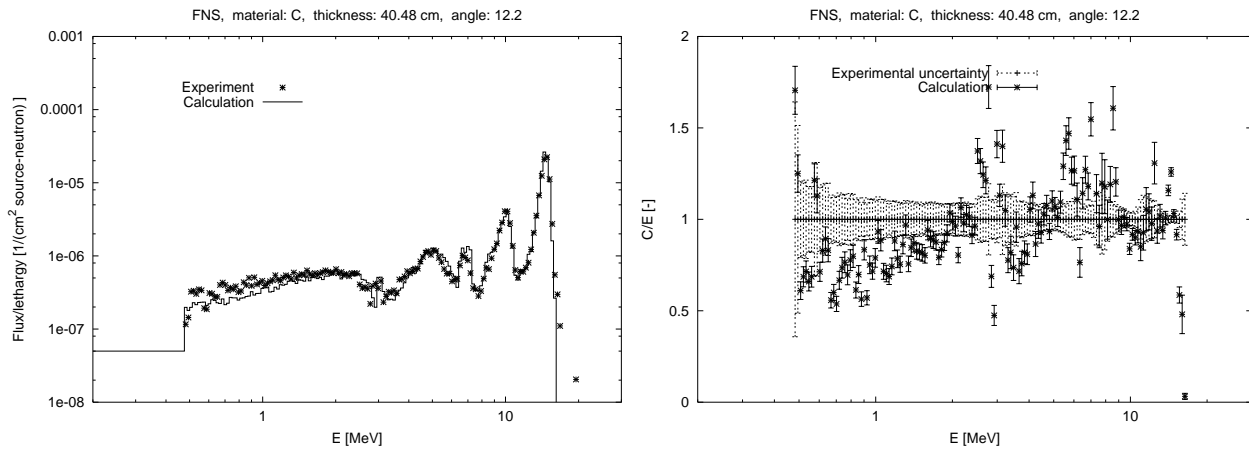


Figure 3.40 Neutron spectrum for the FNS, C, $d=40\text{cm}$ benchmark at 12.2° angle.

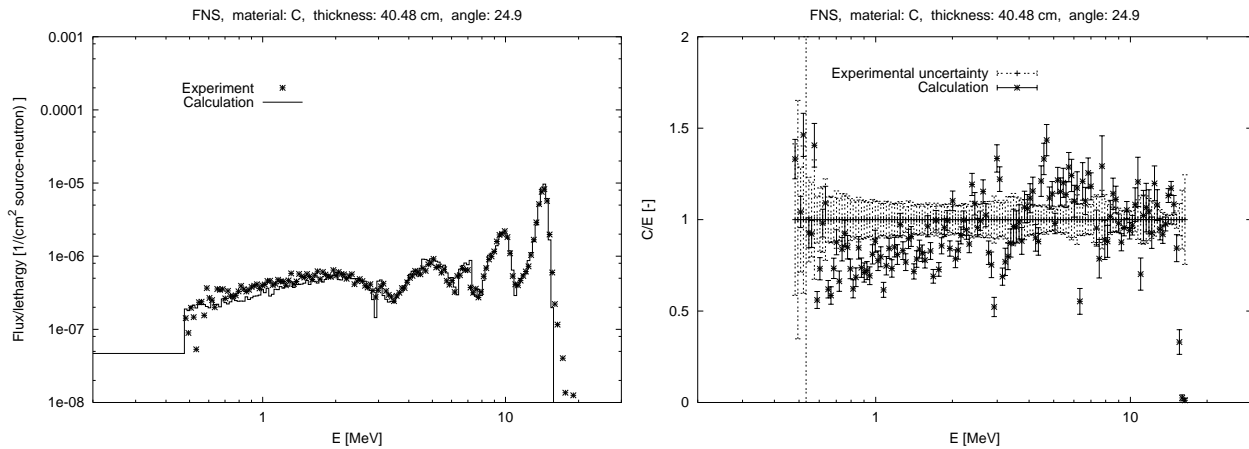


Figure 3.41 Neutron spectrum for the FNS, C, $d=40\text{cm}$ benchmark at 24.9° angle.

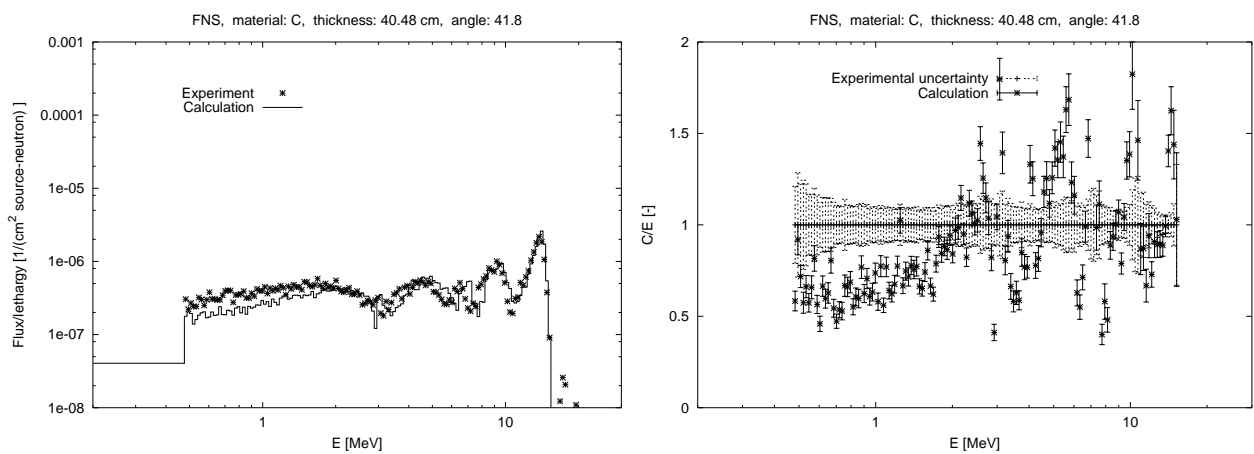


Figure 3.42 Neutron spectrum for the FNS, C, $d=40\text{cm}$ benchmark at 42.8° angle.

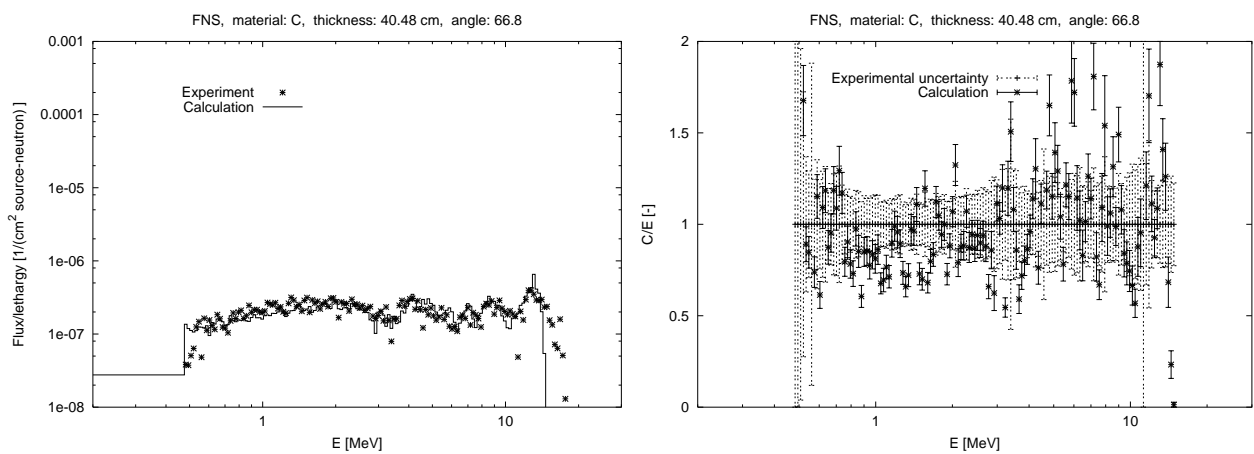


Figure 3.43 Neutron spectrum for the FNS, C, $d=40\text{cm}$ benchmark at 66.8° angle.

energy range		0°	12.2°	24.9°	42.8°	66.8°
0.1–	1.0	0.71 ± 0.01	0.70 ± 0.01	0.80 ± 0.01	0.60 ± 0.02	0.94 ± 0.02
1.0–	5.0	0.78 ± 0.01	0.90 ± 0.01	0.91 ± 0.01	0.86 ± 0.01	0.91 ± 0.01
5.0–	10.0	0.85 ± 0.01	1.02 ± 0.01	1.01 ± 0.01	1.05 ± 0.02	1.12 ± 0.02
10.0–	20.0	1.03 ± 0.01	1.08 ± 0.01	1.09 ± 0.01	1.14 ± 0.02	0.94 ± 0.04

Table 3.16 C/E values for the neutron spectrum of the FNS C 40cm benchmark.

3.2.7 FNS, N, 20 cm

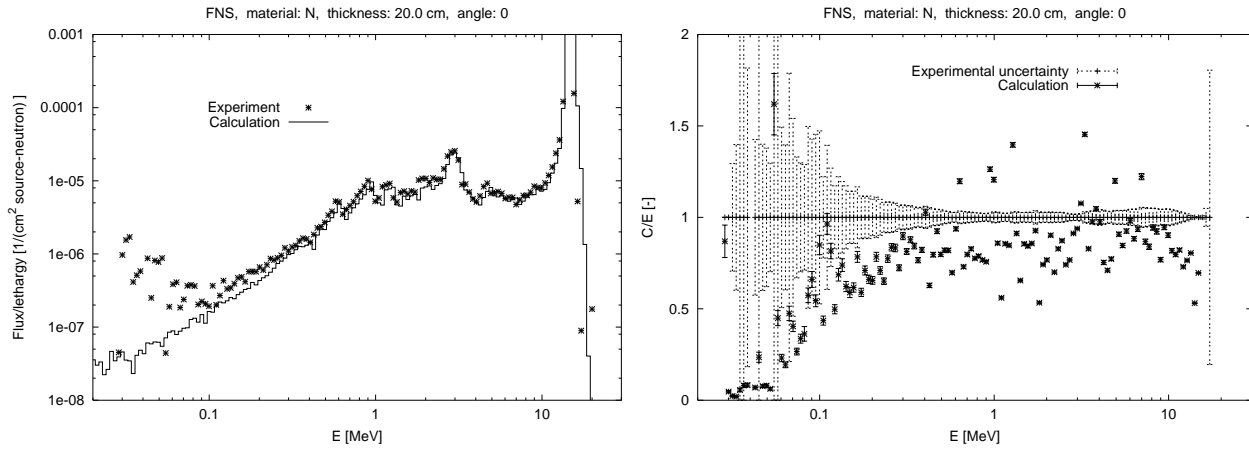


Figure 3.44 Neutron spectrum for the FNS, N, $d=20\text{cm}$ benchmark at 0° angle.

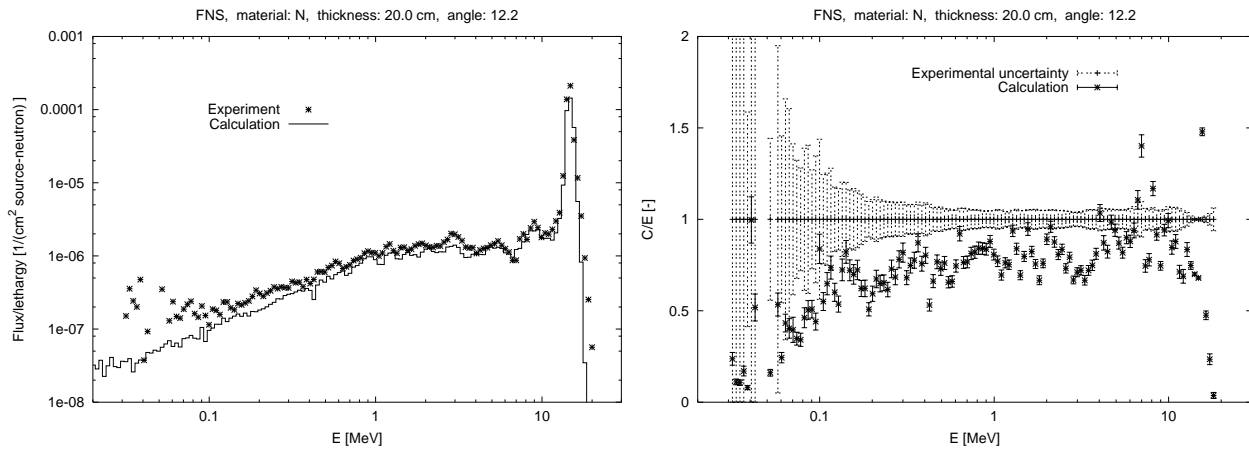


Figure 3.45 Neutron spectrum for the FNS, N, $d=20\text{cm}$ benchmark at 12.2° angle.

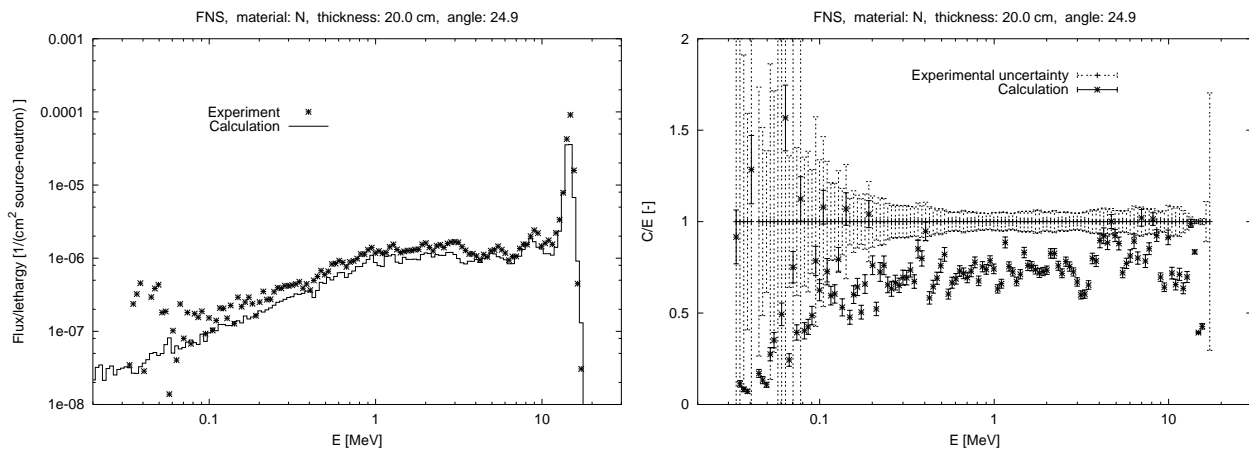


Figure 3.46 Neutron spectrum for the FNS, N, $d=20\text{cm}$ benchmark at 24.9° angle.

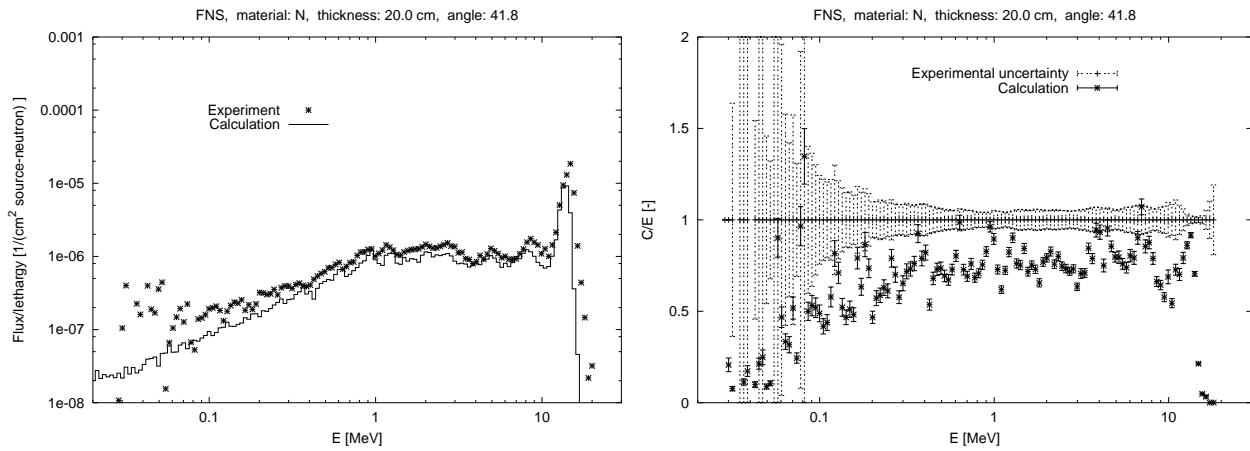


Figure 3.47 Neutron spectrum for the FNS, N, d=20cm benchmark at 42.8° angle.

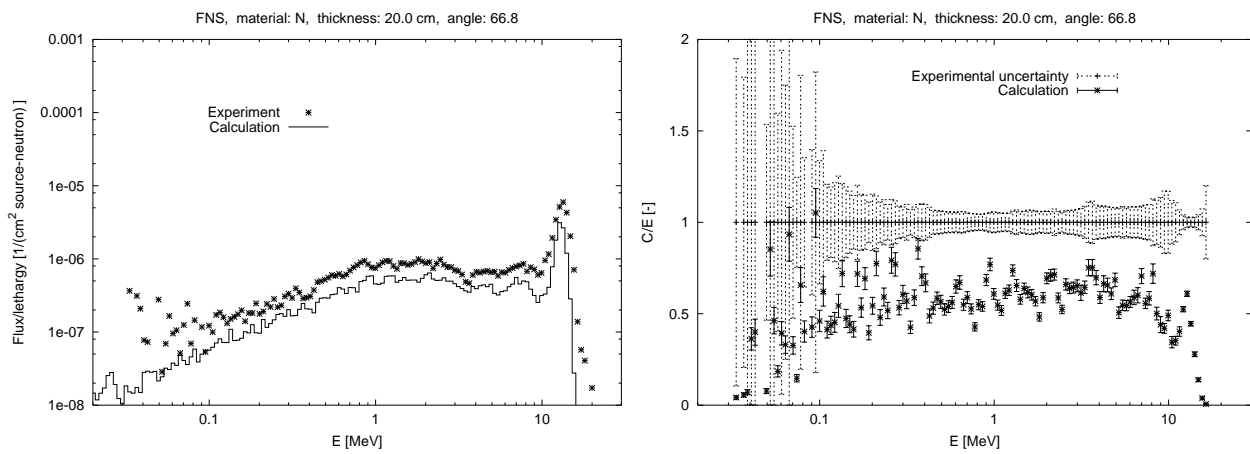


Figure 3.48 Neutron spectrum for the FNS, N, d=20cm benchmark at 66.8° angle.

energy range	0°	12.2°	24.9°	42.8°	66.8°
0.1– 1.0	0.80 ± 0.01	0.72 ± 0.01	0.68 ± 0.01	0.70 ± 0.01	0.56 ± 0.01
1.0– 5.0	0.86 ± 0.01	0.79 ± 0.01	0.75 ± 0.01	0.77 ± 0.01	0.63 ± 0.01
5.0– 10.0	0.92 ± 0.01	0.89 ± 0.01	0.82 ± 0.01	0.78 ± 0.01	0.57 ± 0.02
10.0– 20.0	0.85 ± 0.01	0.76 ± 0.01	0.57 ± 0.01	0.51 ± 0.01	0.42 ± 0.01

Table 3.17 C/E values for the neutron spectrum of the FNS N 20cm benchmark.

3.2.8 FNS, O, 20 cm

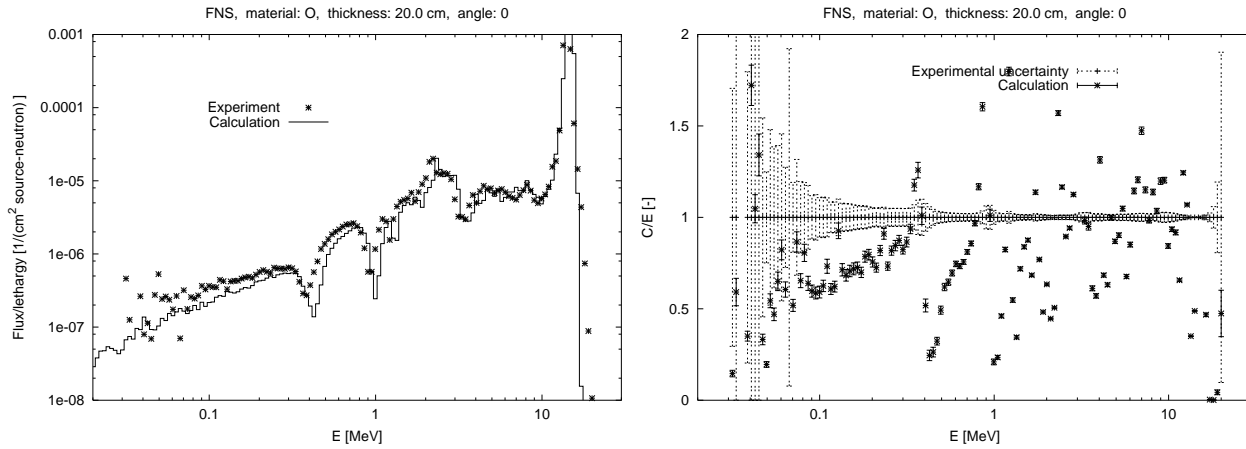


Figure 3.49 Neutron spectrum for the FNS, O, $d=20\text{cm}$ benchmark at 0° angle.

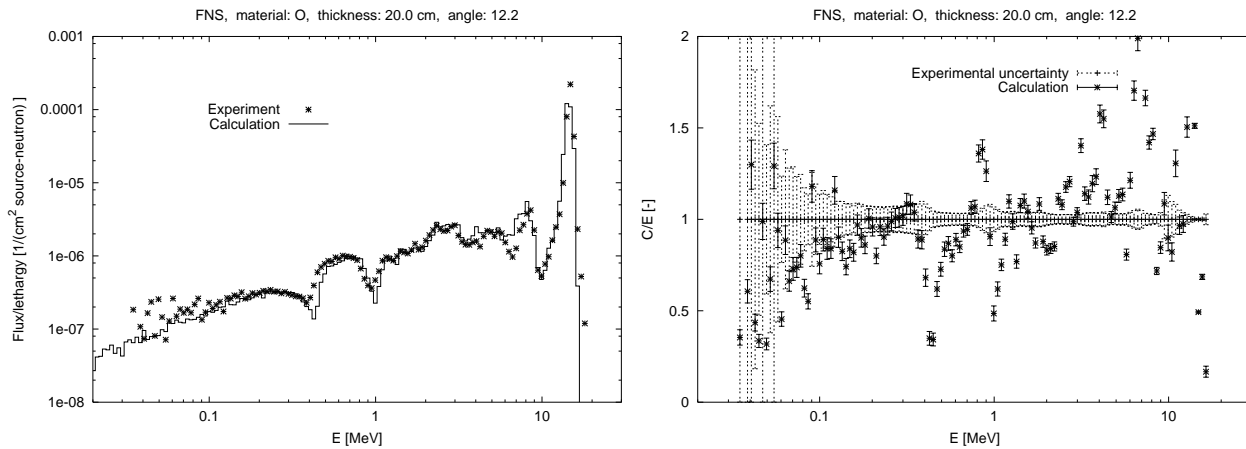


Figure 3.50 Neutron spectrum for the FNS, O, $d=20\text{cm}$ benchmark at 12.2° angle.

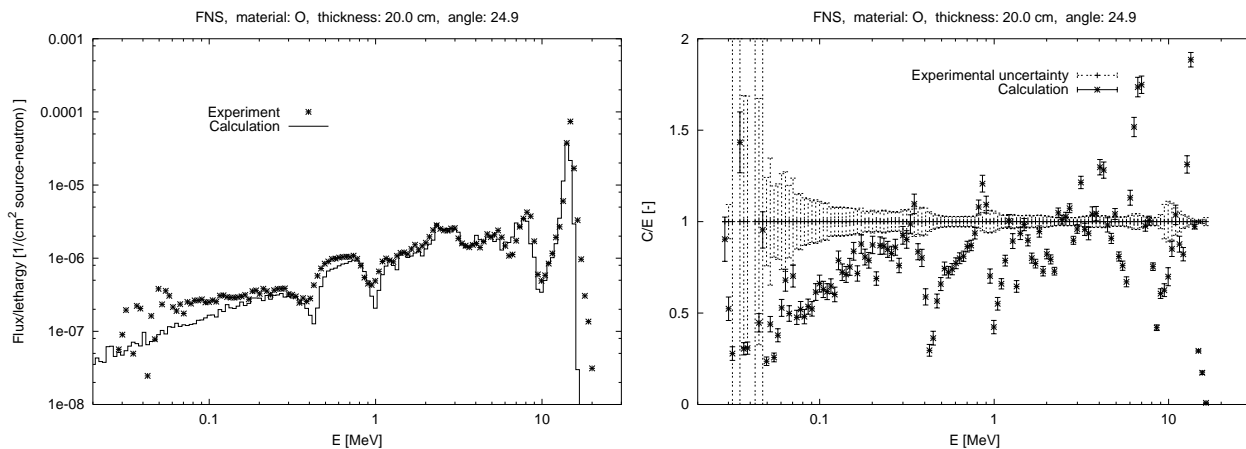


Figure 3.51 Neutron spectrum for the FNS, O, $d=20\text{cm}$ benchmark at 24.9° angle.

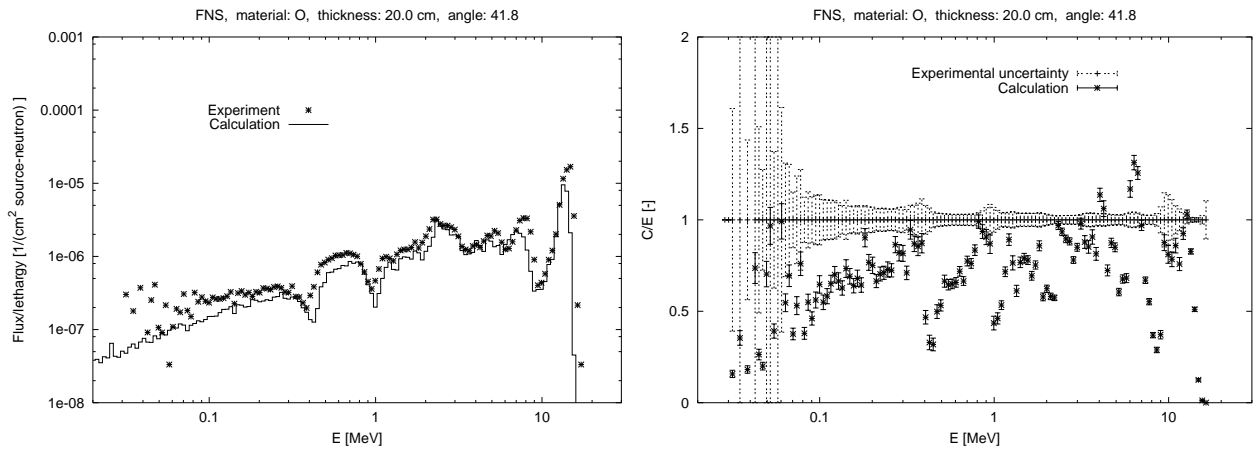


Figure 3.52 Neutron spectrum for the FNS, O, $d=20\text{cm}$ benchmark at 42.8° angle.

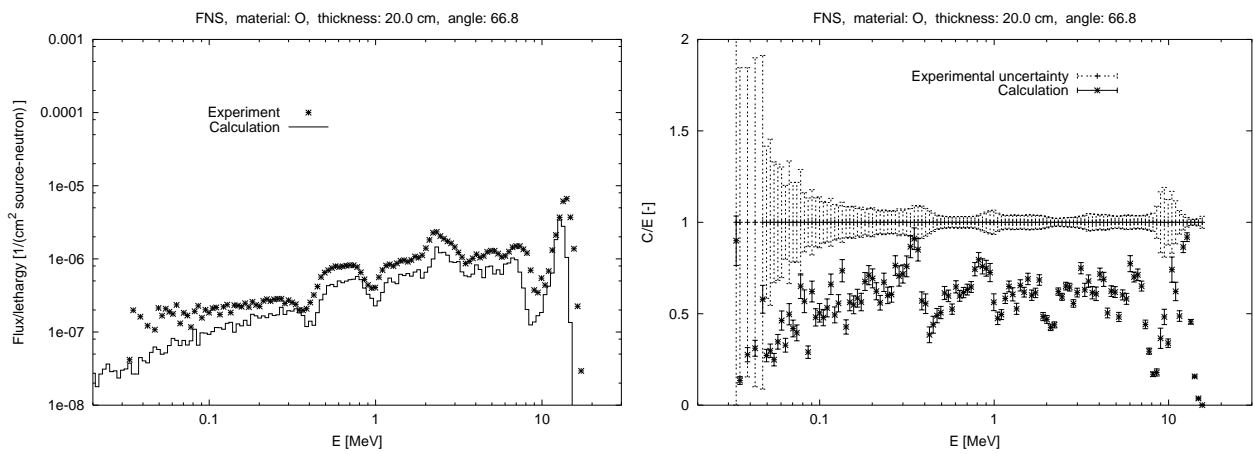


Figure 3.53 Neutron spectrum for the FNS, O, $d=20\text{cm}$ benchmark at 66.8° angle.

energy range	0°	12.2°	24.9°	42.8°	66.8°
0.1– 1.0	0.79 ± 0.01	0.89 ± 0.01	0.78 ± 0.01	0.70 ± 0.01	0.62 ± 0.01
1.0– 5.0	0.84 ± 0.01	1.03 ± 0.01	0.91 ± 0.01	0.78 ± 0.01	0.58 ± 0.01
5.0– 10.0	1.07 ± 0.01	1.32 ± 0.01	0.95 ± 0.01	0.74 ± 0.01	0.55 ± 0.01
10.0– 20.0	0.89 ± 0.01	0.81 ± 0.01	0.55 ± 0.01	0.51 ± 0.01	0.41 ± 0.01

Table 3.18 C/E values for the neutron spectrum of the FNS O 20cm benchmark.

3.2.9 FNS, Fe, 5 cm

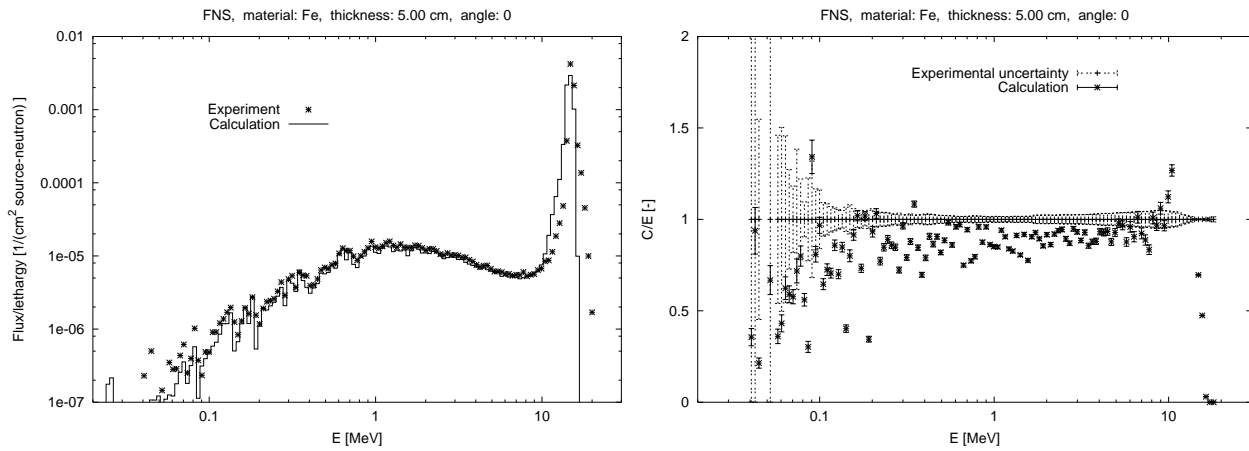


Figure 3.54 Neutron spectrum for the FNS, Fe, $d=5\text{cm}$ benchmark at 0° angle.

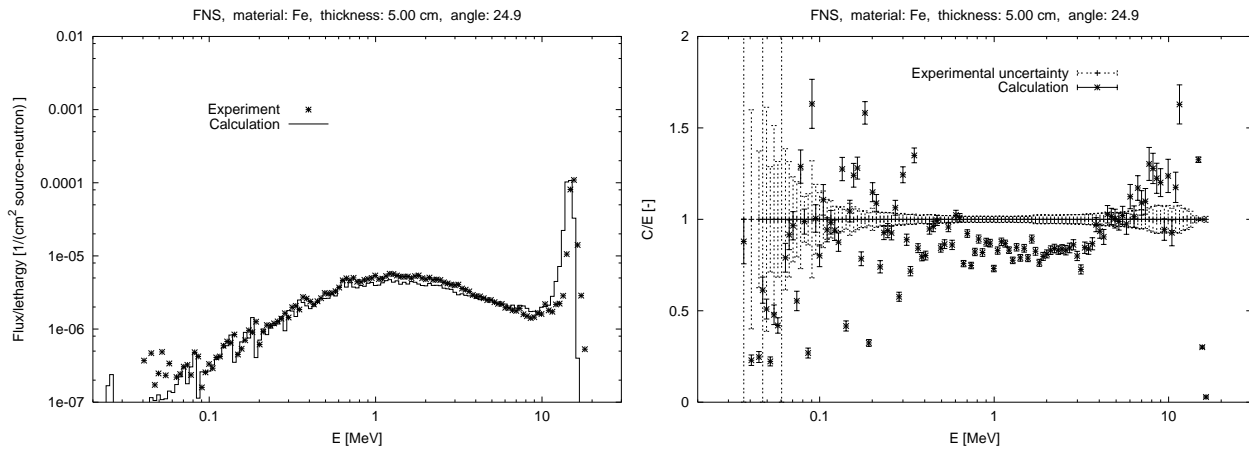


Figure 3.55 Neutron spectrum for the FNS, Fe, $d=5\text{cm}$ benchmark at 24.9° angle.

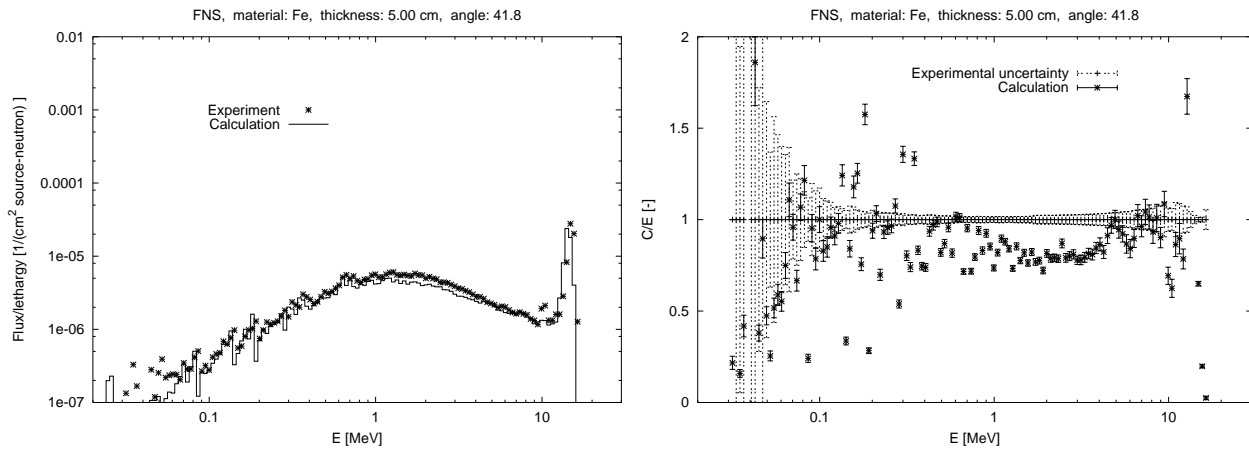


Figure 3.56 Neutron spectrum for the FNS, Fe, $d=5\text{cm}$ benchmark at 42.8° angle.

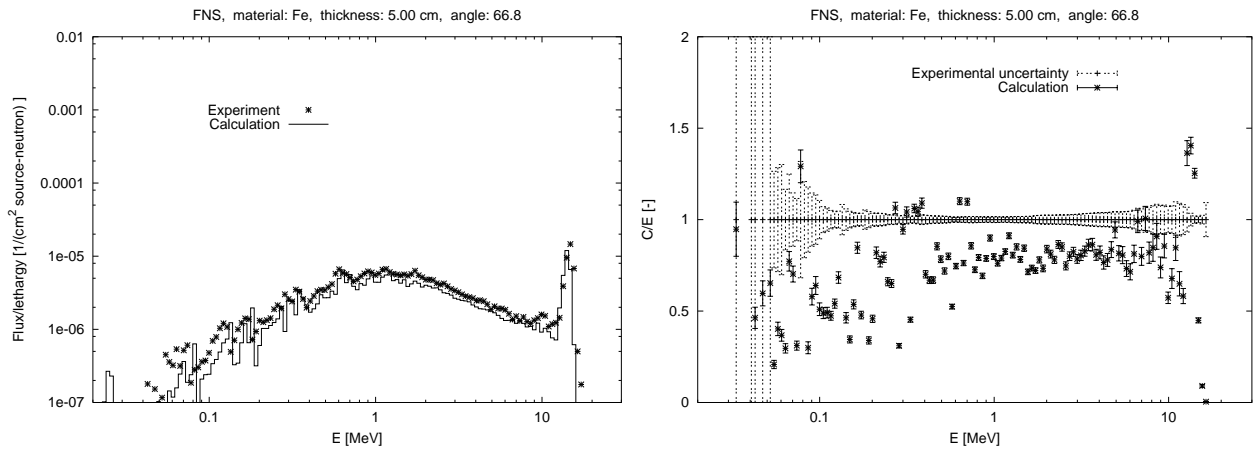


Figure 3.57 Neutron spectrum for the FNS, Fe, d=5cm benchmark at 66.8° angle.

energy range	0°	12.2°	24.9°	42.8°	66.8°
0.1— 1.0	0.83 ± 0.01		0.85 ± 0.01	0.84 ± 0.01	0.76 ± 0.01
1.0— 5.0	0.90 ± 0.01		0.85 ± 0.01	0.83 ± 0.01	0.82 ± 0.01
5.0— 10.0	0.95 ± 0.01		1.13 ± 0.02	0.97 ± 0.02	0.85 ± 0.02
10.0— 20.0	0.91 ± 0.01		1.24 ± 0.01	0.92 ± 0.01	0.73 ± 0.01

Table 3.19 C/E values for the neutron spectrum of the FNS Fe 5cm benchmark.

3.2.10 FNS, Fe, 20 cm

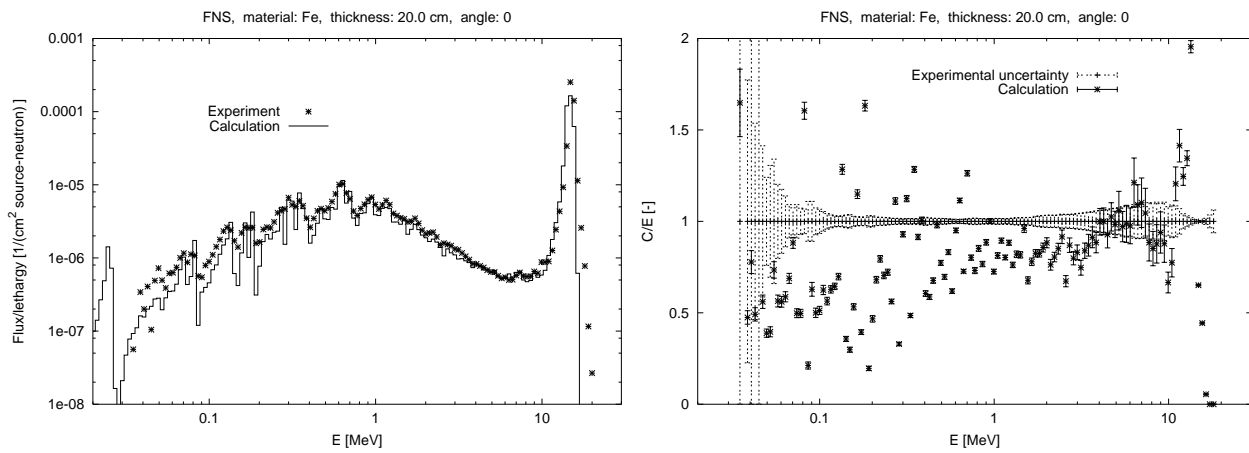


Figure 3.58 Neutron spectrum for the FNS, Fe, $d=20\text{cm}$ benchmark at 0° angle.

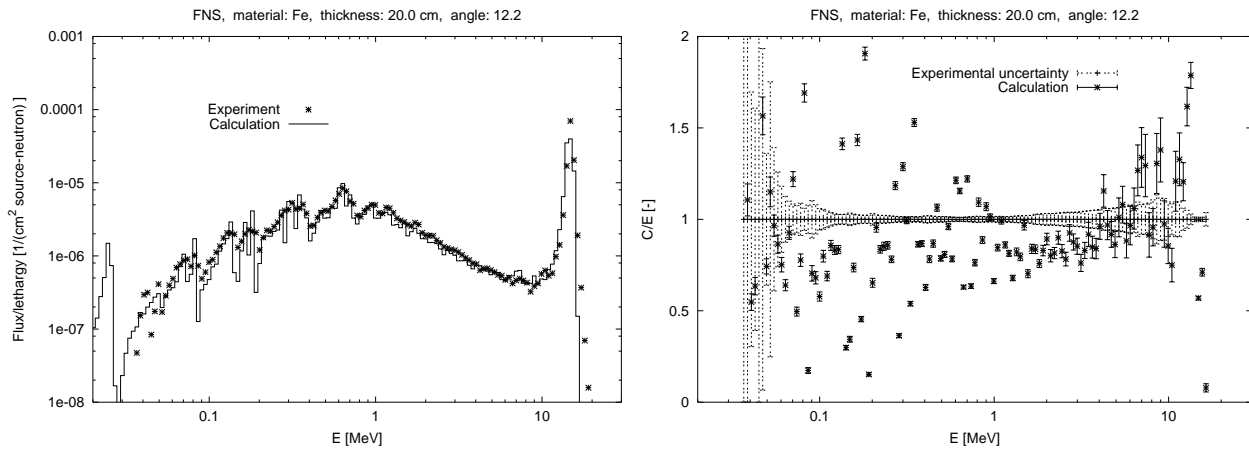


Figure 3.59 Neutron spectrum for the FNS, Fe, $d=20\text{cm}$ benchmark at 12.2° angle.

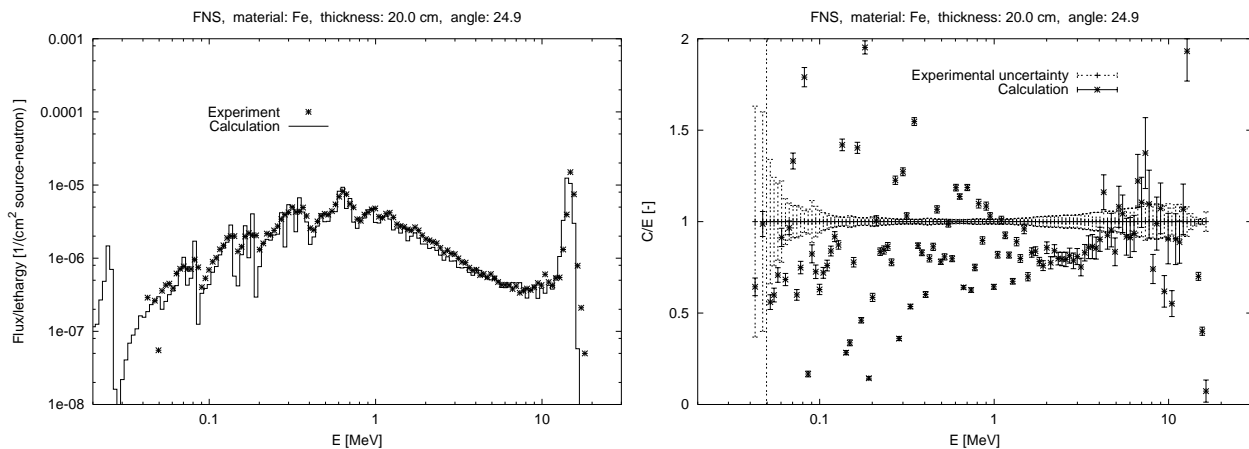


Figure 3.60 Neutron spectrum for the FNS, Fe, $d=20\text{cm}$ benchmark at 24.9° angle.

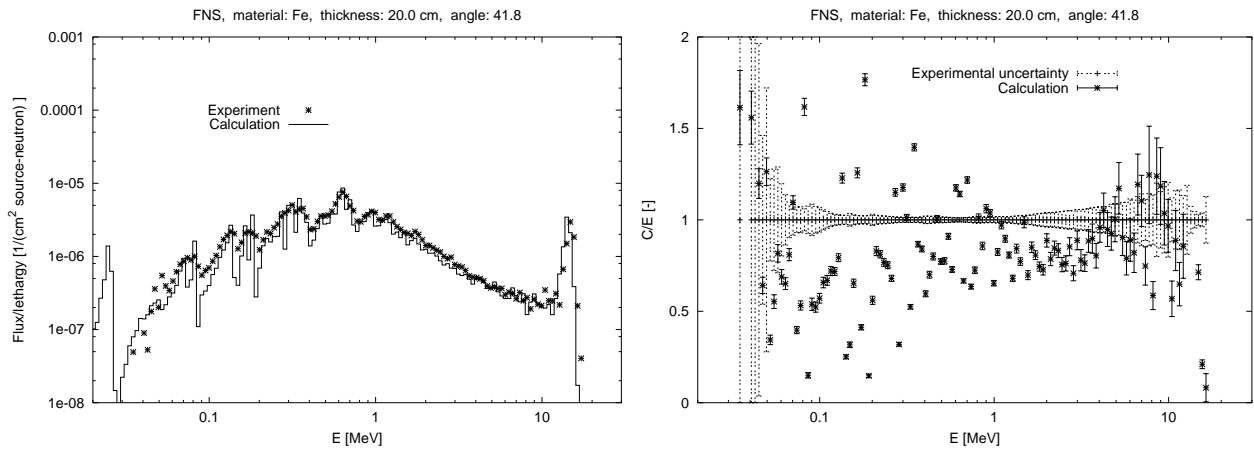


Figure 3.61 Neutron spectrum for the FNS, Fe, d=20cm benchmark at 42.8° angle.

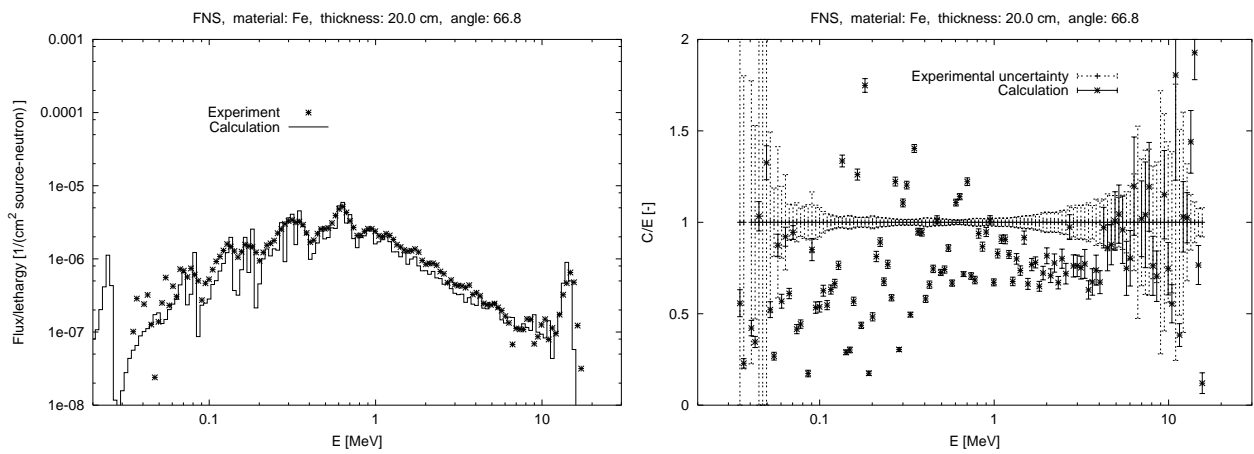


Figure 3.62 Neutron spectrum for the FNS, Fe, d=20cm benchmark at 66.8° angle.

energy range	0°	12.2°	24.9°	42.8°	66.8°
0.1– 1.0	0.82 ± 0.01	0.89 ± 0.01	0.89 ± 0.01	0.85 ± 0.01	0.85 ± 0.01
1.0– 5.0	0.88 ± 0.01	0.88 ± 0.01	0.88 ± 0.01	0.87 ± 0.01	0.83 ± 0.01
5.0– 10.0	0.96 ± 0.03	1.09 ± 0.03	1.01 ± 0.03	1.02 ± 0.04	1.11 ± 0.06
10.0– 20.0	0.82 ± 0.01	0.87 ± 0.01	1.03 ± 0.02	1.04 ± 0.03	0.95 ± 0.05

Table 3.20 C/E values for the neutron spectrum of the FNS Fe 20cm benchmark.

3.2.11 FNS, Fe, 40 cm

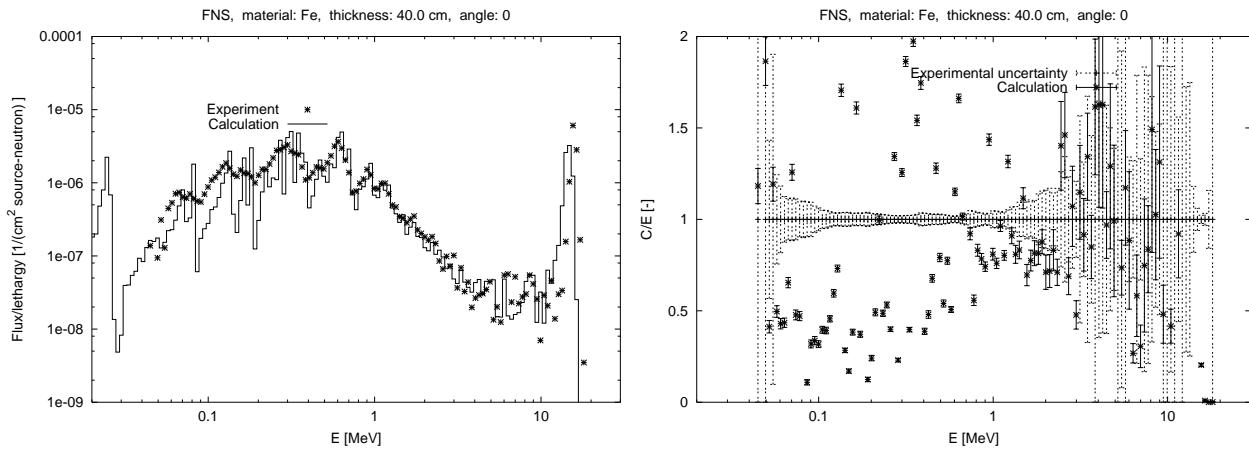


Figure 3.63 Neutron spectrum for the FNS, Fe, $d=40\text{cm}$ benchmark at 0° angle.

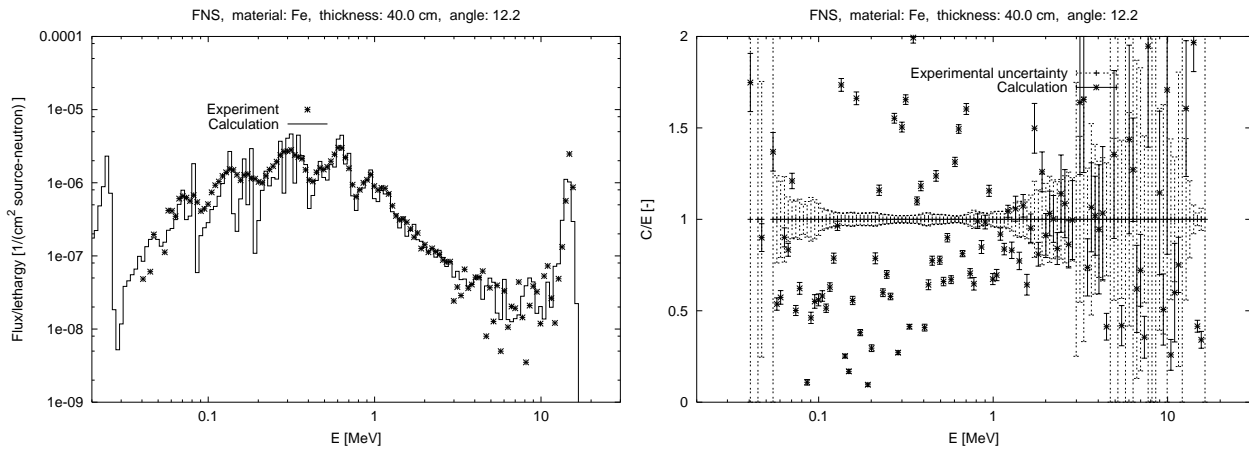


Figure 3.64 Neutron spectrum for the FNS, Fe, $d=40\text{cm}$ benchmark at 12.2° angle.

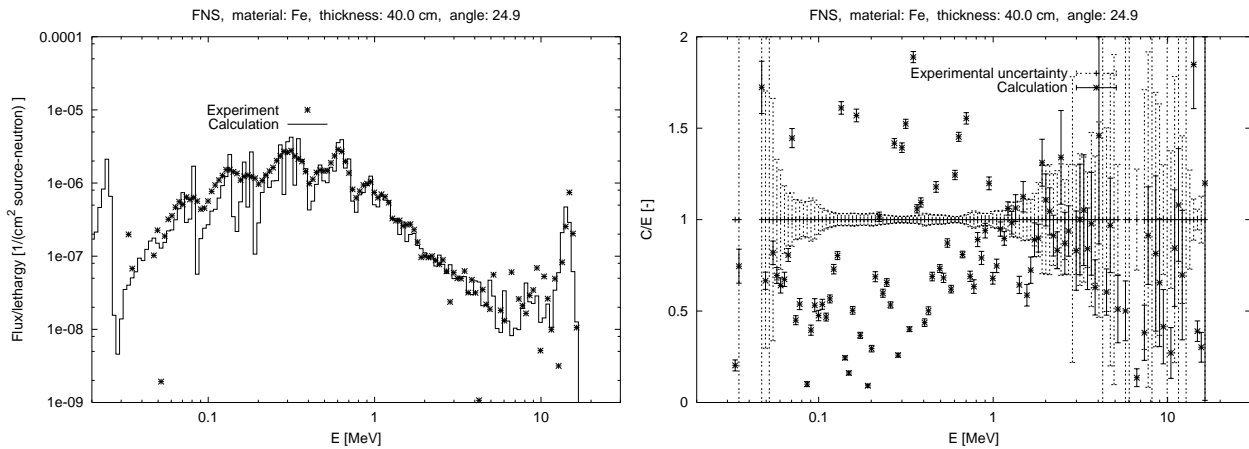


Figure 3.65 Neutron spectrum for the FNS, Fe, $d=40\text{cm}$ benchmark at 24.9° angle.

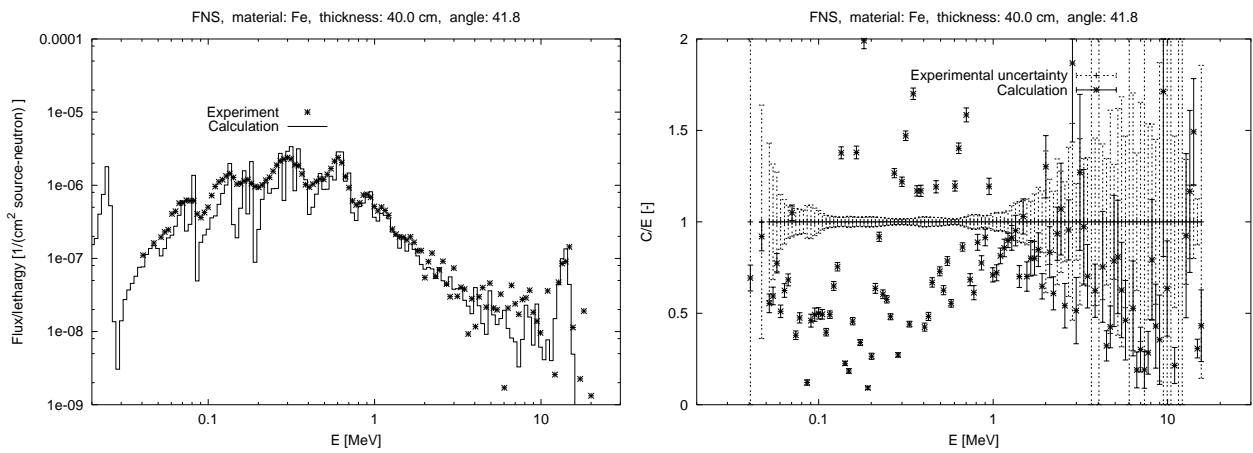


Figure 3.66 Neutron spectrum for the FNS, Fe, $d=40\text{cm}$ benchmark at 42.8° angle.

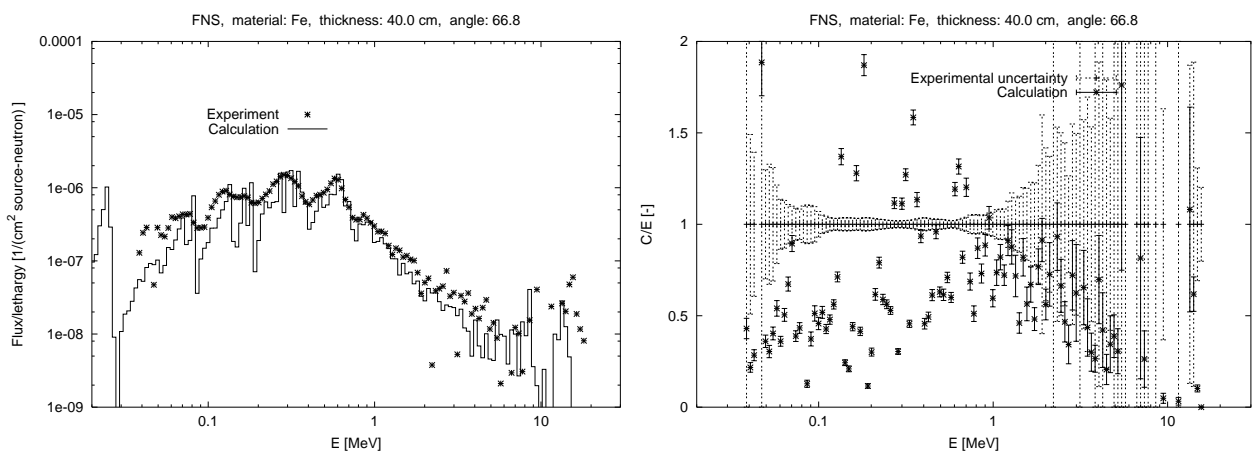


Figure 3.67 Neutron spectrum for the FNS, Fe, $d=40\text{cm}$ benchmark at 66.8° angle.

energy range		0°	12.2°	24.9°	42.8°	66.8°
0.1–	1.0	0.91 ± 0.01	0.97 ± 0.01	0.91 ± 0.01	0.85 ± 0.01	0.77 ± 0.01
1.0–	5.0	0.98 ± 0.01	1.01 ± 0.01	1.01 ± 0.02	0.91 ± 0.02	0.77 ± 0.03
5.0–	10.0	0.95 ± 0.12	1.32 ± 0.11	1.07 ± 0.13	0.66 ± 0.15	0.00 ± 0.28
10.0–	20.0	0.76 ± 0.02	0.71 ± 0.05	0.86 ± 0.08	0.84 ± 0.14	0.39 ± 0.25

Table 3.21 C/E values for the neutron spectrum of the FNS Fe 40cm benchmark.

3.2.12 FNS, Fe, 60 cm

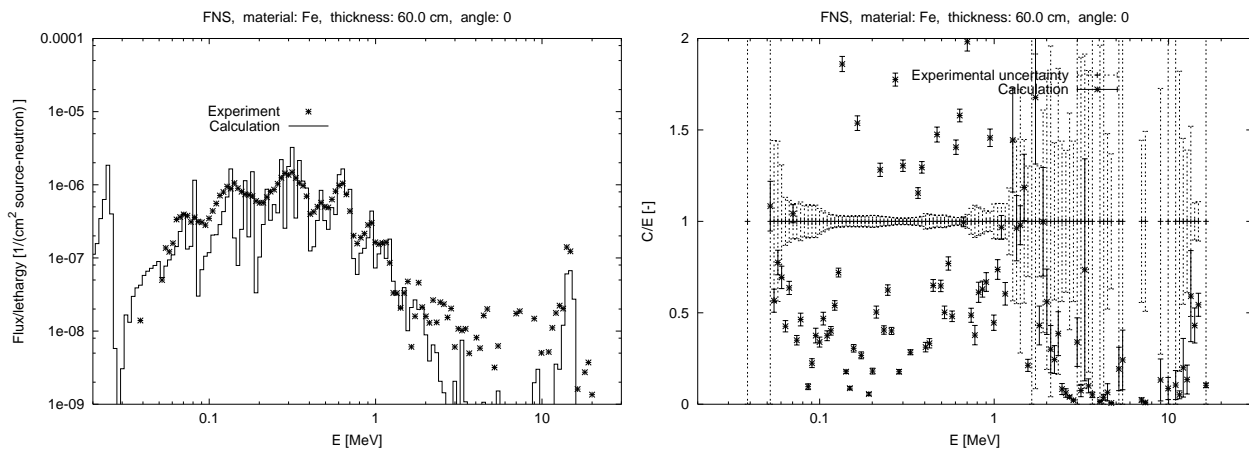


Figure 3.68 Neutron spectrum for the FNS, Fe, $d=60\text{cm}$ benchmark at 0° angle.

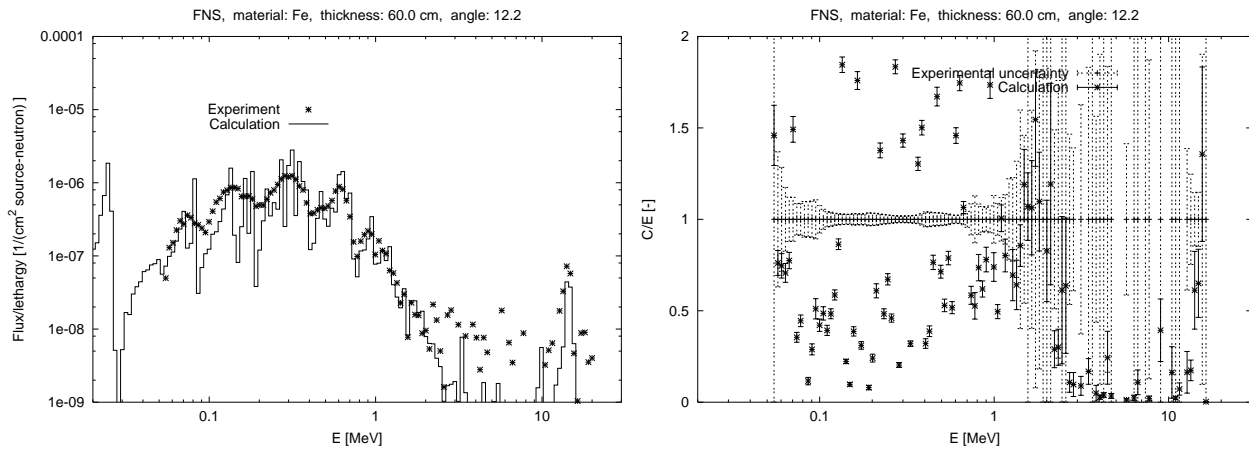


Figure 3.69 Neutron spectrum for the FNS, Fe, $d=60\text{cm}$ benchmark at 12.2° angle.

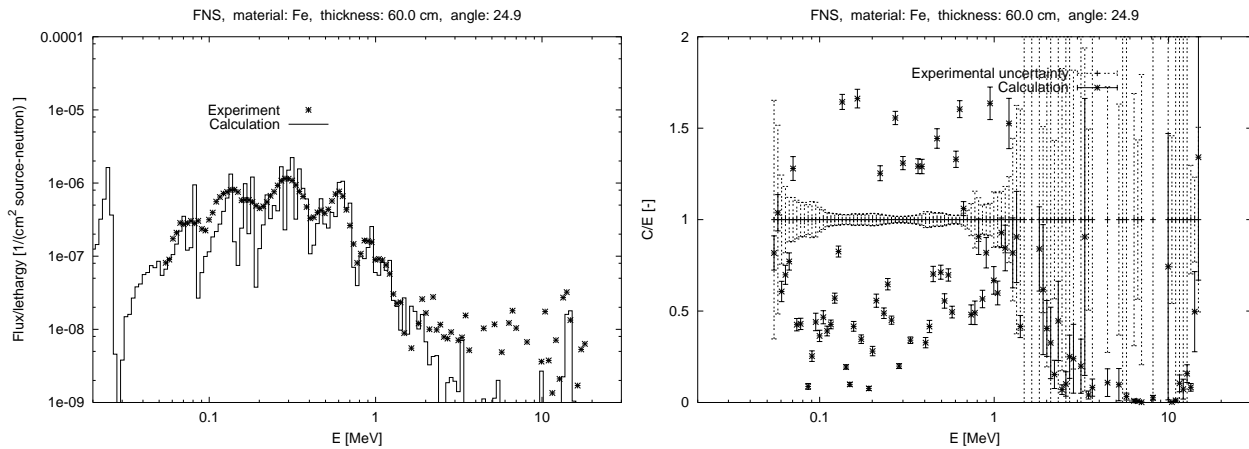


Figure 3.70 Neutron spectrum for the FNS, Fe, $d=60\text{cm}$ benchmark at 24.9° angle.

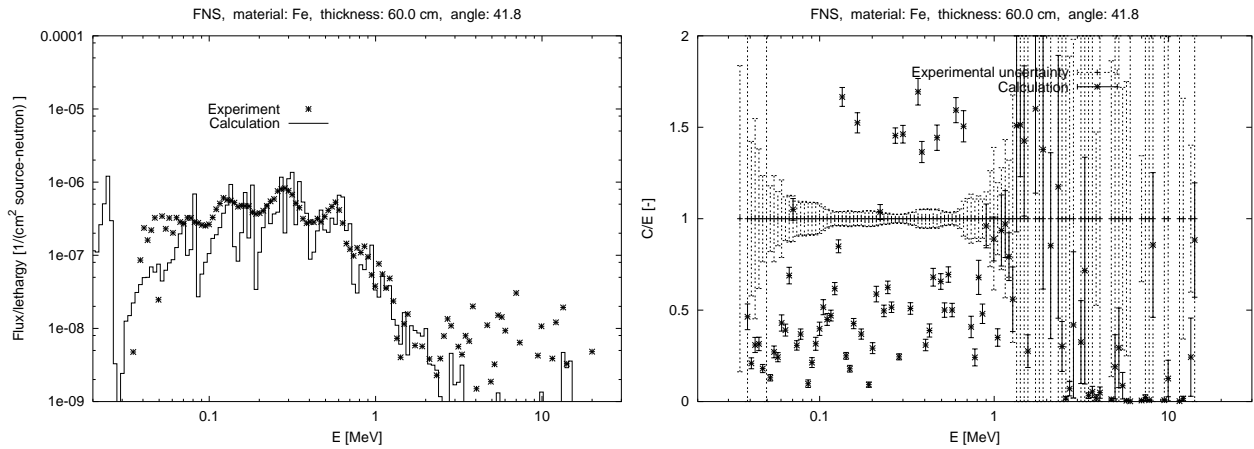


Figure 3.71 Neutron spectrum for the FNS, Fe, d=60cm benchmark at 42.8° angle.

energy range		0°	12.2°	24.9°	42.8°
0.0–	0.1	3.30 ± 0.01	10.02 ± 0.01	7.00 ± 0.01	1.10 ± 0.01
0.1–	1.0	0.91 ± 0.01	0.98 ± 0.01	0.90 ± 0.01	0.91 ± 0.01
1.0–	5.0	0.85 ± 0.03	0.94 ± 0.03	1.04 ± 0.04	0.90 ± 0.07
5.0–	10.0	0.33 ± 0.32	0.00 ± 0.30	0.12 ± 0.47	0.08 ± 0.39
10.0–	20.0	0.52 ± 0.10	0.49 ± 0.19	0.39 ± 0.29	1.90 ± 0.38

Table 3.22 C/E values for the neutron spectrum of the FNS Fe 60cm benchmark.

3.2.13 FNS, Pb, 5 cm

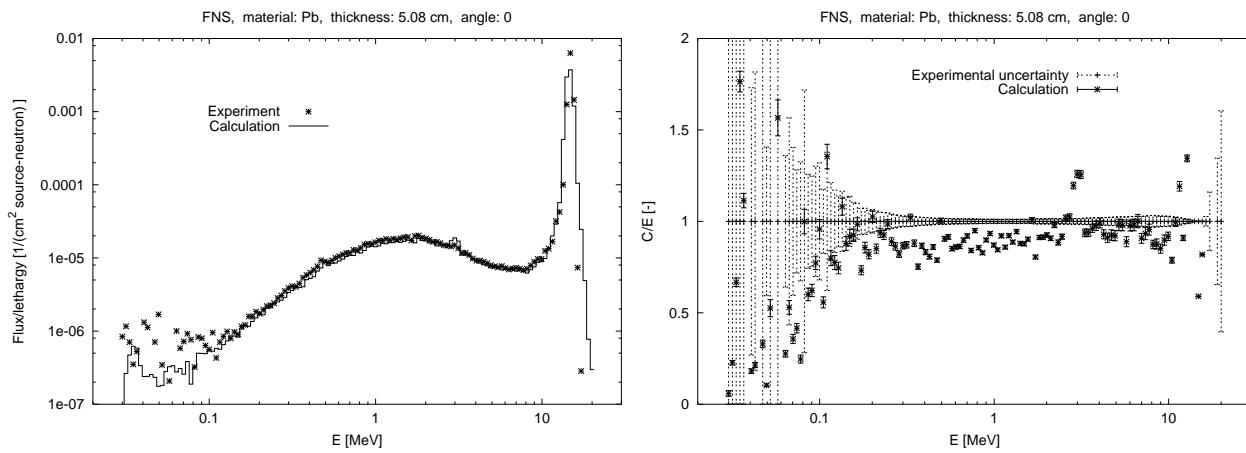


Figure 3.72 Neutron spectrum for the FNS, Pb, d=5cm benchmark at 0° angle.

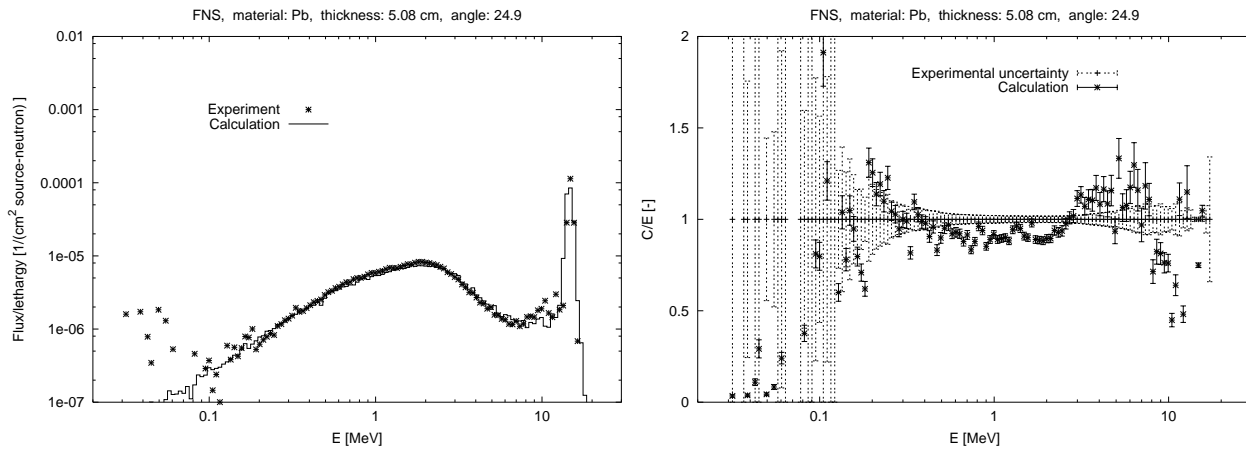


Figure 3.73 Neutron spectrum for the FNS, Pb, d=5cm benchmark at 24.9° angle.

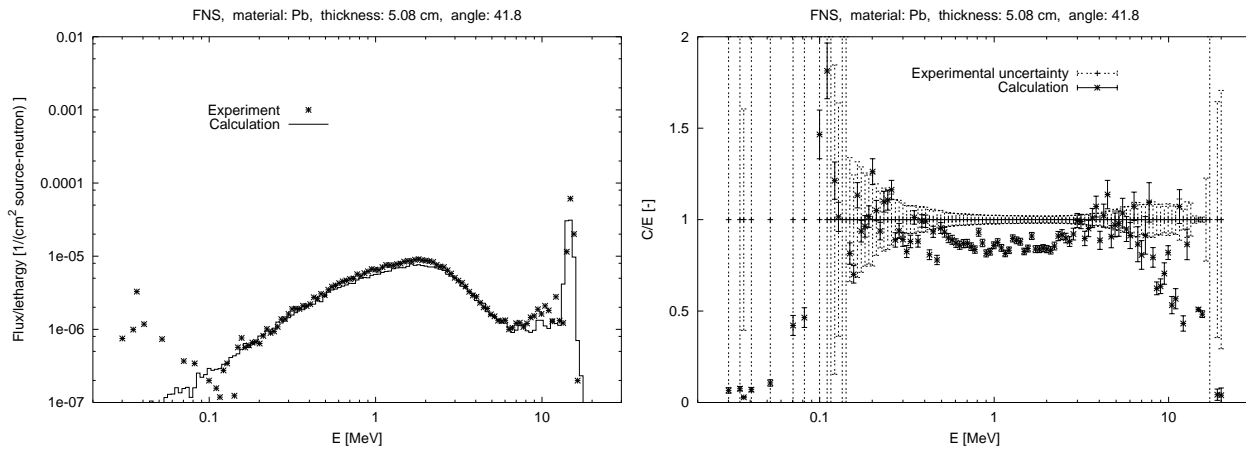


Figure 3.74 Neutron spectrum for the FNS, Pb, d=5cm benchmark at 42.8° angle.

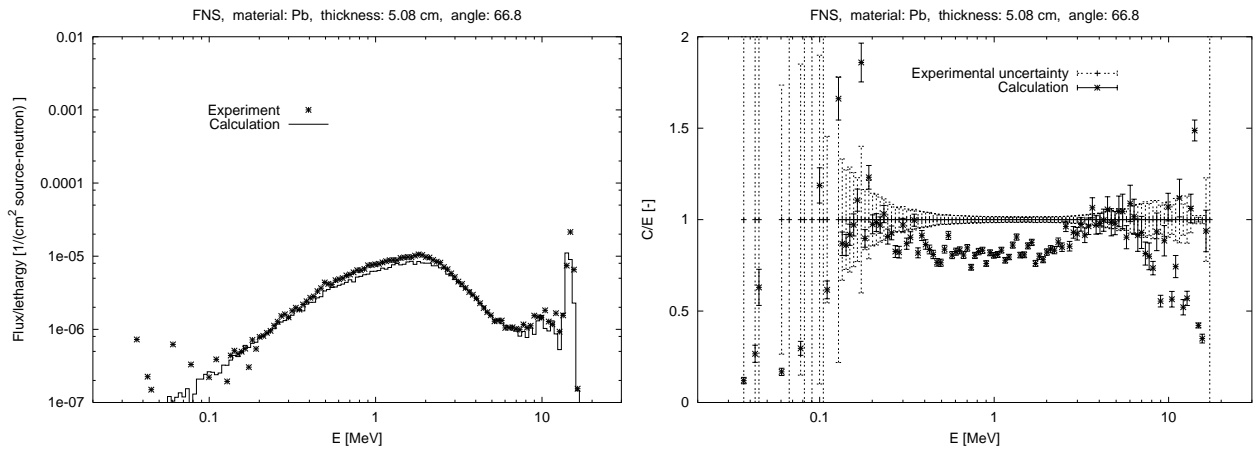


Figure 3.75 Neutron spectrum for the FNS, Pb, d=5cm benchmark at 66.8° angle.

energy range	0°	12.2°	24.9°	42.8°	66.8°
0.1— 1.0	0.83 ± 0.01		0.88 ± 0.01	0.85 ± 0.01	0.80 ± 0.01
1.0— 5.0	0.96 ± 0.01		0.98 ± 0.01	0.90 ± 0.01	0.88 ± 0.01
5.0— 10.0	0.91 ± 0.01		1.02 ± 0.02	0.87 ± 0.02	0.90 ± 0.02
10.0— 20.0	0.93 ± 0.01		1.12 ± 0.01	0.81 ± 0.01	0.69 ± 0.02

Table 3.23 C/E values for the neutron spectrum of the FNS Pb 5cm benchmark.

3.2.14 FNS, Pb, 20 cm

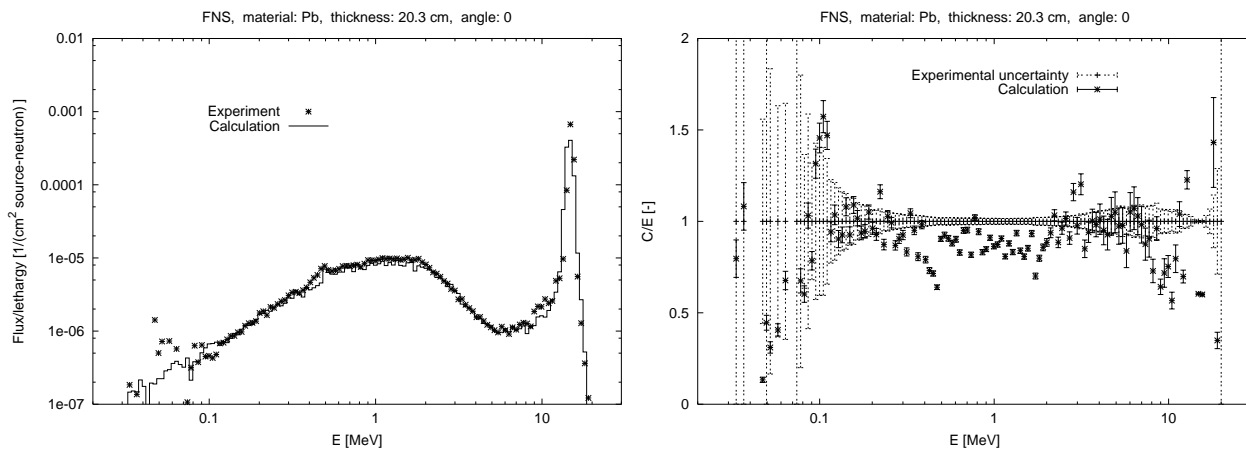


Figure 3.76 Neutron spectrum for the FNS, Pb, d=20cm benchmark at 0° angle.

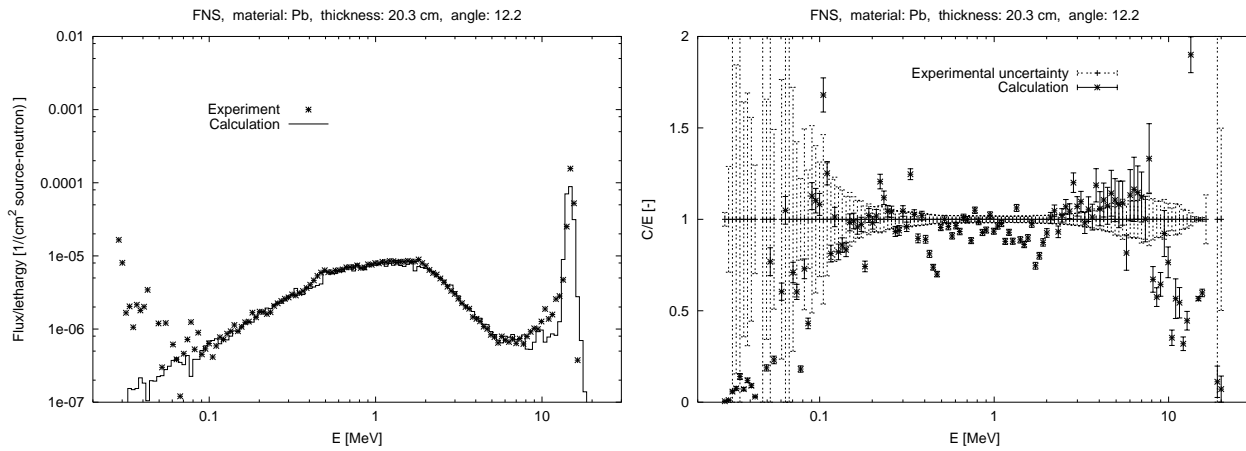


Figure 3.77 Neutron spectrum for the FNS, Pb, d=20cm benchmark at 12.2° angle.

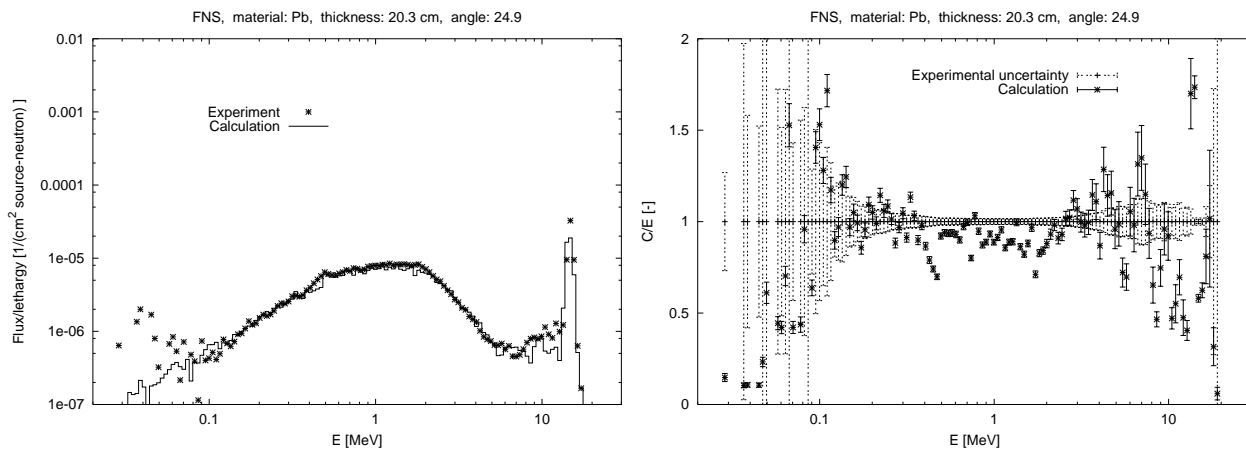


Figure 3.78 Neutron spectrum for the FNS, Pb, d=20cm benchmark at 24.9° angle.

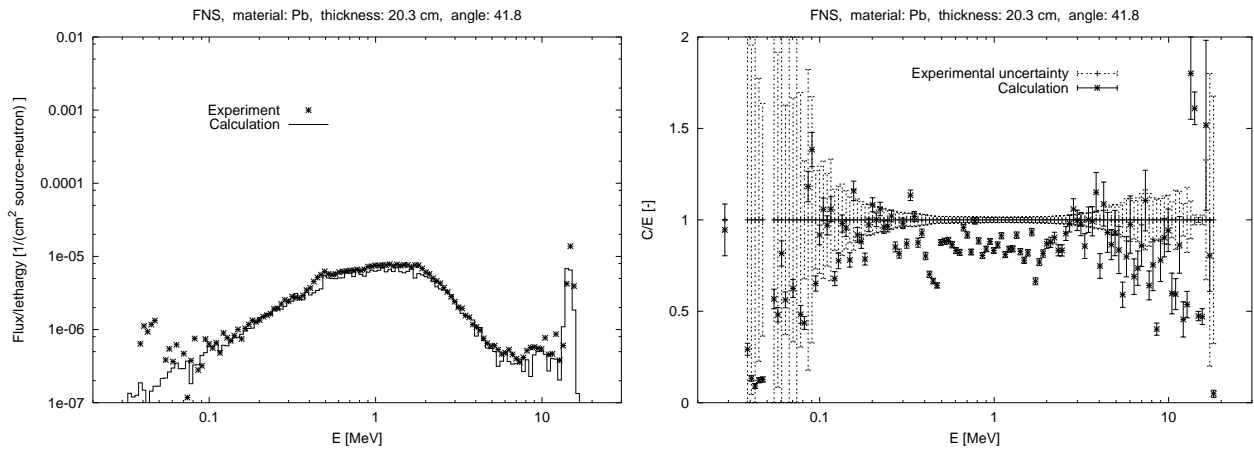


Figure 3.79 Neutron spectrum for the FNS, Pb, $d=20\text{cm}$ benchmark at 42.8° angle.

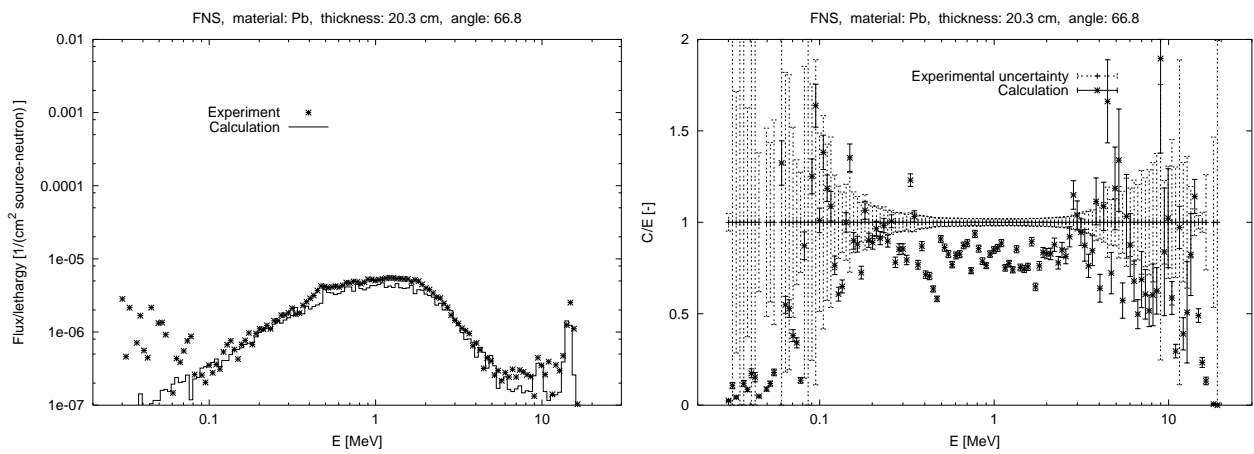


Figure 3.80 Neutron spectrum for the FNS, Pb, $d=20\text{cm}$ benchmark at 66.8° angle.

energy range	0°	12.2°	24.9°	42.8°	66.8°
0.1– 1.0	0.85 ± 0.01	0.91 ± 0.01	0.89 ± 0.01	0.83 ± 0.01	0.80 ± 0.01
1.0– 5.0	0.93 ± 0.01	0.99 ± 0.01	0.95 ± 0.01	0.90 ± 0.01	0.86 ± 0.01
5.0– 10.0	0.84 ± 0.03	0.92 ± 0.03	0.88 ± 0.04	0.78 ± 0.04	0.83 ± 0.07
10.0– 20.0	0.93 ± 0.01	0.84 ± 0.01	0.81 ± 0.02	0.73 ± 0.03	0.63 ± 0.05

Table 3.24 C/E values for the neutron spectrum of the FNS Pb 20cm benchmark.

3.2.15 FNS, Pb, 40 cm

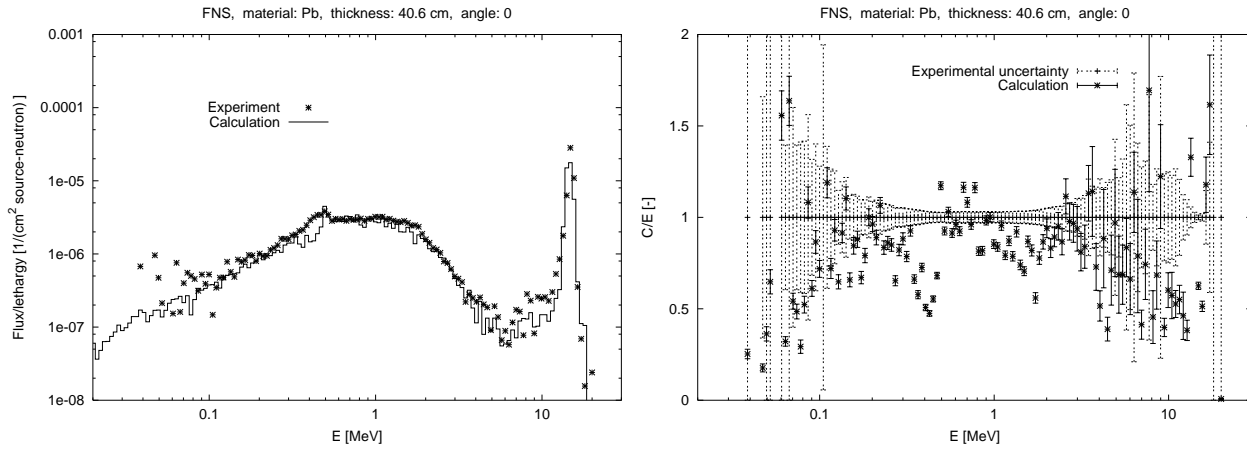


Figure 3.81 Neutron spectrum for the FNS, Pb, $d=40\text{cm}$ benchmark at 0° angle.

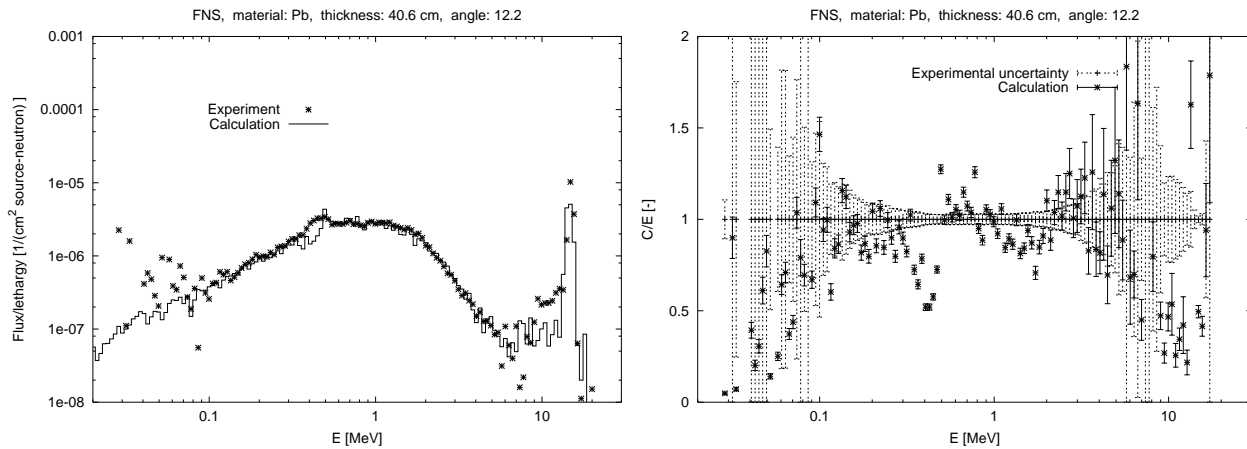


Figure 3.82 Neutron spectrum for the FNS, Pb, $d=40\text{cm}$ benchmark at 12.2° angle.

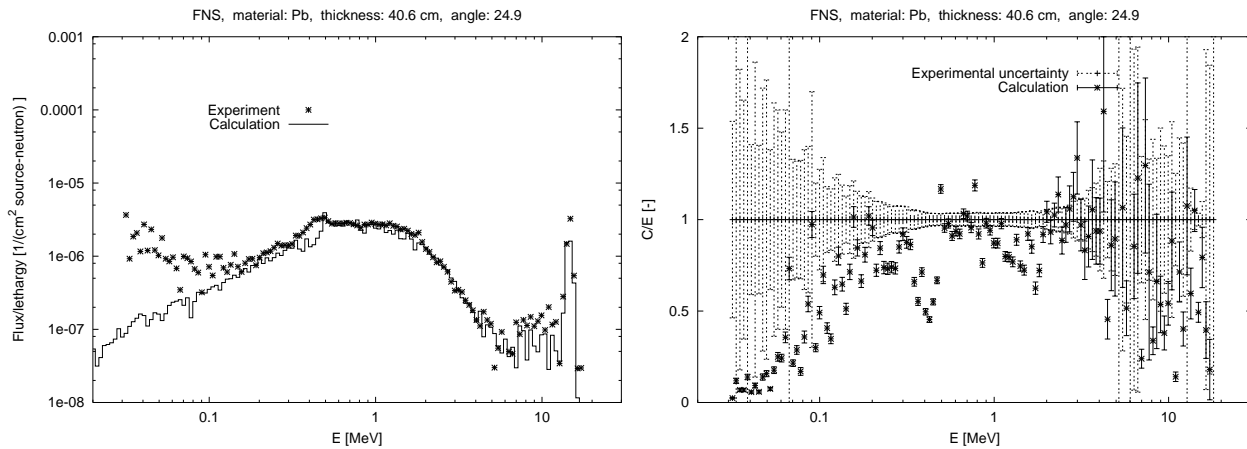


Figure 3.83 Neutron spectrum for the FNS, Pb, $d=40\text{cm}$ benchmark at 24.9° angle.

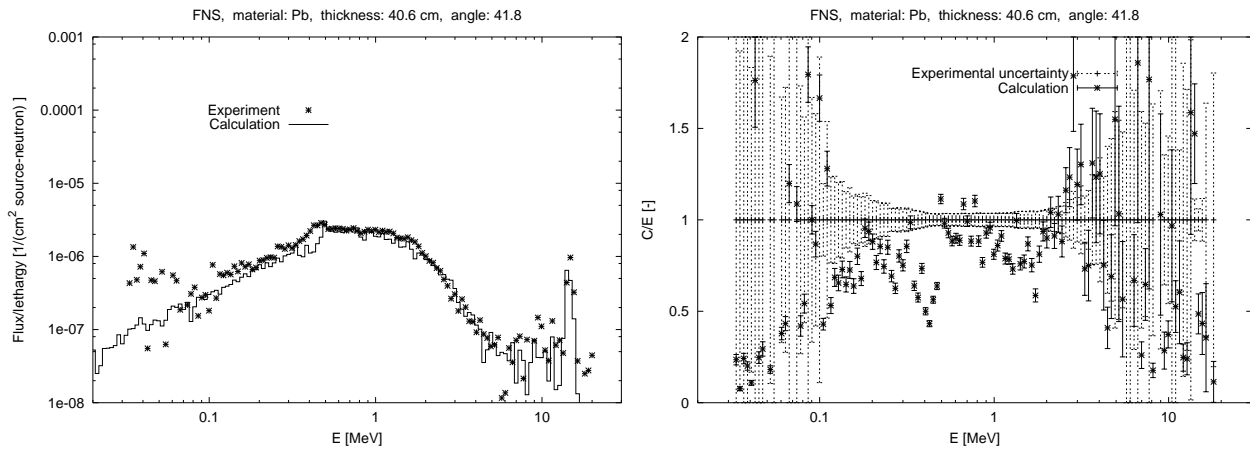


Figure 3.84 Neutron spectrum for the FNS, Pb, $d=40\text{cm}$ benchmark at 42.8° angle.

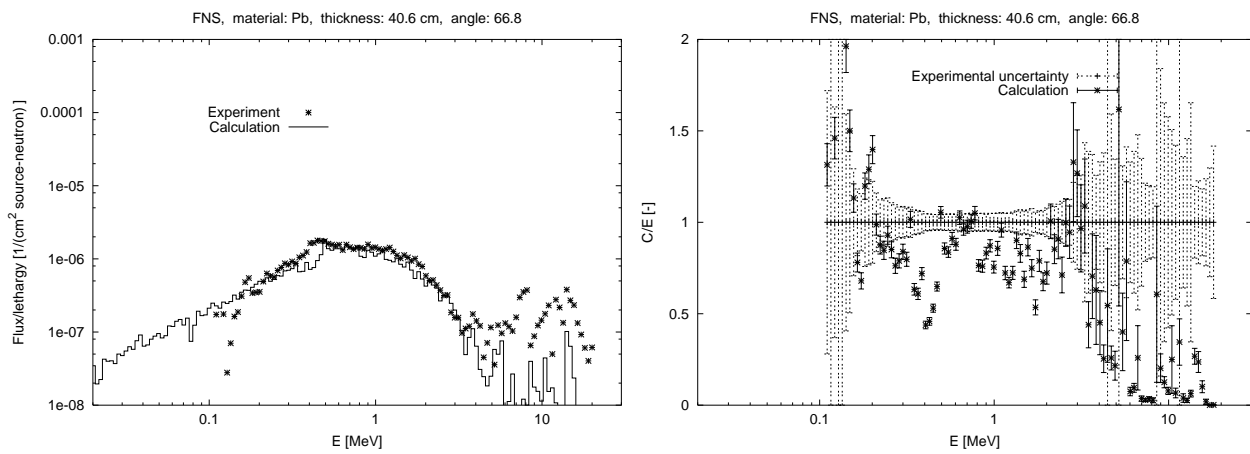


Figure 3.85 Neutron spectrum for the FNS, Pb, $d=40\text{cm}$ benchmark at 66.8° angle.

energy range		0°	12.2°	24.9°	42.8°	66.8°
0.1–	1.0	0.84 ± 0.01	0.90 ± 0.01	0.80 ± 0.01	0.79 ± 0.01	0.84 ± 0.01
1.0–	5.0	0.89 ± 0.01	0.99 ± 0.01	0.92 ± 0.01	0.92 ± 0.01	0.84 ± 0.01
5.0–	10.0	0.64 ± 0.08	0.92 ± 0.10	0.75 ± 0.12	0.84 ± 0.13	0.16 ± 0.20
10.0–	20.0	0.85 ± 0.02	0.72 ± 0.04	0.67 ± 0.06	0.71 ± 0.11	0.13 ± 0.14

Table 3.25 C/E values for the neutron spectrum of the FNS Pb 40cm benchmark.

3.3 LLNL Pulsed Spheres

3.3.1 LLNL Pulsed Spheres, ${}^6\text{Li}$

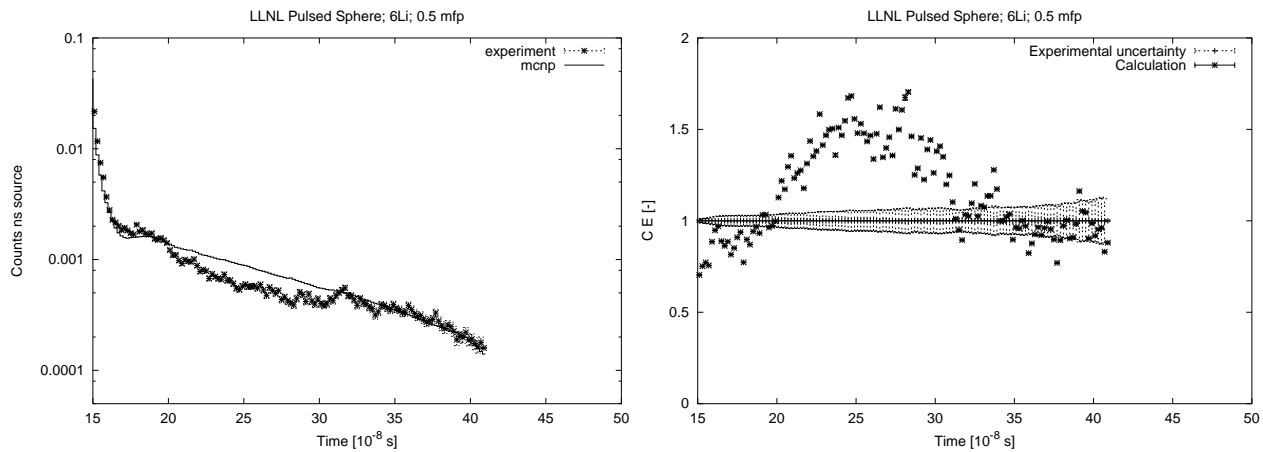


Figure 3.86 Neutron spectrum for the LLNL Pulsed Sphere, ${}^6\text{Li}$ (0.5 mfp) benchmark.

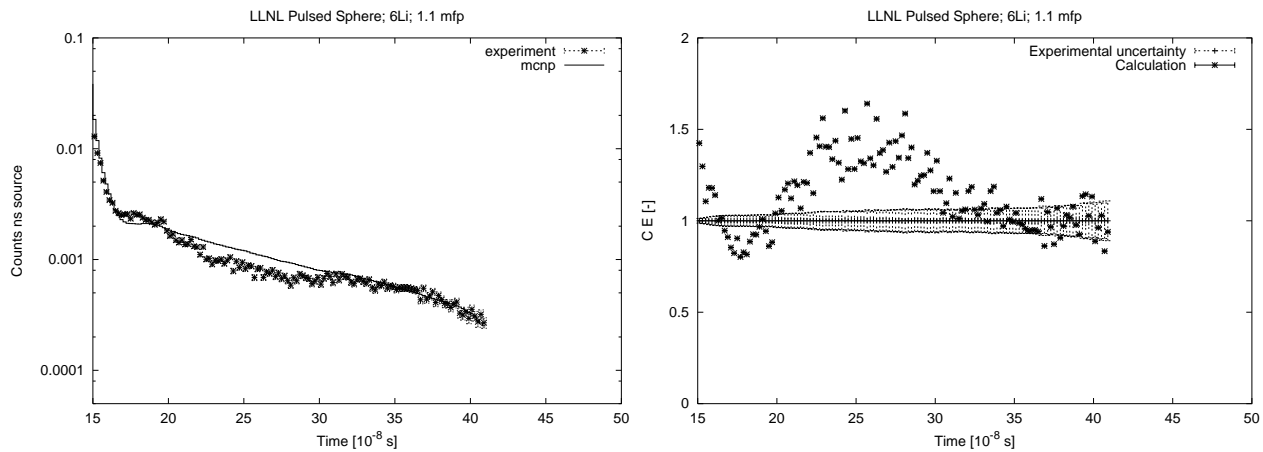


Figure 3.87 Neutron spectrum for the LLNL Pulsed Sphere, ${}^6\text{Li}$ (1.1 mfp) benchmark.

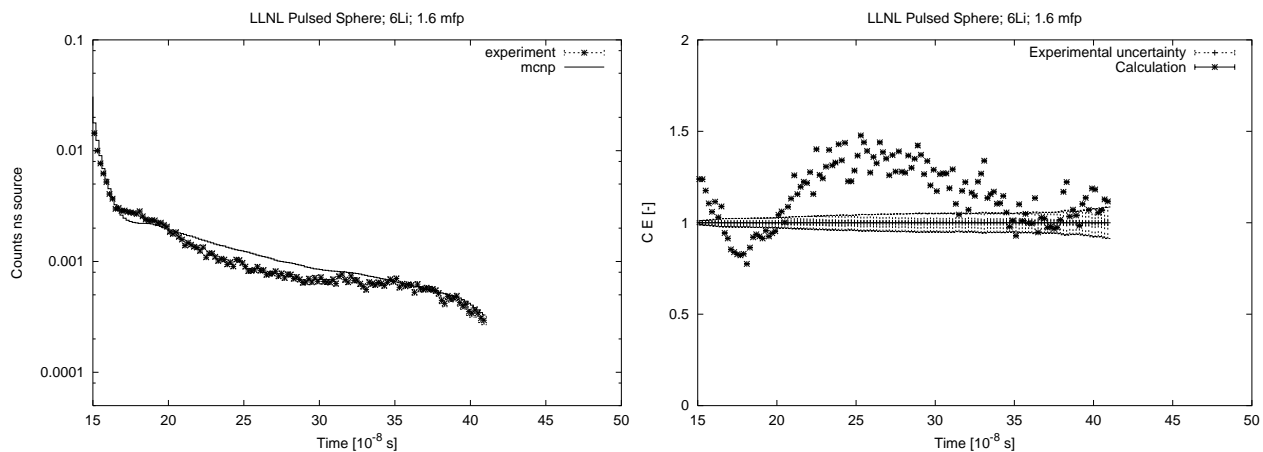


Figure 3.88 Neutron spectrum for the LLNL Pulsed Sphere, ${}^6\text{Li}$ (1.6 mfp) benchmark.

3.3.2 LLNL Pulsed Spheres, ${}^7\text{Li}$

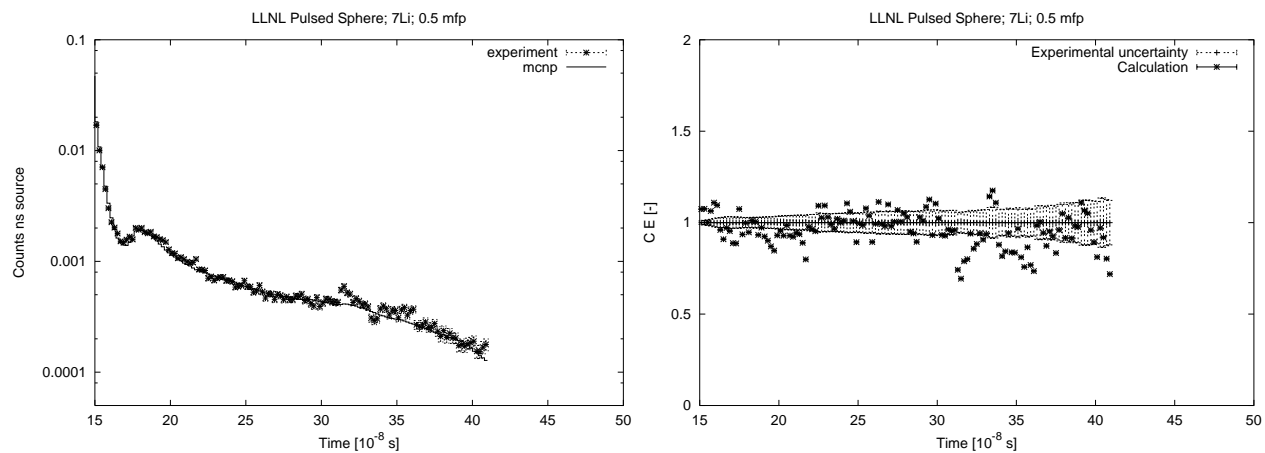


Figure 3.89 Neutron spectrum for the LLNL Pulsed Sphere, ${}^7\text{Li}$ (0.5 mfp) benchmark.

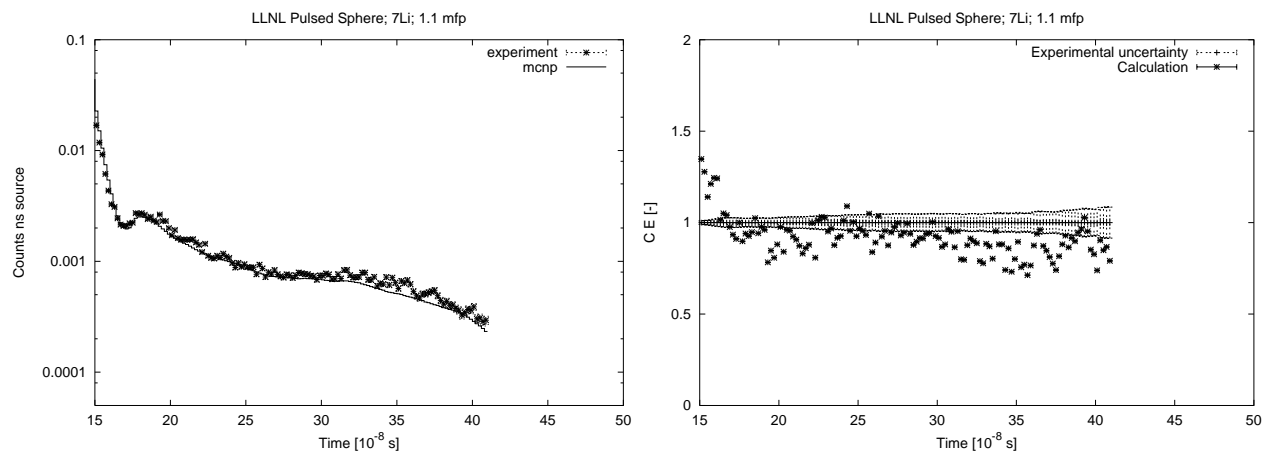


Figure 3.90 Neutron spectrum for the LLNL Pulsed Sphere, ${}^7\text{Li}$ (1.1 mfp) benchmark.

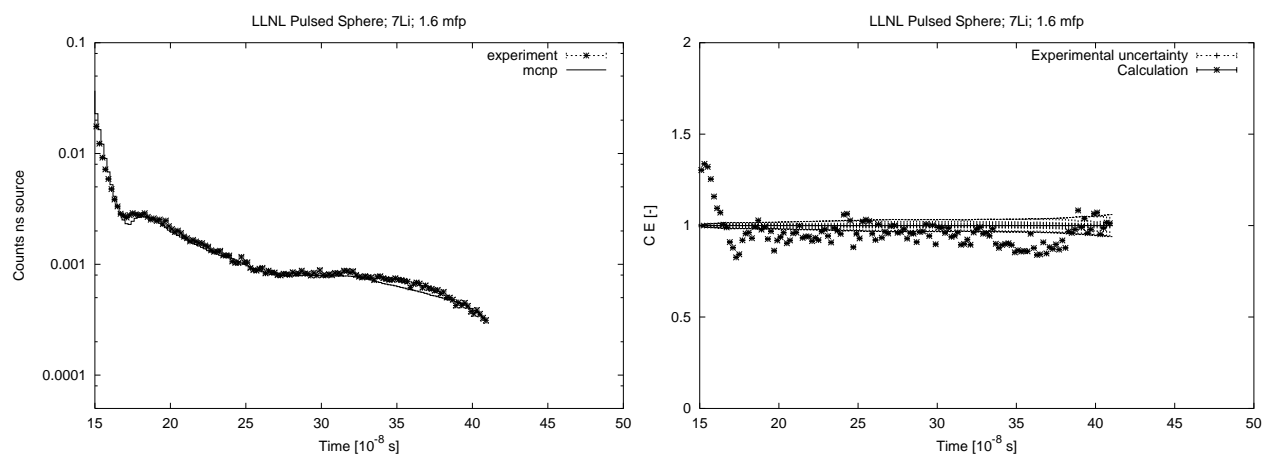


Figure 3.91 Neutron spectrum for the LLNL Pulsed Sphere, ${}^7\text{Li}$ (1.6 mfp) benchmark.

3.3.3 LLNL Pulsed Spheres, Be

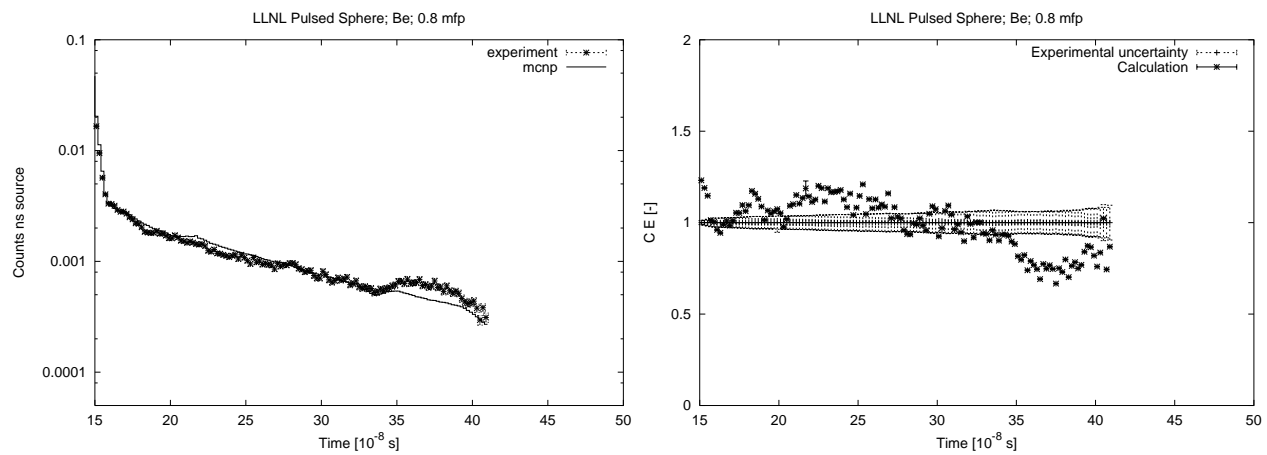


Figure 3.92 Neutron spectrum for the LLNL Pulsed Sphere, Be (0.8 mfp) benchmark.

3.3.4 LLNL Pulsed Spheres, C

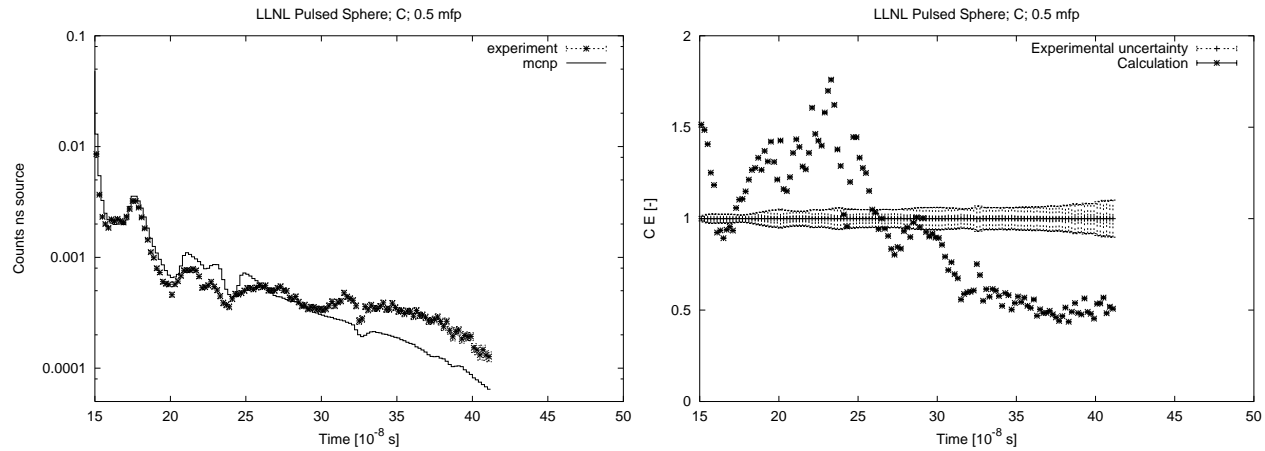


Figure 3.93 Neutron spectrum for the LLNL Pulsed Sphere, C (0.5 mfp) benchmark.

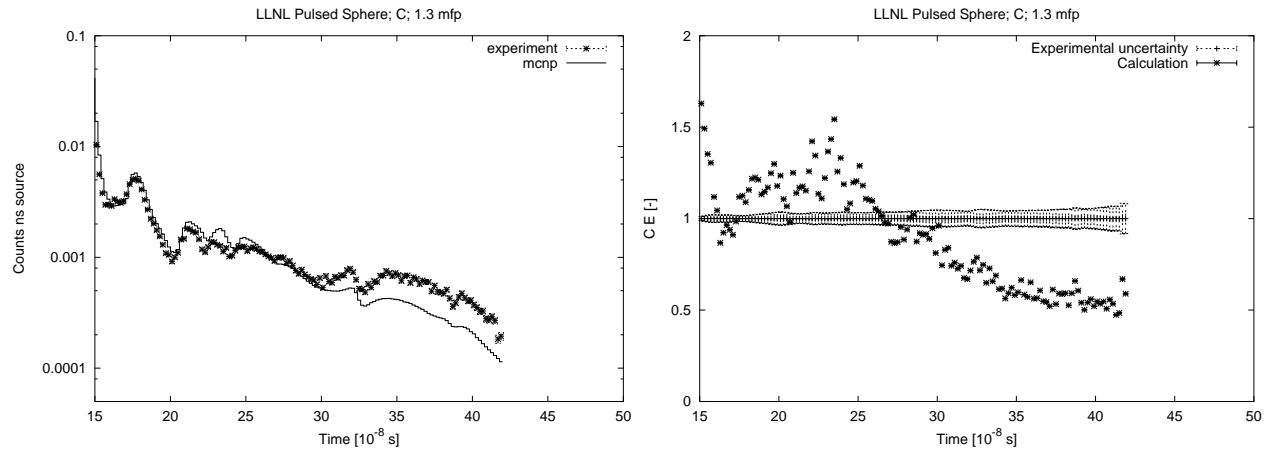


Figure 3.94 Neutron spectrum for the LLNL Pulsed Sphere, C (1.3 mfp) benchmark.

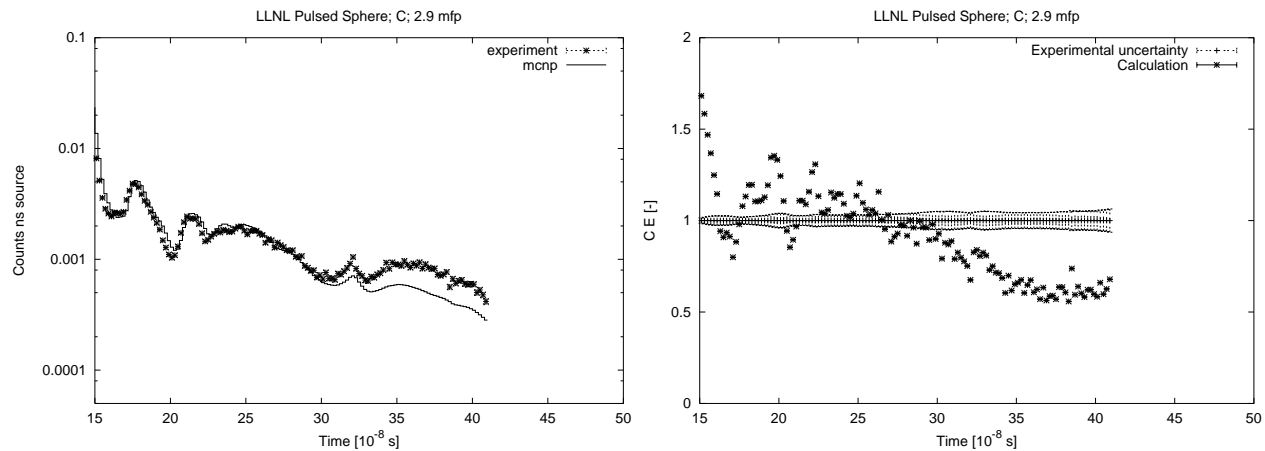


Figure 3.95 Neutron spectrum for the LLNL Pulsed Sphere, C (2.9 mfp) benchmark.

3.3.5 LLNL Pulsed Spheres, N

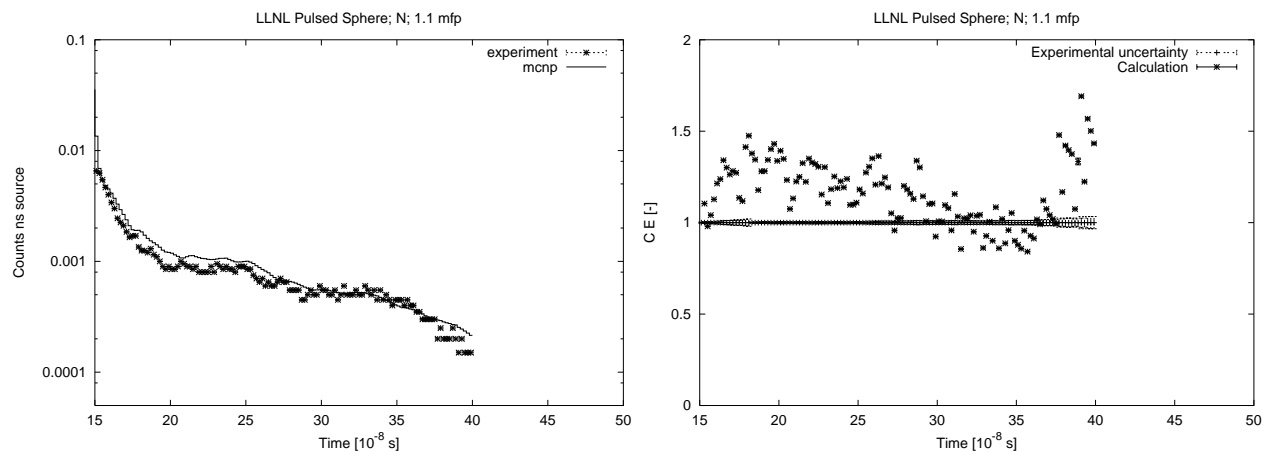


Figure 3.96 Neutron spectrum for the LLNL Pulsed Sphere, N (1.1 mfp) benchmark.

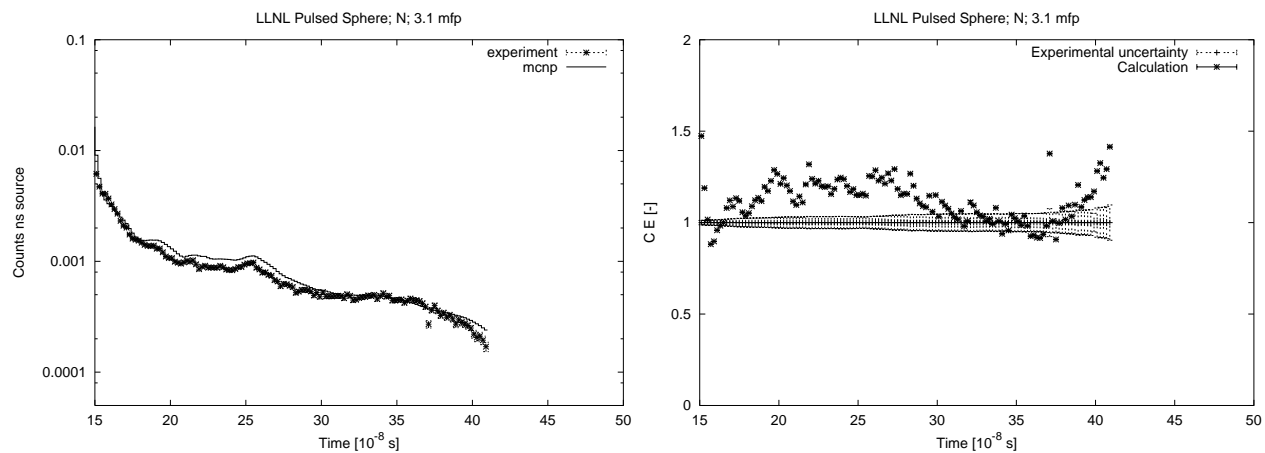


Figure 3.97 Neutron spectrum for the LLNL Pulsed Sphere, N (3.1 mfp) benchmark.

3.3.6 LLNL Pulsed Spheres, O

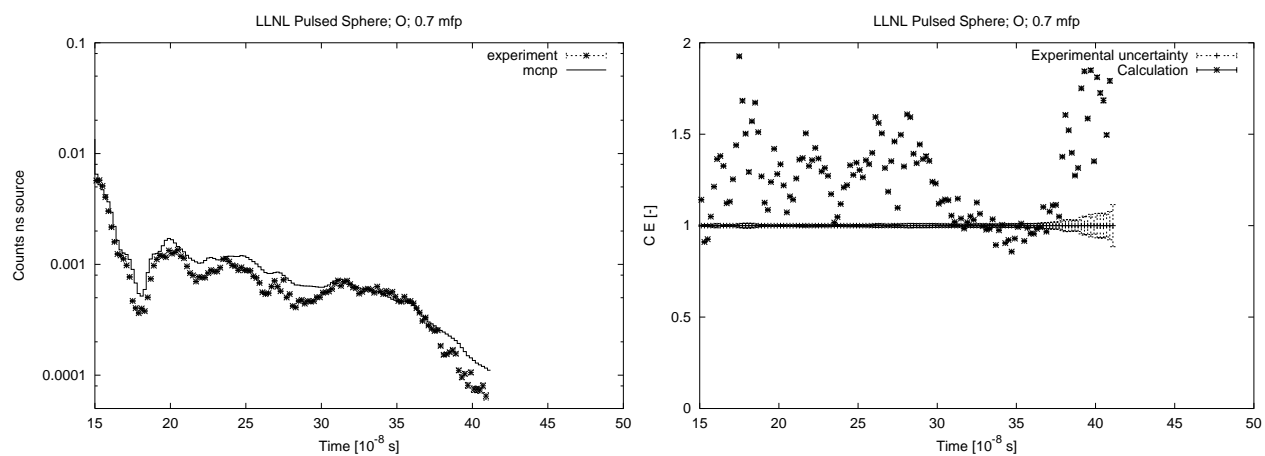


Figure 3.98 Neutron spectrum for the LLNL Pulsed Sphere, O (0.7 mfp) benchmark.

3.3.7 LLNL Pulsed Spheres, Mg

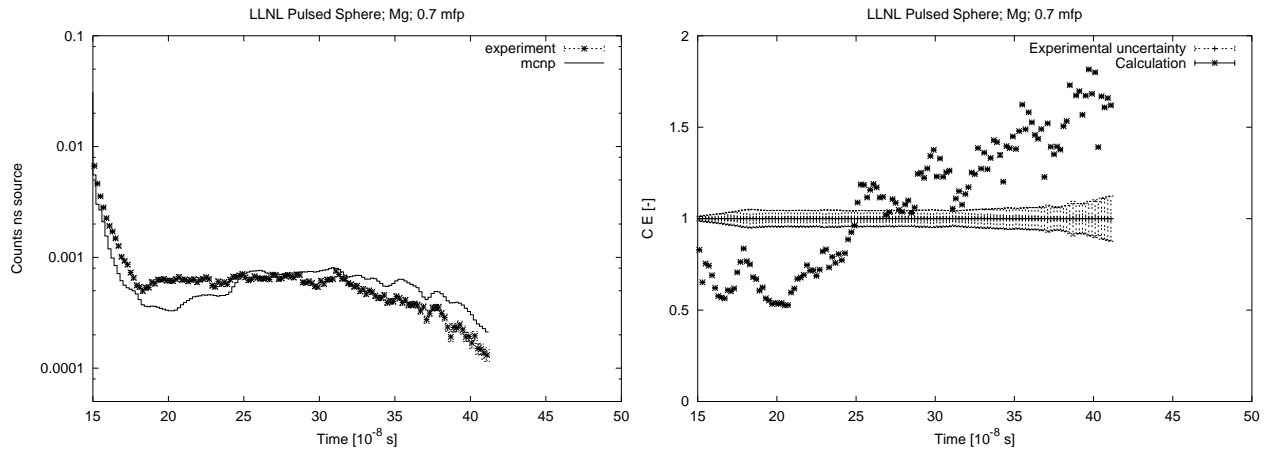


Figure 3.99 Neutron spectrum for the LLNL Pulsed Sphere, Mg (0.7 mfp) benchmark.

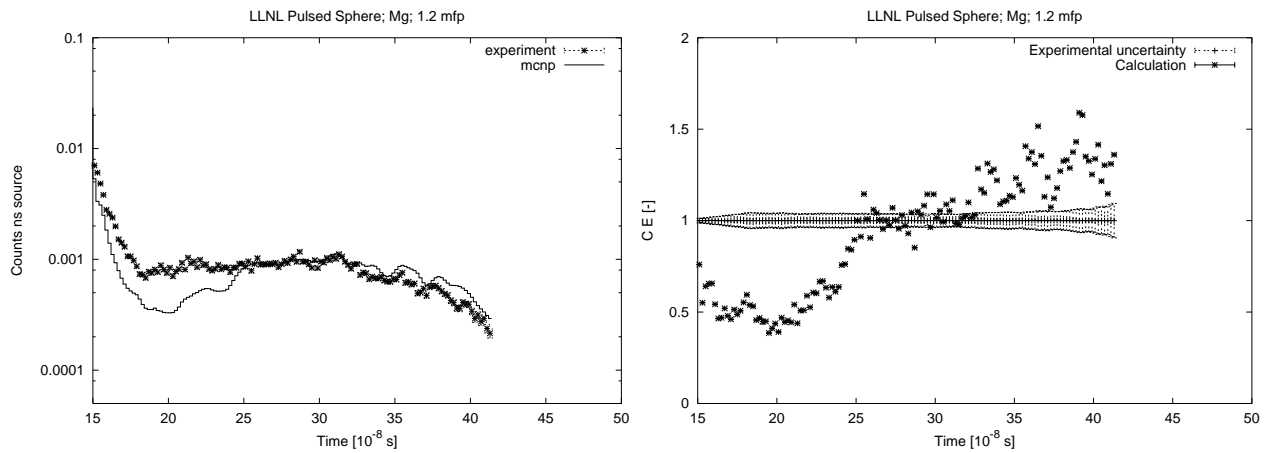


Figure 3.100 Neutron spectrum for the LLNL Pulsed Sphere, Mg (1.2 mfp) benchmark.

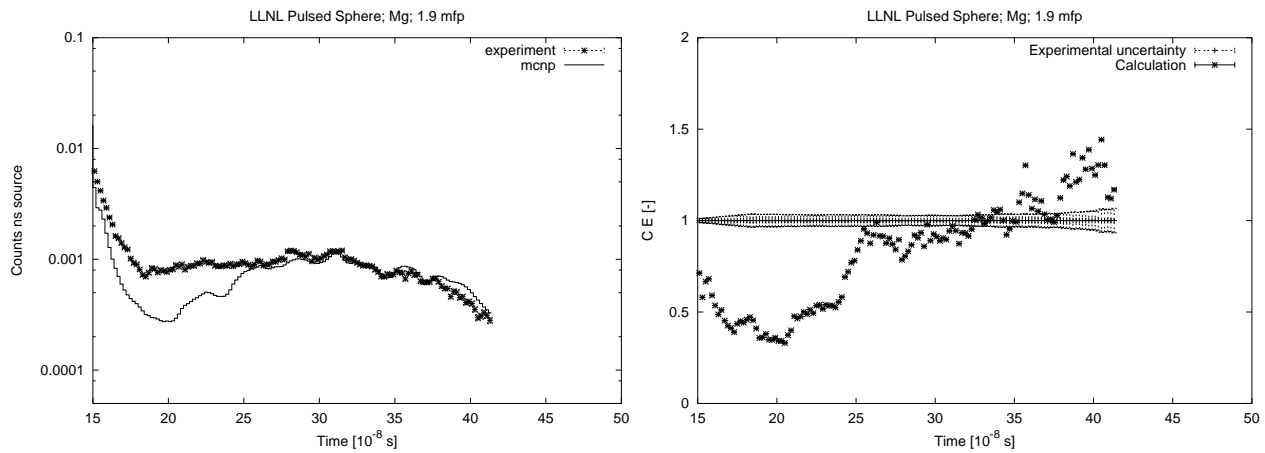


Figure 3.101 Neutron spectrum for the LLNL Pulsed Sphere, Mg (1.9 mfp) benchmark.

3.3.8 LLNL Pulsed Spheres, Al

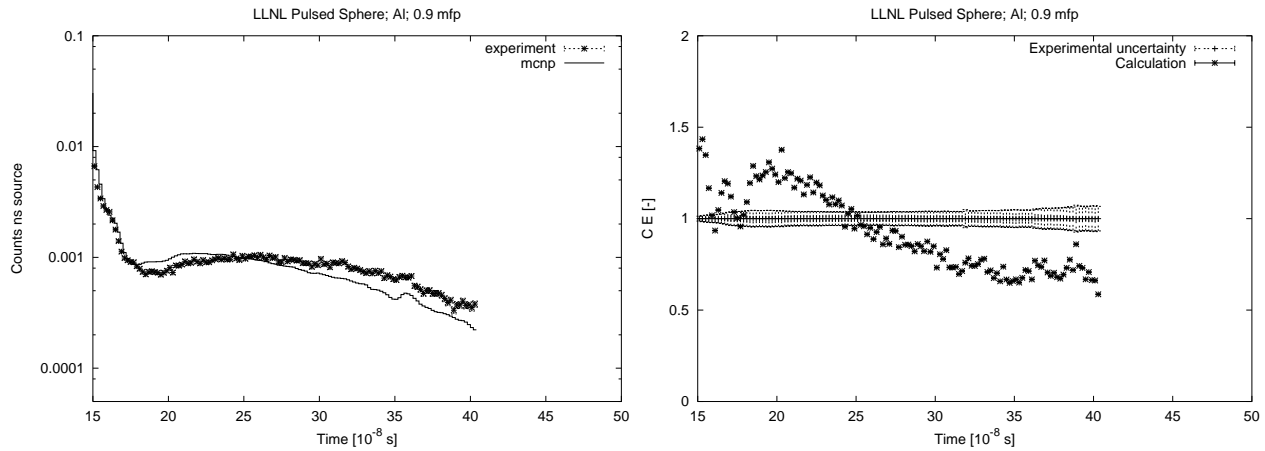


Figure 3.102 Neutron spectrum for the LLNL Pulsed Sphere, Al (0.9 mfp) benchmark.

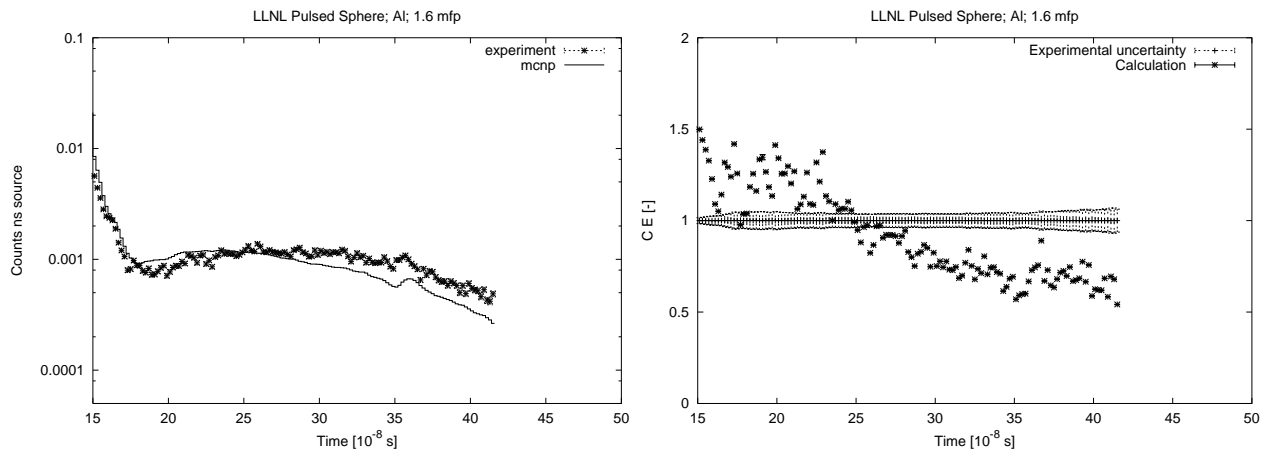


Figure 3.103 Neutron spectrum for the LLNL Pulsed Sphere, Al (1.6 mfp) benchmark.

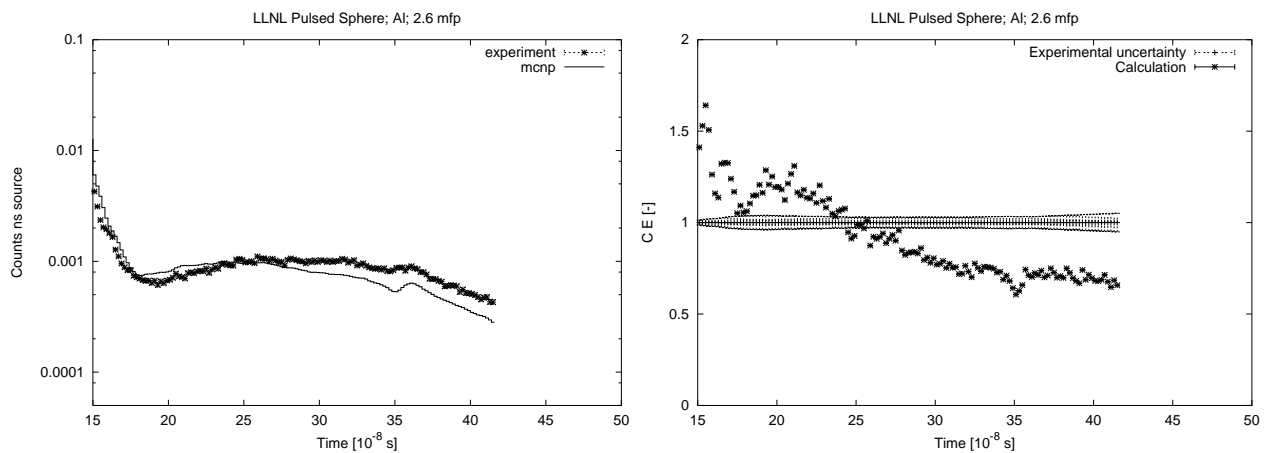


Figure 3.104 Neutron spectrum for the LLNL Pulsed Sphere, Al (2.6 mfp) benchmark.

3.3.9 LLNL Pulsed Spheres, Ti

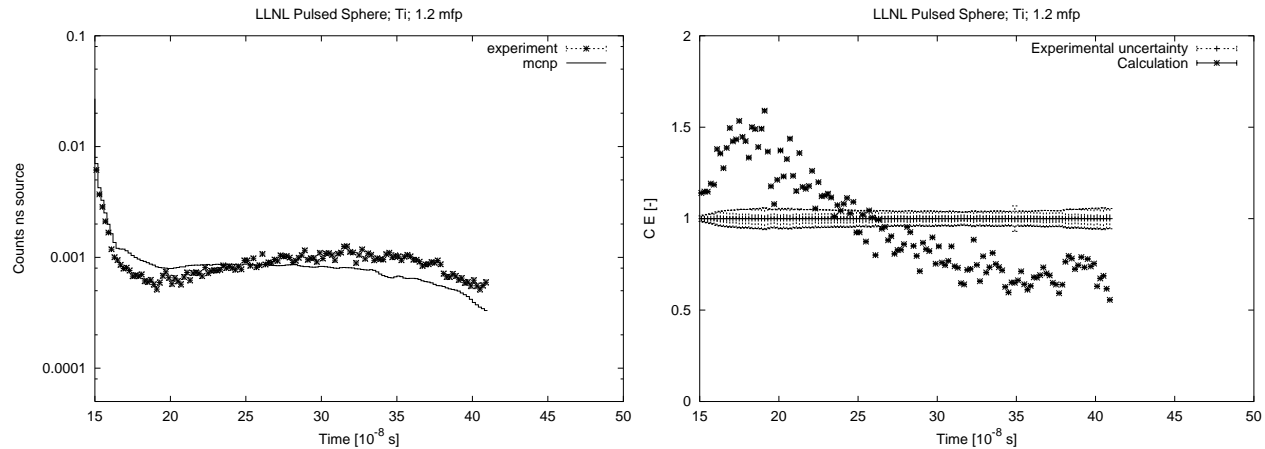


Figure 3.105 Neutron spectrum for the LLNL Pulsed Sphere, Ti (1.2 mfp) benchmark.

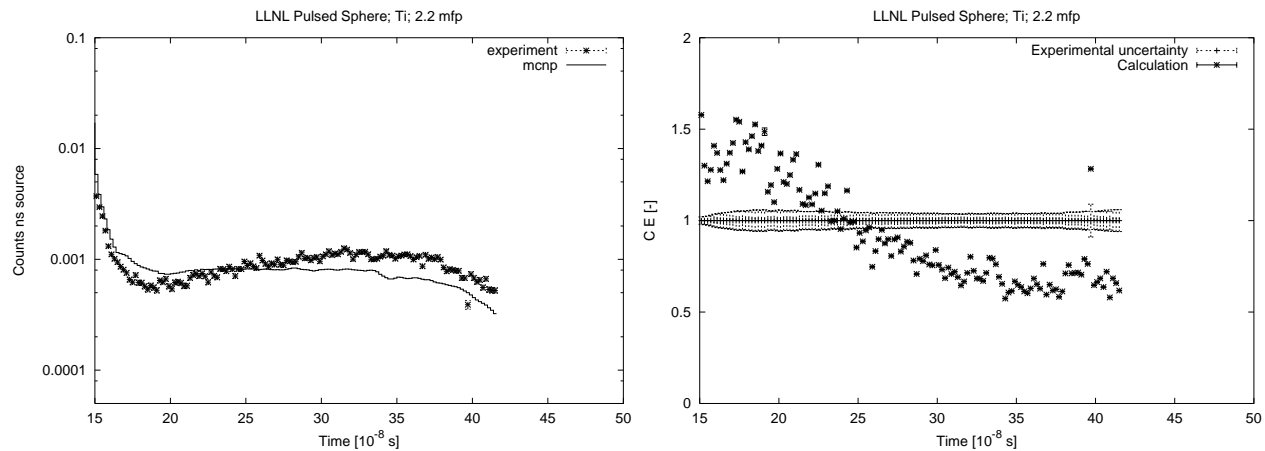


Figure 3.106 Neutron spectrum for the LLNL Pulsed Sphere, Ti (2.2 mfp) benchmark.

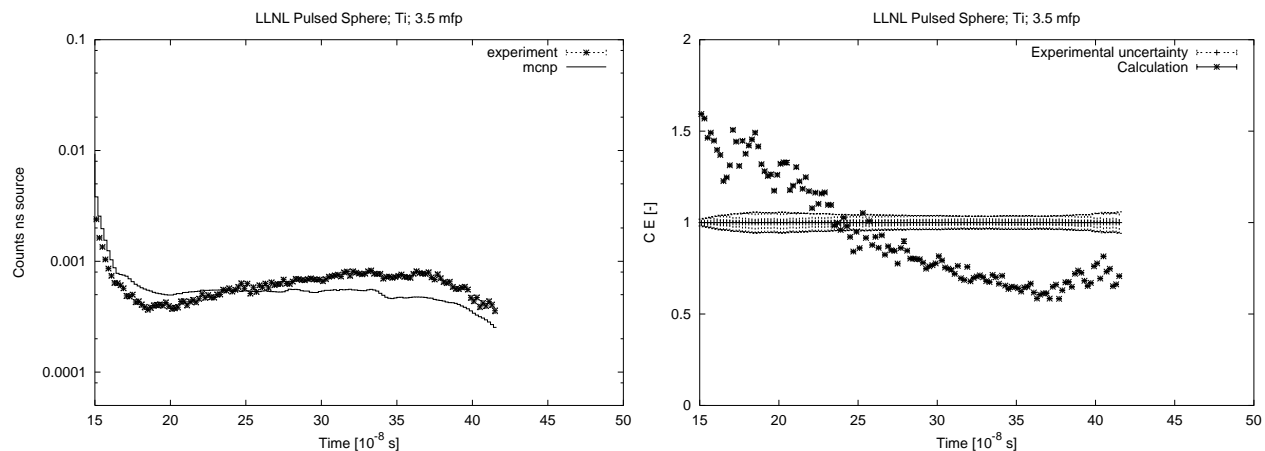


Figure 3.107 Neutron spectrum for the LLNL Pulsed Sphere, Ti (3.5 mfp) benchmark.

3.3.10 LLNL Pulsed Spheres, Fe

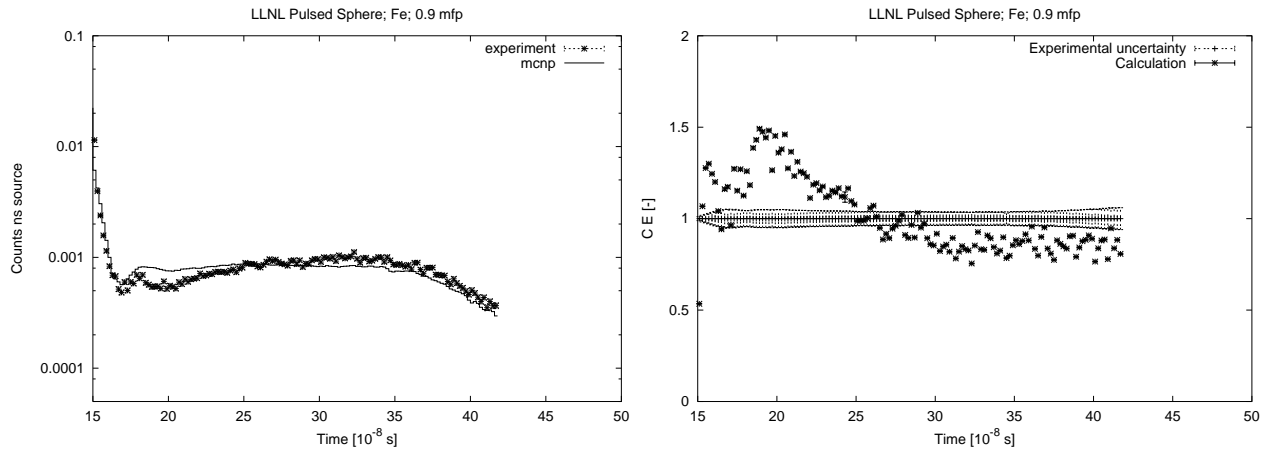


Figure 3.108 Neutron spectrum for the LLNL Pulsed Sphere, Fe (0.9 mfp) benchmark.

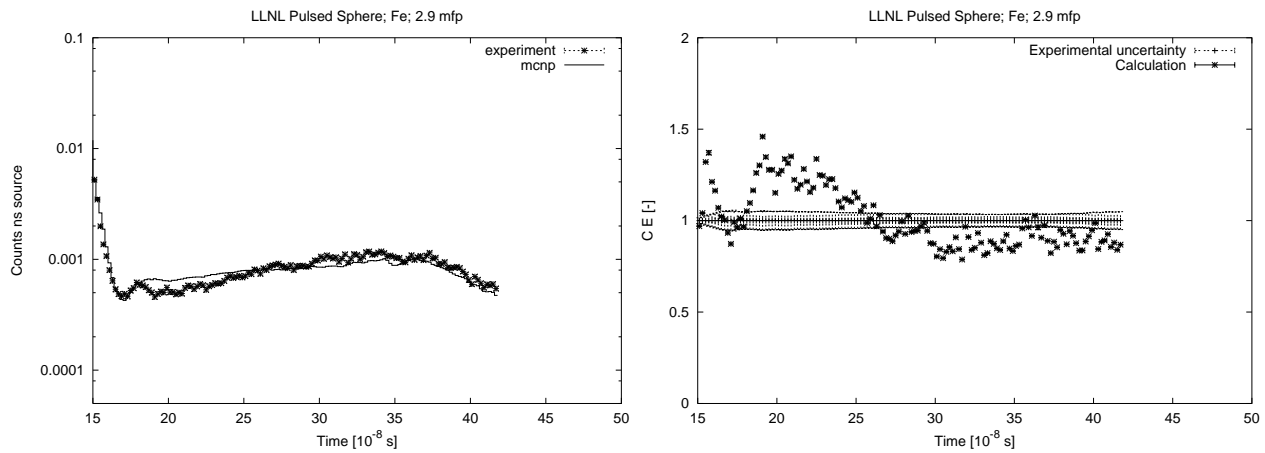


Figure 3.109 Neutron spectrum for the LLNL Pulsed Sphere, Fe (2.9 mfp) benchmark.

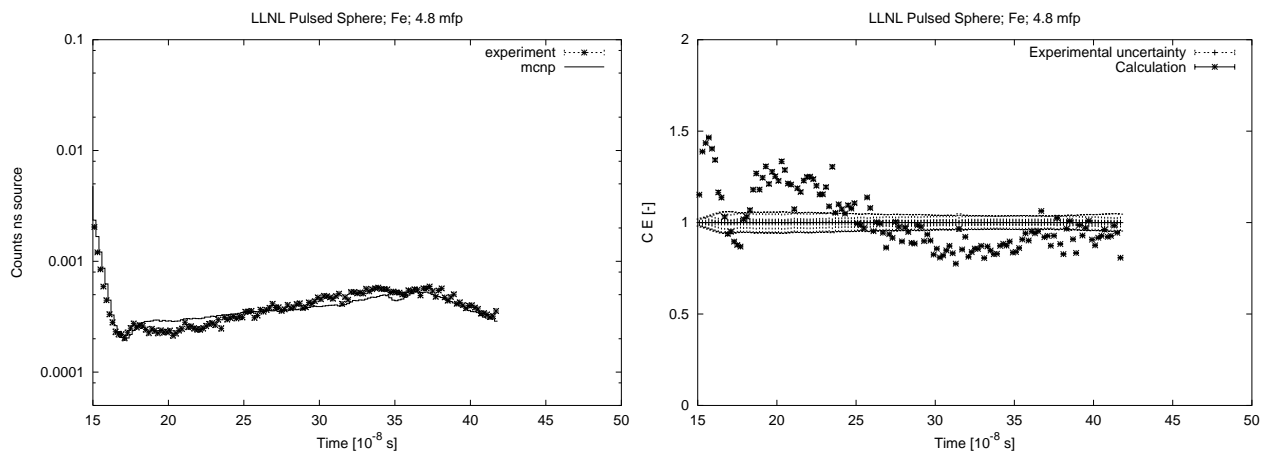


Figure 3.110 Neutron spectrum for the LLNL Pulsed Sphere, Fe (4.8 mfp) benchmark.

3.3.11 LLNL Pulsed Spheres, Pb

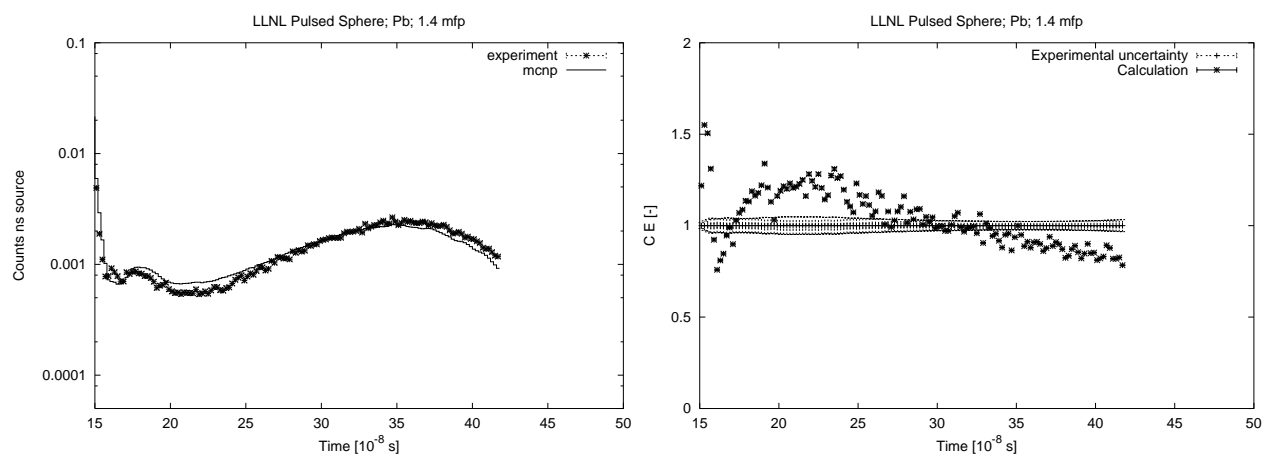


Figure 3.111 Neutron spectrum for the LLNL Pulsed Sphere, Pb (1.4 mfp) benchmark.

3.3.12 LLNL Pulsed Spheres, D₂O

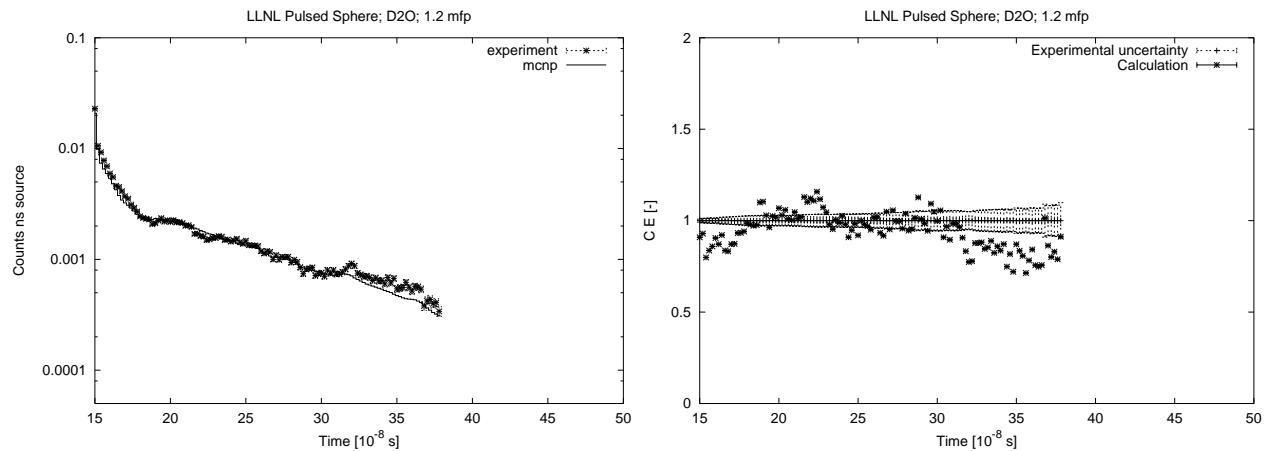


Figure 3.112 Neutron spectrum for the LLNL Pulsed Sphere, D₂O (1.2 mfp) benchmark.

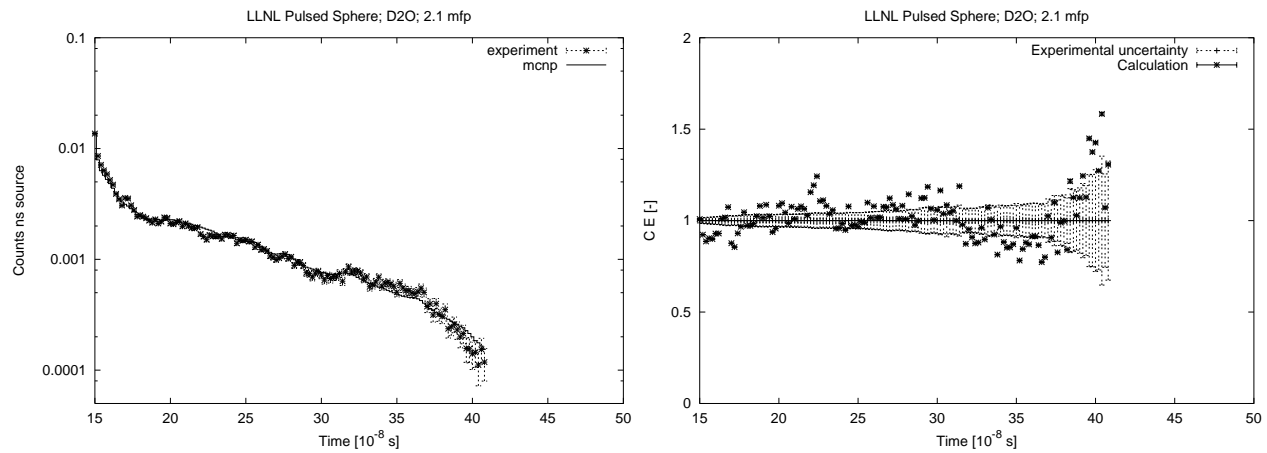


Figure 3.113 Neutron spectrum for the LLNL Pulsed Sphere, D₂O (2.1 mfp) benchmark.

3.3.13 LLNL Pulsed Spheres, H₂O

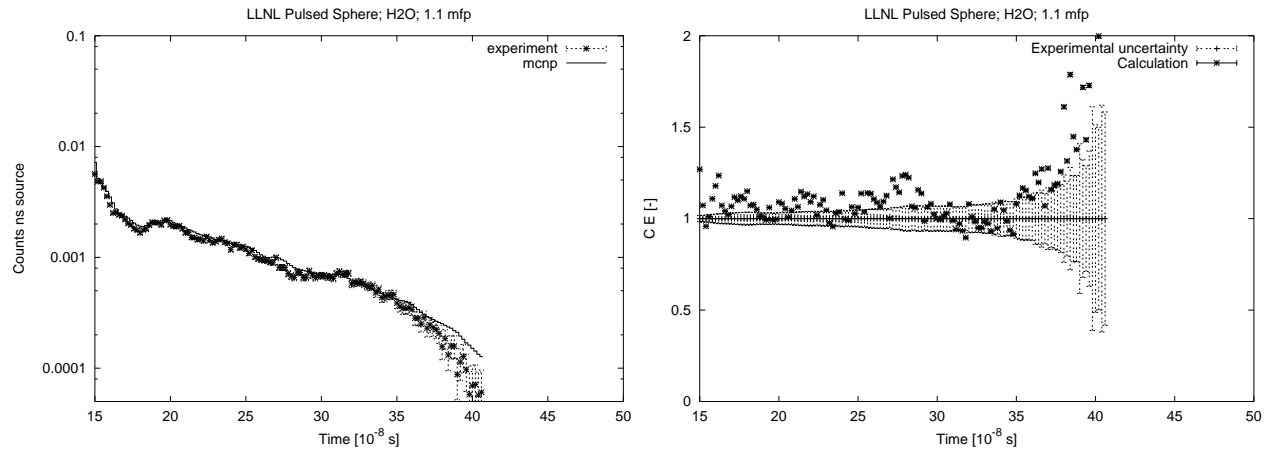


Figure 3.114 Neutron spectrum for the LLNL Pulsed Sphere, H₂O (1.1 mfp) benchmark.

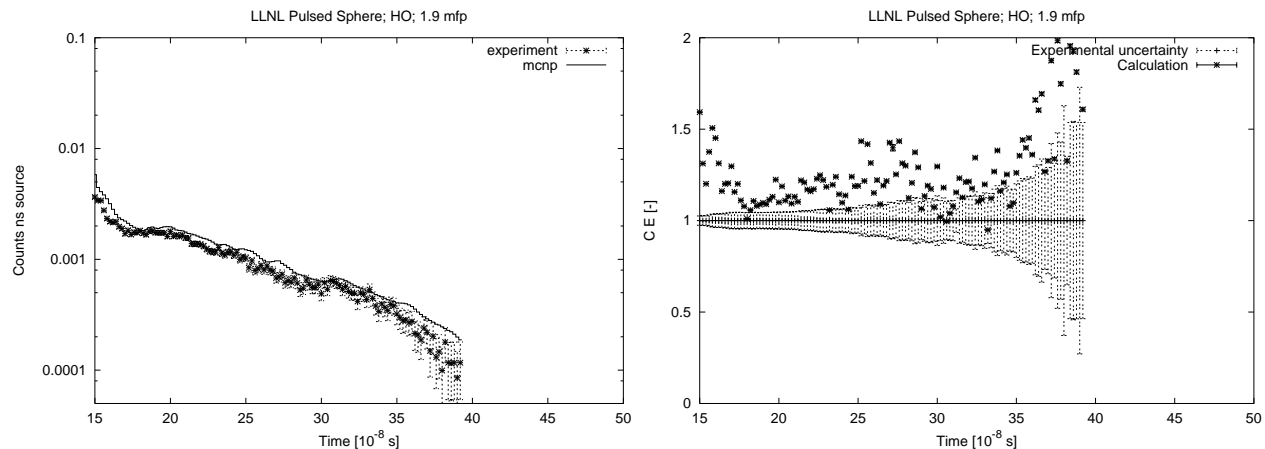


Figure 3.115 Neutron spectrum for the LLNL Pulsed Sphere, H₂O (1.9 mfp) benchmark.

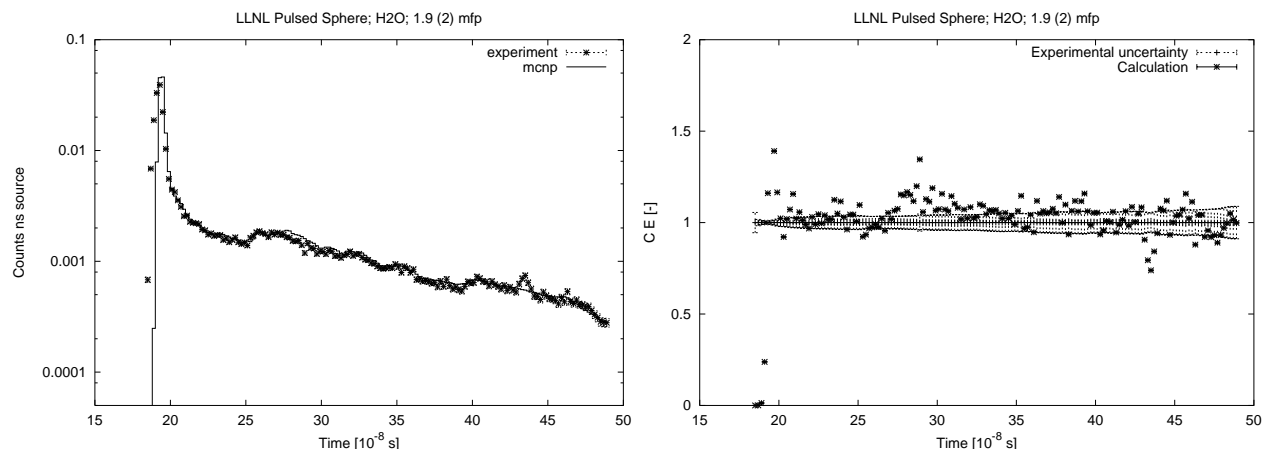


Figure 3.116 Neutron spectrum for the LLNL Pulsed Sphere, H₂O (1.9 (2) mfp) benchmark.

3.3.14 LLNL Pulsed Spheres, Concrete

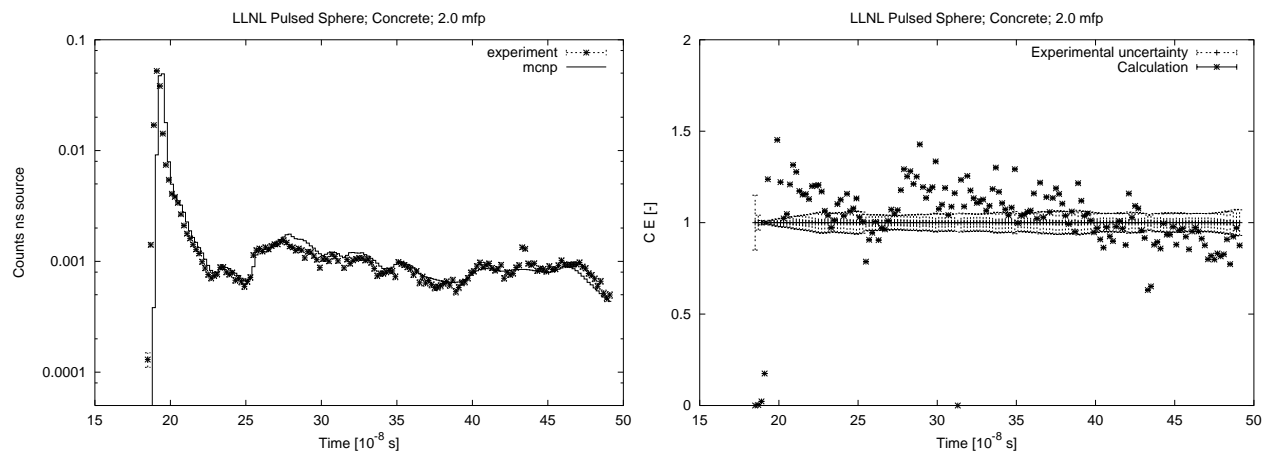


Figure 3.117 Neutron spectrum for the LLNL Pulsed Sphere, con (2.0 mfp) benchmark.

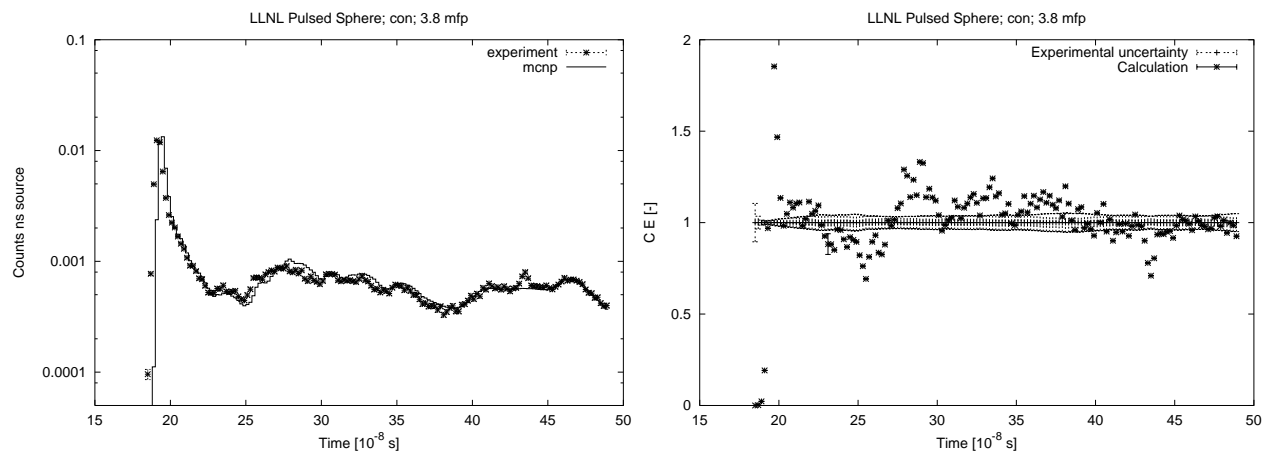


Figure 3.118 Neutron spectrum for the LLNL Pulsed Sphere, con (3.8 mfp) benchmark.

3.3.15 LLNL Pulsed Spheres, Polyethylene

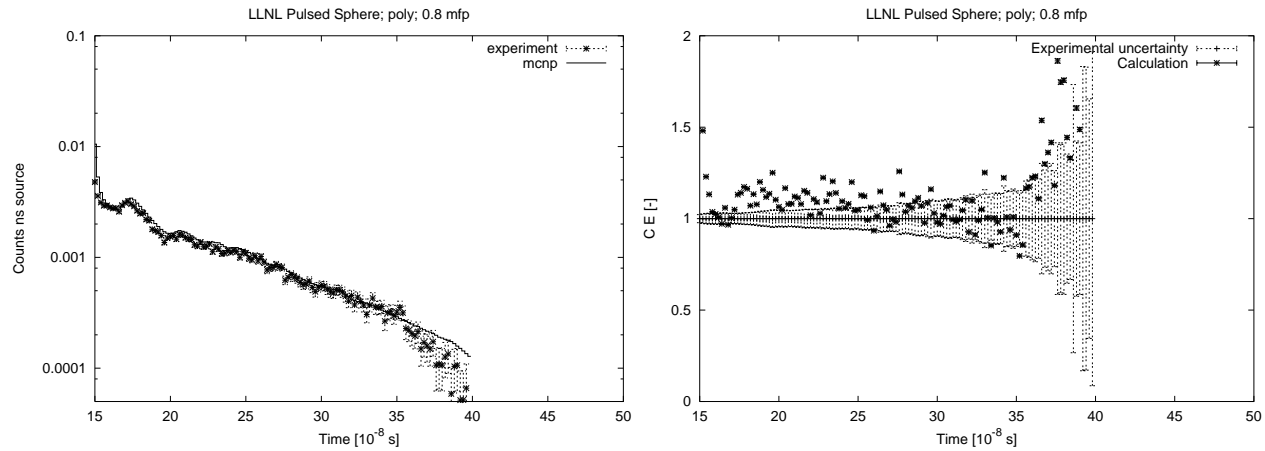


Figure 3.119 Neutron spectrum for the LLNL Pulsed Sphere, poly (0.8 mfp) benchmark.

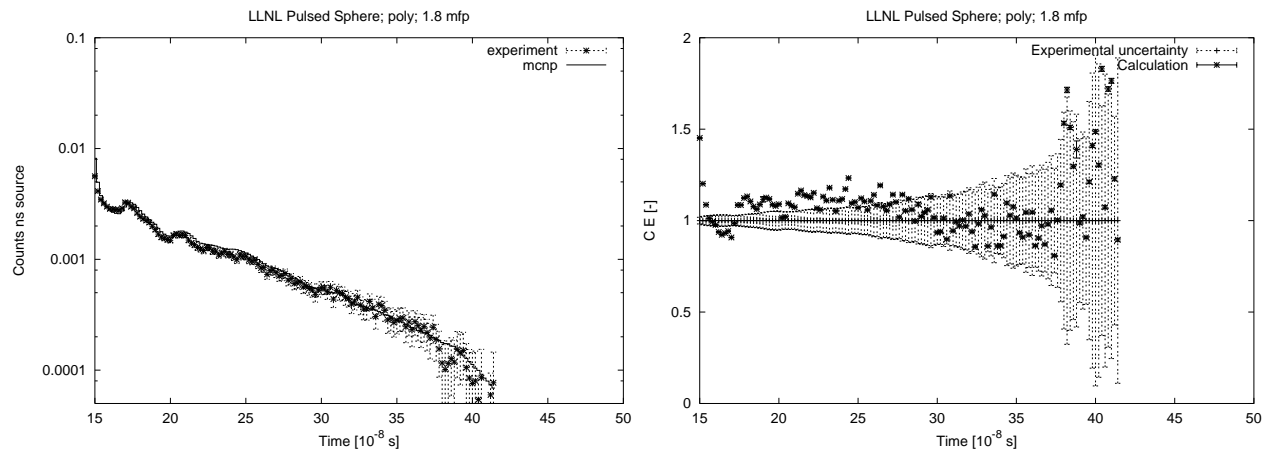


Figure 3.120 Neutron spectrum for the LLNL Pulsed Sphere, poly (1.8 mfp) benchmark.

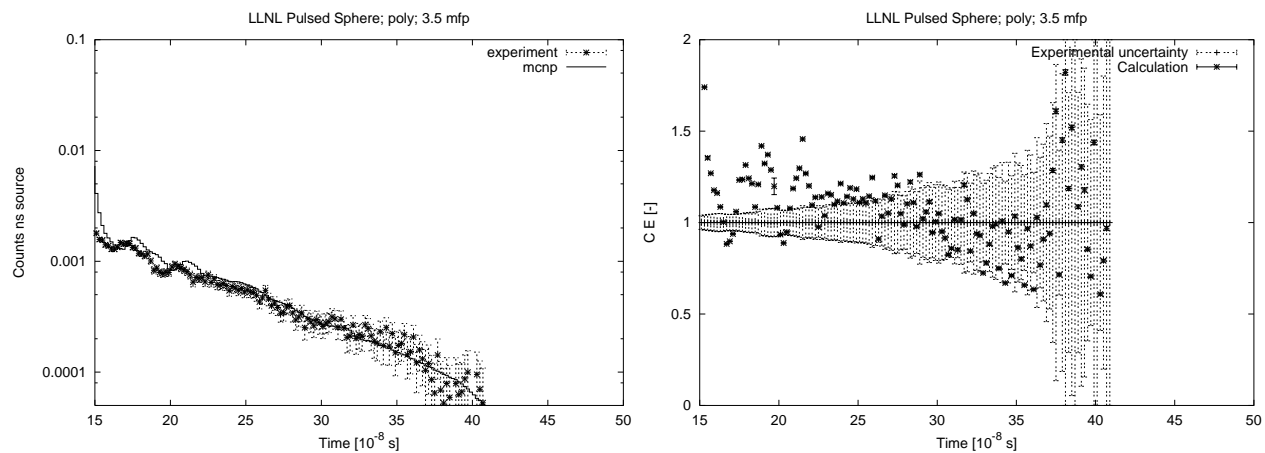


Figure 3.121 Neutron spectrum for the LLNL Pulsed Sphere, poly (3.5 mfp) benchmark.

3.3.16 LLNL Pulsed Spheres, Teflon

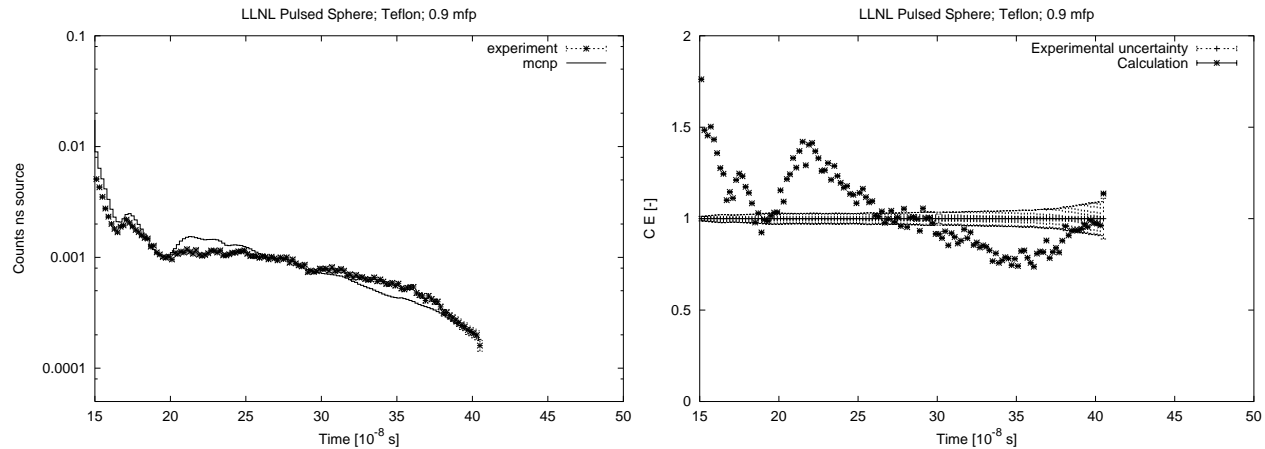


Figure 3.122 Neutron spectrum for the LLNL Pulsed Sphere, Teflon (0.9 mfp) benchmark.

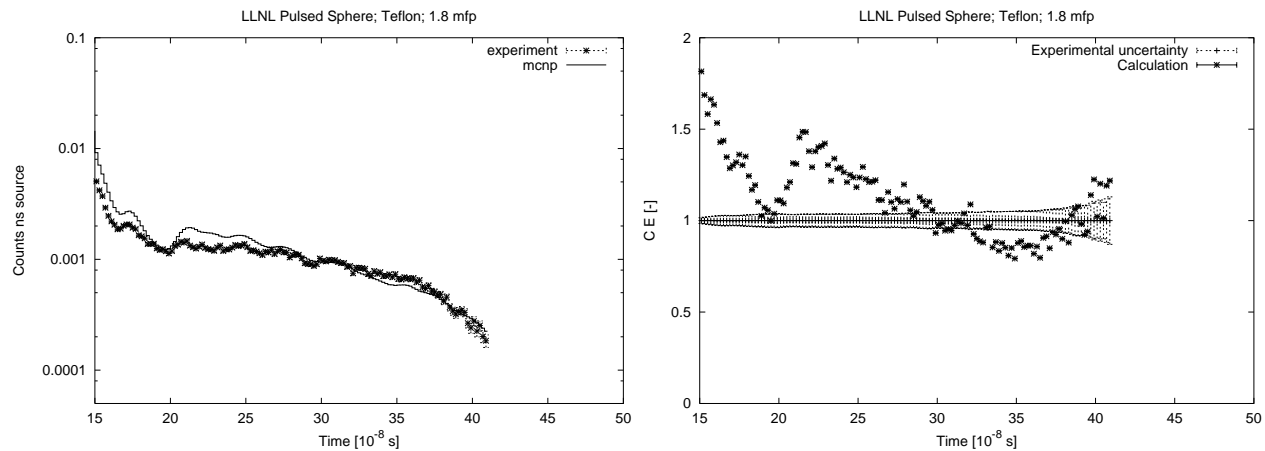


Figure 3.123 Neutron spectrum for the LLNL Pulsed Sphere, Teflon (1.8 mfp) benchmark.

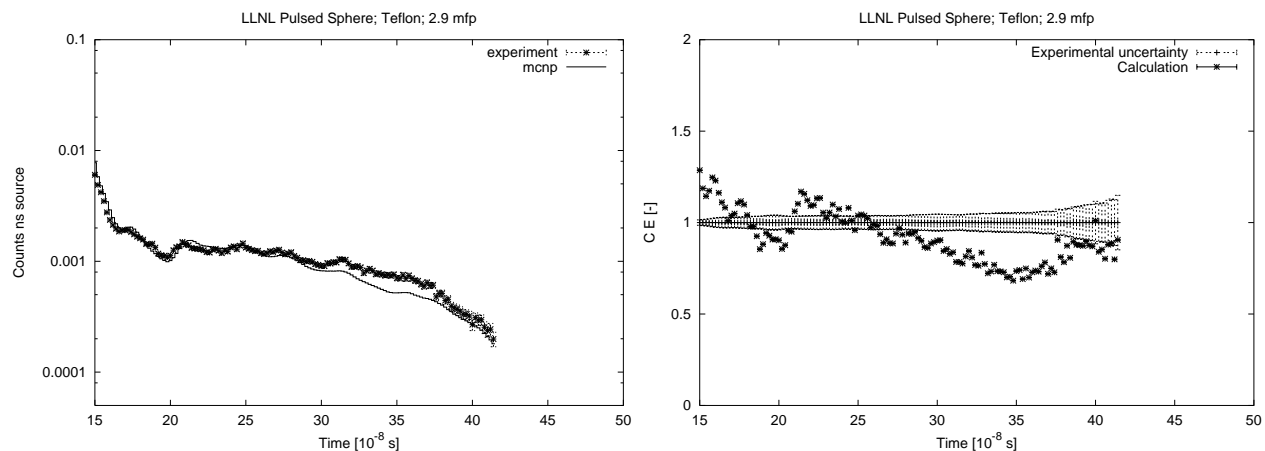


Figure 3.124 Neutron spectrum for the LLNL Pulsed Sphere, Teflon (2.9 mfp) benchmark.

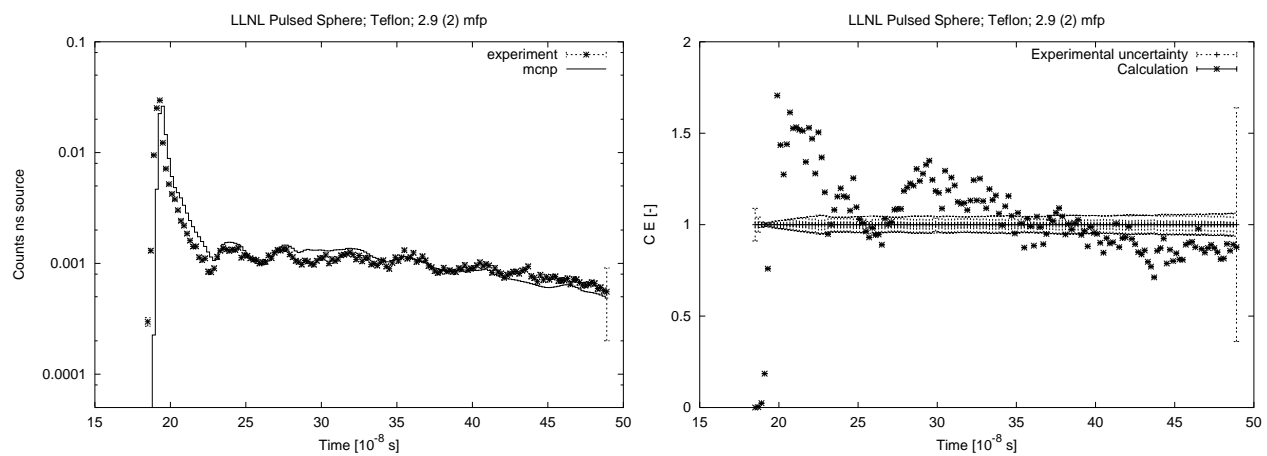


Figure 3.125 Neutron spectrum for the LLNL Pulsed Sphere, Teflon (2.9 (2) mfp) benchmark.

3.4 NIST Water Spheres

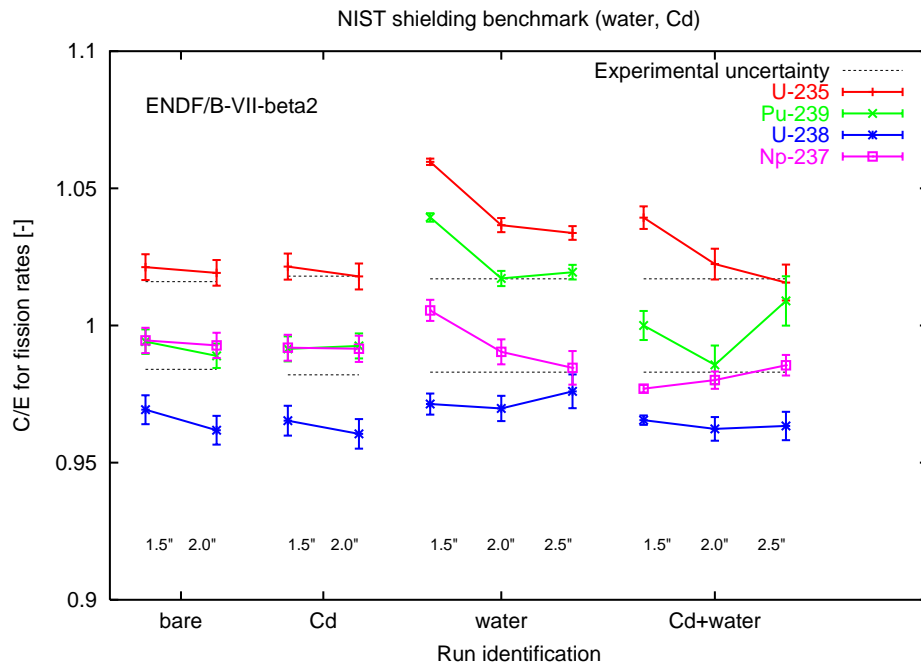


Figure 3.126 C/E values for the fission rate in fission foils in the NIST experiments.

material	radius	U-235	Pu-239	U-238	Np-237
bare	1.5"	1.021±0.005	0.994±0.004	0.969±0.005	0.995±0.005
bare	2.0"	1.019±0.005	0.989±0.004	0.962±0.005	0.993±0.005
Cd	1.5"	1.021±0.005	0.991±0.005	0.965±0.005	0.992±0.005
Cd	2.0"	1.018±0.005	0.993±0.005	0.961±0.005	0.992±0.005
H ₂ O	1.5"	1.060±0.001	1.039±0.002	0.971±0.004	1.006±0.004
H ₂ O	2.0"	1.037±0.003	1.017±0.003	0.970±0.005	0.990±0.005
H ₂ O	2.5"	1.034±0.002	1.019±0.003	0.976±0.006	0.985±0.006
Cd+H ₂ O	1.5"	1.039±0.004	1.000±0.005	0.965±0.002	0.977±0.001
Cd+H ₂ O	2.0"	1.022±0.006	0.986±0.007	0.962±0.004	0.980±0.003
Cd+H ₂ O	2.5"	1.016±0.007	1.009±0.009	0.963±0.005	0.986±0.004

Table 3.26 C/E values for the fission rates in the NIST benchmark.

4. Summary

The ENDF/B-VII beta2 general purpose library has been tested, using MCNP-4C3, with the shielding benchmarks Oktavian, FNS, LLNL Pusled Spheres, and NIST Water spheres. The first three of these are 14 MeV experiments.

This exercise provides insight in the global quality of a data library and also in particular problems of nuclear data for certain elements. Comparison with other data libraries and detailed inspection of the data files could reveal the origin of observed discrepancies. However, this is outside the scope of the present study.

References

- [1] J.F. Briesmeister (Ed.), *MCNP - A General Monte Carlo N-Particle Transport Code, Version 4C*, Technical Report LA-13709-M, Los Alamos National Laboratory, USA (2000)
- J.S. Hendricks, *MCNP4C3*, Report X-5:RN(U)-JSH-01-17, Los Alamos National Laboratory, USA (2001)
- [2] M.C. Duijvestijn, A. Hogenbirk, S.C. van der Marck, *ENDF/B-VI.8-PBMR - Contents of the ENDF/B-VI.8 based MCNP neutron transport cross section libraries for PBMR*, NRG Report 21526/05.64901/C FAI/MD/AK (2005)
- [3] www-nds.iaea.or.at/fendl2/validation/benchmarks/jaerim94014/oktavian/n-leak
- [4] C. Ichihara, I. Kimura, S.A. Hayashi, J. Yamamoto, and A. Takahashi, *Measurement of leakage neutron spectra from a spherical pile of zirconium irradiated with 14 MeV neutrons and validation of its nuclear data*, *J. Nucl. Sci. Techn.* **40** (2003) 417–422
- [5] www-nds.iaea.or.at/fendl2/validation/benchmarks/jaerim94014/fns-tof
- [6] Y. Oyama, S. Yamaguchi, and H. Maekawa *Measurements and analyses of angular neutron flux spectra on graphite and lithium-oxide slabs irradiated with 14.8 MeV neutrons*, *J. Nucl. Sci. Techn.* **25** (1988) 419–428
- [7] C. Wong, J.D. Anderson, P. Brown, L.F. Hansen, J.L. Kammerdiener, C. Logan, and B. Pohl, *Livermore Pulsed Sphere Program: Program Summary through July 1971*, UCRL-51144, Rev. 1 (1972)
- [8] W. Haeck, *JEFF 3.1 validation results on LLNL pulsed spheres*, JEF/DOC-1141 (2006)
- [9] M.Z. Youssef, A. Kumar, M.A. Abdou, Ch. Konno, F. Maekawa, M. Wada, Y. Oyama, H. Maekawa, and Y. Ikeda, *Verification of ITER shielding capability and FENDL data benchmarking through analysis of bulk shielding experiment on large SS316/water assembly bombarded with 14 MeV neutrons*, *Fusion Engineering and Design* **42** (1998) 235–245
- [10] Sinbad data base, NEA (2004), http://www.nea.fr/html/science/shielding/sinbad/nist_h2o/nist-abs.htm